DOCTORAL THESIS

Advanced Condition Monitoring of High-Voltage Circuit Breaker Utilising Machine Learning

Sajjad Asefi

TALLINNA TEHNIKAÜLIKOOL
TALLINN UNIVERSITY OF TECHNOLOGY
TALLINN 2026

TALLINN UNIVERSITY OF TECHNOLOGY
DOCTORAL THESIS
54/2026

Advanced Condition Monitoring of High-Voltage Circuit Breaker Utilising Machine Learning

SAJJAD ASEFI

TAL TECH PRESS

TALLINN UNIVERSITY OF TECHNOLOGY
School of Engineering
Department of Electrical Power Engineering and Mechatronics

This dissertation was accepted for the defence of the degree 05/07/2026

Supervisor: Professor Jako Kilter,
Department of Electrical Power Engineering and Mechatronics, School of Engineering,
Tallinn University of Technology
Tallinn, Estonia

Co-supervisor: Mart Landsberg, PhD
Department of Electrical Power Engineering and Mechatronics, School of Engineering,
Tallinn University of Technology
Tallinn, Estonia

Opponents: Professor Kaveh Niayesh,
Norwegian University of Science and Technology
Trondheim, Norway

Prof. Dr. Christian M. Franck,
University of ETH Zürich,
Zürich, Switzerland

Defence of the thesis: 08/09/2026, Tallinn

Declaration:
Hereby I declare that this doctoral thesis, my original investigation and achievement, submitted for the doctoral degree at Tallinn University of Technology has not been submitted for doctoral or equivalent academic degree.

Sajjad Asefi

---
signature

European Union
European Regional
Development Fund

Investing
in your future

elering
CONNECTING ENERGIES

Copyright: Sajjad Asefi, 2026

ISSN 2585-6901 (pdf)
ISBN 978-9916-80-545-9 (pdf)
https://doi.org/10.23658/taltech.54/2026

Asefi, S. (2026). *Advanced Condition Monitoring of High-Voltage Circuit Breaker Utilising Machine Learning* [TalTech Press]. https://doi.org/10.23658/taltech.54/2026

TALLINNA TEHNIKAÜLIKOOL
DOKTORITÖÖ
54/2026

Kõrgepinge-võimsuslüliti täiustatud seisundiseire masinõppe abil

SAJJAD ASEFI

TAL TECH
KIRJASTUS

Contents

List of Publications 7

Author's Contributions to the Publications 8

List of Symbols and Abbreviations 9

Introduction 11

1 Principles of Condition Monitoring of Substation Equipment 19
1.1 Substation 19
1.2 Maintenance Strategies 20
1.3 Failure Modes and Mechanisms 22
1.3.1 Mechanical Failures 22
1.3.2 Electrical and Dielectric Failures 23
1.3.3 Auxiliary and Control System Failures 23
1.3.4 Summary 23
1.4 Diagnostic Signals 24
1.4.1 Switching Number 24
1.4.2 SF_6 Gas Pressure 26
1.4.3 Drive Motor Current 26
1.4.4 Trip/Close Coil Current 27
1.4.5 Contact Travel Curve 28
1.4.6 Contact Resistance Measurement 29
1.4.7 Other methodologies 30
1.4.8 Summary 30
1.5 Health Index Evaluation Techniques 30
1.6 Remarks 31

2 Condition Monitoring of High-Voltage Circuit Breaker 33
2.1 Architecture and Operational Principles of SF_6 Gas Circuit Breakers 33
2.1.1 The SF_6 Gas Arc Extinguishing Medium 33
2.1.2 Operating Mechanisms and Control Circuits 35
2.2 Failure Analysis Based on Service Application 38
2.3 Theoretical Framework of Equipment Failure 39
2.3.1 The Bathtub Curve Concept 39
2.3.2 Weibull Distribution Limitations 40
2.4 Proposed Methodology for Remaining Useful Life Estimation 40
2.4.1 Gaussian Function-Based Ageing Model 40
2.4.2 Data Limitations and the Bathtub Curve Analogy 41
2.4.3 Interpolation of the Data and Sensitivity Analysis 42
2.4.4 Integration of Service Type via Normalisation 44
2.4.5 Computational Implementation 45
2.5 Remarks 46

3 Condition Monitoring of HVCB Based on Coil Current Measurements 47
3.1 Commercial Measurement Equipment 47
3.2 Coil Current Measurement Experimental Setup 48
3.2.1 Emulator Architecture 49
3.2.2 Comparative Analysis of Current Sensors 52

3.2.3 Comparison of Denoising Algorithms 54
3.2.4 Defect Emulation Scenarios 56
3.3 Feature Extraction Framework 57
3.4 Selection of Savitzky-Golay Parameters 59
3.5 Machine Learning Classification Methodology 59
3.6 Feature Importance Specification via SHAP 60
3.7 Signal Comparison via Dynamic Time Warping 63
3.8 Proposed Monitoring Framework 66
3.9 Mathematical Modelling of Health Index 66
3.9.1 Feature Normalisation 66
3.9.2 Overall Health Index Calculation 68
3.9.3 Case Study: Reliability-Based Maintenance Scheduling 68
3.10 Proposed Enhancements and Practical Implementation 71
3.10.1 Real-Time Validation via Hardware-in-the-Loop Frameworks 71
3.10.2 Integration of Measurement Accuracy into the Health Index 72
3.10.3 Practical Implementation Framework for Transmission System Operators 73

Conclusions and Further Work 75

List of Figures 77

List of Tables 79

References 81

Acknowledgements 87

Abstract 89

Kokkuvõte 91

Appendix 1 93

Appendix 2 101

Appendix 3 109

Appendix 4 119

Appendix 5 127

Appendix 6 139

Curriculum Vitae 147

List of Publications

Main Publications: The present Ph.D. thesis is based on the following publications that are referred to within the text by Roman numbers.

I B. Asad, M. U. Sardar, T. Vaimann, A. Kallaste, S. Asefi, and J. Kilter, "High-Voltage Circuit Breaker Charging Motor's Condition Monitoring - Importance, Possibilities, and Challenges," in 2024 International Conference on Diagnostics in Electrical Engineering (Diagnostika), 2024, pp. 1-7.

II S. Asefi, G. Andreesen, M. Leinakse, J. Kilter, T. Kalmet, H. Manninen, and M. Landsberg, "Measurement and Operation Based Condition Monitoring Methodology for High Voltage Circuit Breakers," in 2022 IEEE PES Innovative Smart Grid Technologies Conference Europe (ISGT-Europe), 2022, pp. 1–5.

III S. Asefi, J. Kilter, and M. Landsberg, "Incorporating Service Type in Ageing Failure Model of High-Voltage Circuit Breaker," in 2023 27th International Conference Electronics, 2023, pp. 1-5.

IV S. Asefi, J. Kilter, E. Shayesteh, P. Hilber, and T. Lindquist, "High-Voltage Circuit Breaker Health Index Evaluation Considering Measurement Accuracy," in 2024 IEEE PES Innovative Smart Grid Technologies Europe (ISGT EUROPE), 2024, pp. 1-5.

V S. Asefi and J. Kilter, "Dynamic Time Warping Technique for Condition Monitoring of High-Voltage Circuit Breakers," in 2025 15th International Conference on Power, Energy, and Electrical Engineering (CPEEE), 2025, pp. 38-42.

VI S. Asefi, S. Asefi, H. Afshari, J. Kilter, E. Shayesteh, P. Hilber, and T. Lindquist, "Machine Learning Based High-Voltage Circuit Breaker Defect Classification Utilizing Savitzky-Golay Filter," IEEE Transactions on Instrumentation and Measurement, 2025.

Additional Publications: The following publications were also authored during the Ph.D. studies but are not directly included in the main body of this thesis.

VII S. Asefi, B. Asad, M. Leinakse, H. Manninen, J. Kilter, T. Vaimann, A. Kallaste, M. Tealane, and M. Landsberg, "Review of High-Voltage Instrument Transformer Condition Monitoring," IEEE Transactions on Dielectrics and Electrical Insulation, vol. 31, no. 6, pp. 3331–3341, 2024.

VIII S. Asefi, J. Kilter, N. Akroud, A. Hurtado, I. Gilbert, and I. Orue, "Application of Transfer Learning for Instrument Transformer Condition Monitoring," in 2024 International Conference on Diagnostics in Electrical Engineering (Diagnostika), 2024, pp. 1–4.

IX S. Asefi, G. Andreesen, J. Kilter, and M. Landsberg, "Capacitor Coupled Voltage Transformer Inaccuracy Effect on Circuit Breaker Operation," in 2023 23rd International Scientific Conference on Electric Power Engineering (EPE), 2023, pp. 1–5.

X S. Asefi, J. Kilter, and M. Landsberg, "Non-intrusive defects identification for the high voltage instrument transformers," in 2023 IEEE 17th International Conference on Compatibility, Power Electronics and Power Engineering (CPE-POWERENG), 2023, pp. 1–5.

XI S. Asefi, M. Leinakse, J. Kilter, and M. Landsberg, "Capacitor Coupled Voltage Transformer Defect Identification in the Presence of Tap Changer," in 2023 IEEE PES Innovative Smart Grid Technologies Europe (ISGT EUROPE), 2023, pp. 1–5.

Author's Contributions to the Publications

I In I, Sajjad Asefi participated in writing, contributed to editing the manuscript, and presented the work at the International Conference on Diagnostics in Electrical Engineering (Diagnostika), 2024.

II In II, Sajjad Asefi was the main author and had a major contribution in preparing the algorithm and analysing the experimental results, as well as writing the manuscript. Additionally, he presented the paper at the IEEE PES Innovative Smart Grid Technologies Conference Europe (ISGT-Europe), 2022.

III In III, Sajjad Asefi was the main author, proposed the idea, wrote the simulation program, carried out the simulations and the analysis of the results, prepared the figures, wrote the manuscript, and presented the results at the International Conference Electronics, 2023.

IV In IV, Sajjad Asefi was the main author, proposed the idea, wrote the simulation program, carried out the simulations and the analysis of the results, prepared the figures, wrote the manuscript, and presented the results at the IEEE PES Innovative Smart Grid Technologies Conference Europe (ISGT-Europe), 2024.

V In V, Sajjad Asefi was the main author, proposed the idea, wrote the simulation program, carried out the simulations and the analysis of the results, prepared the figures, wrote the manuscript, and presented the results at the International Conference on Power, Energy, and Electrical Engineering (CPEEE), 2025.

VI In VI, Sajjad Asefi was the main author, proposed the idea, developed the methodology, carried out the simulation, analysed the results, and had a major role in writing the manuscript.

List of Symbols and Abbreviations

Abbreviations

AIS	Air Insulated Switchgear
CBM	Condition Based Maintenance
CIGRE	International Council on Large Electric Systems
CoF	Consequences of Failure
DRM	Dynamic Resistance Measurement
DTW	Dynamic Time Warping
ENS	Energy Not Supplied
EU	European Union
FNR	False Negative Ratio
GIS	Gas Insulated Switchgear
HI	Health Index
HIL	Hardware in the Loop
HVCB	High-Voltage Circuit Breaker
IoT	Internet of Things
KNN	K-Nearest Neighbors
MaF	Major Failure
MiF	Minor Failure
ML	Machine Learning
MPSN	Maximum Permissible Switching Number
MTTF	Mean Time To Failure
PoF	Probability of Failure
RCM	Reliability Centered Maintenance
RMSE	Root Mean Square Error
RTDS	Real Time Digital Simulator
RUL	Remaining Useful Life
SHAP	Shapley Additive Explanations
SNR	Signal to Noise Ratio
SVM	Support Vector Machine
TBM	Time Based Maintenance
TC	Travel Curve
TPR	True Positive Ratio
TSO	Transmission System Operator

Symbols

a_1, a_2		
b_1, b_2	Tunable parameters of Gaussian model	-
c_1, c_2		
A, B, E	Coefficients of operating age	-
C_i	Normalised value of ith feature	-
d	Euclidean distance	-
D	Cost matrix of dynamic time warping	-
f_s	Sampling frequency	Hz
I_{P1}	First peak current	A
I_{P2}	Second peak current	A
n	Noise component of signal	-
N	Number of samples	-
P_{deg}	Polynomial degree of Savitzky-Golay filter	-
S	Standard deviation (Z-score normalisation)	-
t_{op}	Effective operating age	$years$
T	Period of coil current signal	-
T_{P1}	Excitation time	s
T_{P2}	Auxiliary contact operation time	s
T_L	Latching time	s
T_E	Total energising time	s
W_{len}	Window length of Savitzky-Golay filter	-
$\overline{X}$	Mean (Z-score normalisation)	-
α, β	Euclidean distance	-
λ	Failure rate (Hazard rate)	$f/year$
γ	Rate of decay	-
ν	Weibull shape parameter	-
η	Weibull scale parameter	-
σ	Standard deviation	-
μ	Mean	-
ζ	Normalised Z-score	-
ϕ	Generalized function influenced by service type	-
τ	Limit value for normalised feature	-

Introduction

Power System Asset Management

Infrastructure asset management is a comprehensive discipline focused on optimising the financial and operational aspects of complex infrastructure systems [1]. This encompasses both the direct routine management of physical assets and the overall strategic optimisation of their benefits for all stakeholders involved. While rapidly developing nations often prioritise the construction of new infrastructure, established economies face the persistent challenge of renewing existing systems as they reach the end of their operational lifespan [2]. The renewal decision encompasses both technical and economic dimensions. A flawed decision at the outset can lead to inefficiencies and operational challenges that persist for many decades, requiring extensive and costly corrective measures. This highlights the fact that asset management is not a reactive or purely operational function but a crucial strategic discipline. Therefore, the ability to make informed decisions, supported by accurate data on asset condition, ensures the enduring sustainability and cost-effectiveness of critical infrastructure [3].

The landscape of infrastructure asset management is continuously evolving, driven by several contemporary factors. There is an increased focus on sustainability and green energy, integrating environmental consciousness into all phases of asset management. The implementation of predictive maintenance technologies, often leveraging the internet of things and artificial intelligence, is increasingly used to support maintenance planning to enhance efficiency and reliability [4]. Digital twin technology is also emerging as a vital tool, creating virtual representations of physical assets for advanced monitoring and management, particularly beneficial for complex and interconnected utility systems [5]. Furthermore, utilities face ongoing challenges with regulatory requirements, necessitating advanced data analytics and smart grid technologies to automate compliance and operational processes. Enhanced cybersecurity measures are becoming critical as utilities become more interconnected and reliant on digital technologies, increasing the risk of cyber threats [6].

Among all available infrastructure, energy supply infrastructure, specifically modern power grids, are undergoing significant changes [7]. This transformation involves integrating a diverse array of both centralised and distributed power generation, a shift largely driven by global climate change initiatives and the rapid expansion of renewable energy sources, such as large-scale offshore wind farms [8]. This fundamental change significantly escalates the overall system complexity and introduces additional demands on existing infrastructure. The combination of ageing infrastructure, which necessitates substantial replacement investments, and new requirements arising from the energy transition (e.g., the need to connect new power plants and accommodate the growth of electric mobility), places pressure on financial resources, available personnel, and the intricate supply chains for critical components and services [9, 10, 11].

Within this area, substations emerge as fundamental nodes in the power grid [12]. They serve essential functions, including voltage transformation, power distribution, and fault protection. The equipment in substations, such as power transformers [13], circuit breakers [14], disconnectors [15], and voltage/current transformers [16], is inherently capital-intensive and indispensable for power grid operation, thereby demanding accurate asset management strategies [17]. The power system faces a dual challenge, i.e., simultaneously managing the natural ageing of its extensive infrastructure and adapting to a rapid technological and regulatory transformation. This situation means that asset managers cannot simply focus on replacing outdated equipment. Instead, they must strategically

adapt to new paradigms. This necessitates the deployment of advanced tools, including condition monitoring, to effectively prioritise investments that ensure both the continued reliability of the existing system and its adaptability to future demands [18].

The specific focus of this thesis is directed towards the condition monitoring of critical substation equipment. While modern substations include a variety of essential apparatuses, this research critically investigates high-voltage circuit breakers (HVCBs). HVCBs are one of the fundamental components within a substation. The HVCB's role in the power system can be categorised as follows [19, 20]:

- to safely carry the expected power flow corresponding to the maximum rated capacity under normal operating conditions;
- to perform the controlled switching of operating currents, which is essential for connecting/disconnecting various sections of the grid. This facilitates planned maintenance activities and enables dynamic system reconfigurations, which are increasingly necessary for optimising power flow and responding to the evolving demands of a modern grid;
- to rapidly and reliably interrupt short-circuit currents, thereby isolating faults and preventing widespread damage to equipment and cascading failures across the network. By swiftly mitigating electrical hazards and limiting equipment damage during fault conditions, they directly contribute to the protection of personnel and property.

The design and performance of such critical equipment is rigorously governed by strict national and international standards, which mandate specific conditions for operating voltage, current, and environmental factors. Their consistent and reliable operation is a foundation for achieving high levels of availability and overall operational excellence in transmission and distribution systems, playing a vital role in preventing widespread blackouts. Consequently, the need for condition monitoring methods to detect subtle degradation and potential failures before they become critical is amplified, ensuring that such critical equipment can continue to perform its roles effectively in a highly interconnected and dynamic power system [14].

Maintenance Strategies

The asset lifecycle management process is a continuous framework designed to maximise the value and utility of an organisation's asset while minimising costs and risks. It begins with planning, where needs and requirements are defined to ensure that the asset aligns with strategic goals. This leads to acquisition, the phase involving the procurement, purchase, or building of the asset. Once obtained, the asset enters deployment and usage, where it is integrated into the workflow and utilised. To ensure peak performance and longevity, the maintenance stage involves regular monitoring and repairs. Finally, when the asset no longer meets operational needs or becomes costly to maintain, it reaches the replacement or disposal stage, feeding back into the planning phase to start the cycle anew. Fig. 1 illustrates the iterative stages of asset lifecycle management, highlighting the existence of maintenance in this continuous process.

Maintenance and asset management are deeply interdependent, though they operate at different scales. Maintenance is primarily tactical, defined as all actions undertaken throughout an asset's lifecycle to preserve or restore its functional condition. Asset management, conversely, takes a broader strategic view to optimise the financial and operational

dimensions of the entire infrastructure system. While effective maintenance directly reduces equipment failure rates, asset management recognises that overall grid reliability is a much more complex construct. System-wide reliability cannot be achieved by maintenance alone. It is also heavily shaped by network topology, operational redundancy, spare parts availability, and personnel response times. Ultimately, asset management balances these equipment level and system level factors to achieve a degree of supply reliability that is both economically optimal and compliant with legal mandates [21].

Economic asset management necessitates a strict evaluation of the trade-off between operational expenditures and technical reliability. While deferring maintenance may offer immediate financial relief, it inherently compromises supply integrity and elevates the risk of costly interruptions. Consequently, the optimisation of infrastructure requires balancing the marginal costs of enhanced asset quality, driven by maintenance and capital investment, against the socio-economic benefits of reliability. This decision-making process is most impactful during the planning phase, where initial design choices dictate long-term lifecycle costs. However, the contemporary shift toward deregulated markets and incentive-based regulation introduces additional constraints, such as revenue caps and mandated quality benchmarks. To navigate these competing pressures of cost efficiency and regulatory compliance, asset managers must increasingly leverage data-driven methodologies and condition monitoring to ensure strategic, evidence-based maintenance allocation.

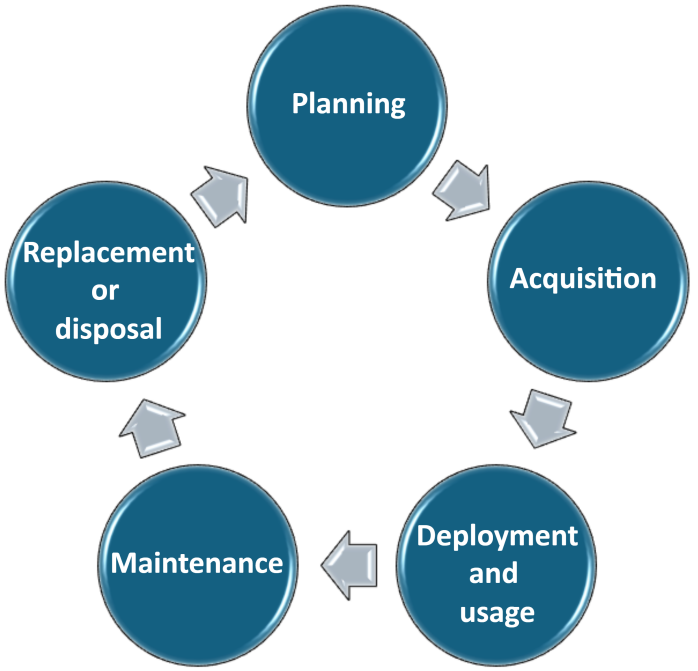


Figure 1: A conceptual framework of the five core stages of the asset lifecycle management

Condition Monitoring

The evolution of maintenance methodologies has seen a significant transition from reactive to more proactive approaches, with condition monitoring emerging as a foundation for modern, data-driven asset management. Historically, maintenance was predominantly reactive, also known as corrective maintenance, only addressing equipment failures after they occurred. This evolved into preventive maintenance, characterised by time-based interventions and scheduled activities. However, the inherent limitation of time-based maintenance (TBM) became apparent. Since a strict correlation between equipment age and its actual failure rate is often absent, considering fixed-interval interventions is inefficient and potentially leads to premature replacements or overlooking impending failures. This inefficiency propelled the adoption of condition-based maintenance (CBM). Empirical evidence indicates that the implementation of preventive maintenance strategies within electric utilities is projected to yield a 30% reduction in system maintenance costs, a 35% to 45% decrease in industrial accidents, and a reduction in operational downtime of 75% [22].

The core principle of CBM dictates that maintenance and replacement decisions are directly linked to the actual technical condition of an asset. This necessitates the continuous or periodic detection of an asset's condition through monitoring or diagnostic procedures. The increasing integration of monitoring systems within power networks is crucial for enhancing the degree of automation and offers a multitude of benefits. These benefits include optimised maintenance, where activities can be scheduled using measured condition information, reducing unnecessary interventions and preventing minor faults from escalating into major system failures [23]. From an economic point of view, while CBM requires initial investments in diagnostic systems and personnel training, its long-term economic advantage stems from minimising failure costs [24]. The delicate balance between reducing maintenance costs and the potential for increased failure rates is a critical consideration in its implementation.

Beyond preventing catastrophic equipment failures, condition monitoring significantly enhances daily grid operations. First, it improves defect management by allowing operators to provide indications of possible degradation and schedule repairs for minor defects before they trigger immediate blackouts. Second, it streamlines real-time network control, optimising tasks such as load management and remote switching. Finally, the continuous stream of diagnostic data provides a long-term strategic advantage, enabling utilities to analyse outage frequencies, minimise network losses, and continuously refine their overall maintenance strategies.

The operational benefits of condition monitoring extend beyond mere asset health, positioning it as a foundational technology for the broader smart grid concept and the transition towards active networks. Modern grids are inherently more complex and characterised by bidirectional power flows, making traditional management approaches insufficient. Consequently, condition monitoring evolves beyond its conventional application as a maintenance tool, emerging as a supporting element for the design and operational optimisation of next-generation power system architectures.

Hypotheses

The foundation of this research is built upon four primary hypotheses that address the available gaps, such as the lack of integrated real-time condition monitoring and the inability to accurately determine real-time failure probabilities in HVCB asset management and condition monitoring. Each hypothesis explores a different facet of the transition

from population-based statistics to individualised, condition aware diagnostics. By challenging the necessity of expensive instrumentation and traditional ageing models, these hypotheses seek to establish a new paradigm for cost-effective grid reliability:

1. **Service-integrated ageing:** An empirical ageing model can describe the observed age-dependent variation in HVCB mean time to failure (MTTF), while incorporating service-type information enables the assessment to account for differences between operational applications.

2. **Information content of coil current:** The developed emulator can reproduce coil current signatures while introducing controlled variations representative of selected operating conditions of the HVCB control and operating mechanism.

3. **Sensor applicability and denoising:** Appropriate signal preprocessing enables the extraction of selected diagnostic features from low-cost coil-current measurements under the investigated laboratory conditions.

4. **Temporal robustness:** A multi-stage diagnostic framework utilising dynamic time warping (DTW) and the machine learning (ML) classification model can distinguish temporal shifts from waveform changes associated with the investigated emulated conditions.

Research Questions

To test the validity of the aforementioned hypotheses, this thesis addresses a set of interconnected research questions. Each question is designed to bridge the gap between theoretical modelling and the practical application in substation environments. By answering these questions, the research aims to provide a clear roadmap for the deployment of intelligent monitoring systems in modern power systems:

1. **RQ1 (linked to Hypothesis 1):** To what extent can an empirical ageing model represent the available age-dependent HVCB failure statistics compared with conventional models, and how can service-type information be incorporated into this assessment?

2. **RQ2 (linked to Hypothesis 2):** Can the developed emulator generate repeatable coil current signatures and controlled feature variations suitable for evaluating condition monitoring algorithms?

3. **RQ3 (linked to Hypothesis 3):** Can proper signal filtering enable low-cost current sensors to achieve feature extraction fidelity suitable for fault identification?

4. **RQ4 (linked to Hypothesis 4):** How does temporal alignment affect coil-current signal comparison, and how effectively can ML classifiers distinguish the investigated emulated conditions?

Fig. 2 illustrates the conceptual framework of this thesis, systematically mapping the core domains of substation asset management to the specific research questions formulated and their corresponding publications. The research trajectory is categorised into four interconnected domains that progress sequentially from theoretical degradation modelling to actionable maintenance scheduling.

The first domain, focusing on asset degradation and failure modelling, investigats how different service applications and operational stresses impact the lifespan of critical

substation equipment. This domain directly addresses RQ1, which seeks to improve remaining useful life (RUL) estimations through proper modeling and normalised service-type integration, and its core findings are disseminated in publications I and III.

Building upon this theoretical basis, the second domain transitions into the practical realm of data acquisition and signal-processing. Within this stage, the viability of utilising low-cost sensors coupled with denoising techniques to extract coil current features is evaluated. This phase answers RQ2 and RQ3, demonstrating that the selected features could be extracted from the investigated low-cost measurements without relying on cost-prohibitive commercial analysers, as detailed extensively in publications II and VI.

The features extracted and processed in the second phase subsequently feed into the third domain, which is automated diagnostics and classification. This stage tackles RQ4 by implementing DTW to appropriately align temporally shifted signals. By mitigating these benign timing variations, the system effectively minimises false positive rates. This enables the subsequent deployment of supervised ML classifiers to accurately identify and categorise specific HVCB defect modes. The methodological advancements achieved in this area are the primary focus of publications V and VI.

Finally, the fourth domain synthesises these automated diagnostic outputs into health index (HI) evaluation and maintenance scheduling. By translating the technical condition and classification results into an actionable, weighted HI that explicitly accounts for measurement accuracy and temporal decay, the framework provides a direct mechanism for system operators to optimise maintenance interventions. This culmination of the research, effectively bridging the gap between raw automated diagnostics and strategic asset management decision-making, is comprehensively presented in Publication IV.

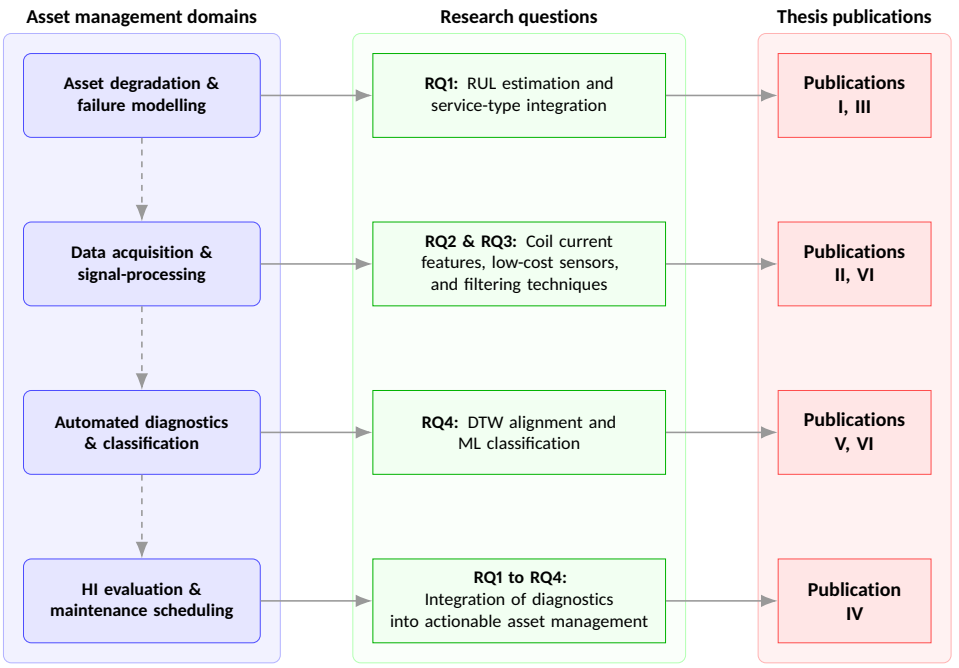


Figure 2: Mapping the core domains of asset management to the specific research questions and corresponding publications

Objectives of the Thesis

The primary objective of this work is to provide a comprehensive framework for HVCB condition assessment that is both economically and technically viable. This involves the integration of low-cost hardware, sophisticated signal-processing, and statistical modelling to create an actionable asset management tool. The following sub-objectives outline the systematic steps taken to fulfil these research requirements:

- To analyse HVCB failure modes based on international CIGRE survey data and identify the most critical diagnostic signals for capturing mechanical health.
- To design and construct a laboratory-scale coil current emulator capable of physically simulating common defects such as latch stiffness, auxiliary contact malfunctions, and voltage fluctuations.
- To evaluate various signal-processing techniques for noise reduction, specifically focusing on those that preserve the geometric integrity and transient peaks of the waveform.
- To develop a supervised ML pipeline for automated defect classification using labelled experimental datasets and feature importance analysis.
- To propose a mathematical HI model that fuses diverse measurement sources while accounting for sensor accuracy and the temporal decay of high-precision data.

Contribution of the Thesis

The research presented in this thesis offers both academic insights and practical tools for the power utility industry. By combining experimental validation with theoretical modelling, the work provides a holistic approach to HVCB maintenance. The contributions are categorised into theoretical advancements in reliability modelling and practical implementations in monitoring technology.

Theoretical contributions:

- A Gaussian function-based ageing model formulated for better representation of the traditional bathtub failure curve to map MTTF trajectories over operational life.
- A service type normalisation framework using Z-scores to adjust failure probabilities based on the specific duty of the HVCB.
- Investigation of DTW for reducing the influence of temporal misalignment on coil-current waveform comparison.
- Comparative evaluation of four supervised machine-learning classifiers using diagnostic features extracted from emulated coil-current signals.
- A weighted HI formulation that introduces a temporal decay factor to manage the uncertainty between periodic high-precision offline tests and continuous low-cost online monitoring.

Practical contributions:

- Development and laboratory evaluation of a coil-current measurement setup using low-cost components

- An automated feature extraction algorithm using cumulative maximums and segmentation to identify critical kinematic points, even in noisy signal environments.
- Demonstration of coil-current acquisition and feature extraction using healthy measurements from a real 110 kV HVCB in a laboratory hardware in the loop (HIL) setup.

Outline of the Thesis

The thesis begins with an introduction presenting the research background, hypotheses, research questions, objectives, and contributions. The main body comprises three chapters, organised as follows:

- **Chapter 1:** provides a comprehensive review of the evolution of maintenance strategies, common failure modes of substation equipment based on international CIGRE surveys, and the diagnostic signals typically employed for health assessment.
- **Chapter 2:** focuses on the specific architecture of SF_6 gas circuit breakers, the statistical analysis of failure rates relative to service application, and the development of a Gaussian function-based ageing model for exploratory population-level analysis.
- **Chapter 3:** details the core experimental work of the thesis, including the design of a low-cost measurement setup, the application of the Savitzky-Golay filter for noise reduction, and the implementation of ML algorithms for automated defect classification.

The thesis concludes by summarising the main findings in relation to the research questions, discussing the limitations of the proposed methods, and identifying directions for further research.

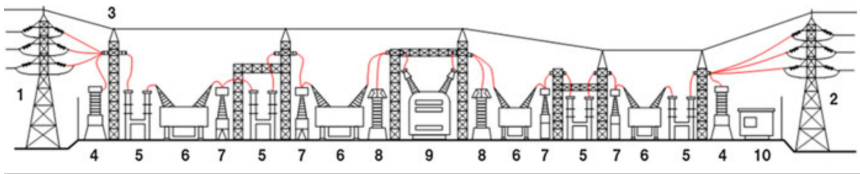
1 Principles of Condition Monitoring of Substation Equipment

This chapter presents a review of literature relevant to the thesis and contemporary research in the field of condition monitoring for substation equipment, establishing the theoretical framework for the research presented in this thesis.

The chapter begins by establishing the foundational role of substations within the power grid. Following this overview, it explores the evolution of maintenance strategies, tracing the progression from a corrective approach to the principles of preventive maintenance. The review then delves into the common failure modes and mechanisms inherent to high-voltage equipment, utilising surveys from CIGRE, which provide essential context on the degradation processes that condition monitoring aims to detect. Subsequently, the discussion focuses on the variety of diagnostic signals and measurement techniques employed to capture data indicative of an asset's health, examining how raw measurements are processed to yield meaningful information. Finally, an analysis of health index evaluation techniques is provided, surveying the methods used to fuse data from multiple sensors into a single, quantitative metric that facilitates decision-making and optimises asset lifecycle management. This chapter is based on publications I and II.

1.1 Substation

Substations are vital components of the global power system, connecting generation, transmission, and distribution to deliver energy to consumers. When substations were first installed, they were considered to be associated with a single generating station. Hence the name "substations" was first used. Substations function as crucial nodes within the power network. Their primary technical function is to transform voltages between different levels and provide essential switching capabilities to connect lines and sources. Critically, modern substations assure network stability and safety by providing sensing functions to detect line faults and rapidly isolating them, thereby protecting the grid and its components [18]. Fig. 3 demonstrates a schematic of a typical AC substation configuration together with the commonly available equipment in a substation [19].



1. Incoming overhead line;
2. Outgoing overhead line;
3. Ground wire;
4. Voltage transformer;
5. Disconnecting switch;
6. Circuit breaker;
7. Current transformer;
8. Surge arrester;
9. Power transformer;
10. Control cabinet with protective relay units.

Figure 3: A typical AC substation schematics [19]

The planning stage of a substation project involves selecting the type of equipment to be used. Based on the CIGRE definition, a substation designer can choose from three main types of switchgear to implement the most appropriate solution:

- Air-insulated switchgear (AIS): Switchgear where insulation to earth and between phase conductors is mainly provided by air at atmospheric pressure, and some live parts are not enclosed (IEC 6050-605-02-13).

- Gas-insulated switchgear (GIS): Metal-enclosed switchgear where insulation is obtained, at least partly, by an insulating gas other than air, such as SF_6 or a mixture of gases (IEC 62271-203).
- Mixed technology switchgear (MTS): Equipment developed from AIS or GIS, often combining technologies.

The selection of switchgear for a substation is primarily determined by a trade-off between cost and land usage. AIS is the cheapest option and is easy to modify, making it ideal for sites where inexpensive land is available and where the environment is relatively clean. However, it requires more space relative to GIS, and the equipment is exposed to the environment. Conversely, GIS is expensive but is extremely compact and fully enclosed, making it the best and sometimes only solution for substations in high-cost, limited-space urban areas or sites suffering from severe pollution. MTS offers a balance, providing a compact solution that is significantly cheaper than GIS, suitable for moderate land-cost areas, or for extending existing AIS substations where space is highly constrained. Fig. 4 and Fig. 5 demonstrated an AIS and a GIS substation, respectively.



Figure 4: Air insulated substation [19]



Figure 5: Gas insulated substation [19]

The equipment in substations is inherently capital-intensive and indispensable for power grid operation, thereby demanding accurate asset management and maintenance strategies. This thesis excludes a detailed study of well-documented equipment like power transformers [25, 26, 27], and focuses entirely on developing diagnostic and asset management frameworks specifically for HVCBs.

1.2 Maintenance Strategies

Effective management of high-voltage assets plays an important role in the reliability of the power system. A key component of this management is the implementation of a coherent maintenance strategy, which dictates the timing and nature of interventions performed on equipment throughout its operational life. The choice of strategy directly influences operational expenditures, asset availability, and overall grid reliability. These strategies have evolved from purely reactive measures to highly sophisticated, data-driven proactive frameworks [28]. The primary classification of maintenance divides the approaches into two fundamental categories: corrective and preventive maintenance, as illustrated in Fig. 6.

Corrective maintenance, often referred to as “run to failure”, is the most straightforward strategy. In this approach, maintenance or repair actions are only performed after a component fails or its performance degrades to an unacceptable level [30]. While this strategy minimises advanced planning, its reactive nature carries significant disadvantages. Unplanned outages resulting from failures can lead to substantial economic losses, collateral damage to adjacent equipment, and potential safety hazards. Consequently, for

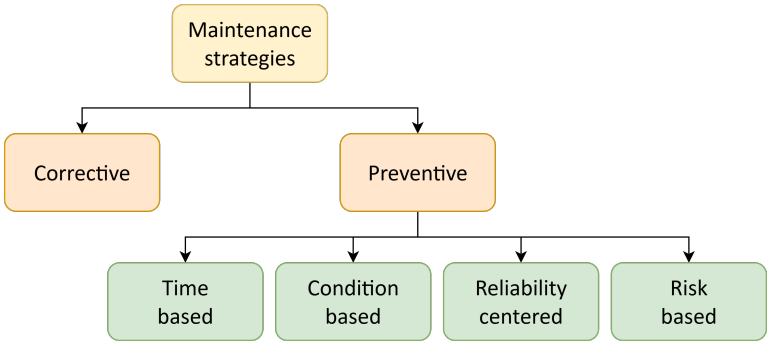


Figure 6: Classification of maintenance strategies [29]

critical high-voltage apparatus where reliability is a priority, a purely corrective approach is generally considered unjustified. To mitigate the risks associated with unexpected failures, preventive maintenance was established. The core principle of preventive maintenance is to perform maintenance actions proactively, before a failure occurs, with the goal of extending asset life and reducing the likelihood of failures during operation [31]. This broad category encompasses a spectrum of strategies that have become progressively more sophisticated over time.

The most traditional form of preventive maintenance is TBM, also known as scheduled maintenance. Under a TBM regime, interventions are carried out at fixed-intervals based on calendar time or operational counters, e.g., hours of operation or the number of switching cycles. These intervals are typically recommended by the original equipment manufacturer or derived from historical failure statistics. While TBM is simple to schedule and can prevent many age-related failures, it suffers from a critical inefficiency, i.e., it does not account for the actual condition of the individual asset. This can lead to either unnecessary maintenance on healthy equipment, which introduces economic inefficiency and a risk of human error, or a failure occurring before the scheduled intervention if the asset degrades faster than anticipated.

A more advanced and efficient approach is CBM, which represents a paradigm shift from a time-based scheme. CBM relies on the direct monitoring of an asset's health through various diagnostic signals and measurements [32]. Maintenance actions are only initiated when collected data indicate a deviation from normal operating conditions or the emergence of an incipient fault. By aligning maintenance with actual need, CBM optimises resource allocation and minimises unnecessary downtime, which leads to an improvement in overall reliability.

A more systematic approach to prioritising preventive actions is found in reliability-centred maintenance (RCM), which prioritises activities based on the criticality or importance of an asset to the overall system. Within this framework, the specific technical condition is considered indirectly, often taken into account statistically through metrics like the average failure rate when calculating system-level indicators such as energy not supplied.

The strategy is further refined by risk-based maintenance (RBM), which builds directly upon the principles of RCM by introducing a more formal and quantitative assessment of risk. This strategy explicitly quantifies risk, commonly defined as the product of an asset's probability of failure (PoF) and the resulting consequences of that failure (CoF), i.e., Risk = PoF $\times$ CoF. The consequences can encompass a wide range of factors, including economic losses, safety hazards, and environmental impact [29]. Furthermore, an RBM framework

often incorporates an economic dimension, weighing the cost of preventive maintenance against the projected costs of a potential outage. A critical aspect of implementing this strategy is the careful definition and evaluation of acceptable risk thresholds, which guide the decision-making process.

It is to be noted that all the above-mentioned strategies are applicable to all critical substation assets, including both switching apparatus, e.g., circuit breakers, and the measurement/protection devices, e.g., instrument transformers, that enable their operation [18]. While the CIGRE survey on HVCBs does not provide failure rates for different maintenance schemes, the report on instrument transformers, as shown in Table 1, offers valuable insight [33]. In general, CBM appeared to produce lower failure frequencies. Since CBM strategy forms the foundation of modern condition monitoring systems, it is a central theme of this thesis.

Table 1: Comparison of instrument transformer failure frequency based on the applied maintenance scheme (data from [33])

Maintenance scheme	**TBM**	**CBM**
Failure frequency (per 100 instrument transformer-years)	0.0625	0.0351

1.3 Failure Modes and Mechanisms

An essential prerequisite for developing an effective condition monitoring system for any equipment is a thorough understanding of the potential failure modes and the underlying physical mechanisms of degradation of that specific equipment. Failures in high-voltage equipment are rarely instantaneous, i.e., they are typically the culmination of a gradual deterioration process. An effective monitoring strategy must be designed to detect the incipient signs of these degradation processes long before they escalate into a catastrophic failure.

While specific vulnerabilities depend on asset design and technology, international reliability surveys, such as those conducted by CIGRE [33, 34], provide a statistical basis for classifying the principal failure modes of critical substation apparatus into distinct categories. Generally, the failures can be classified into two categories: major failures (MaFs) and minor failures (MiFs). Failure of the equipment (or part of the equipment) that causes the cessation of one or more of its fundamental functions is called MaF. The MiFs represent a degradation of the performance and smaller changes in the operating characteristics of the equipment. Analysis of this data reveals that failures can be broadly grouped by their physical nature. Consequently, this section focuses exclusively on the common failure modes of HVCBs to demonstrate how their physical characteristics dictate their degradation pathways.

1.3.1 Mechanical Failures

Mechanical failures are associated with components that perform or are subjected to physical motion and stress. For the switching apparatus, this is the most critical failure category. Based on the CIGRE survey report for HVCBs, the operating mechanism is the largest contributor to MaFs, being the responsible component in approximately 50% of cases. As shown in Fig. 7, the dominant failure modes of MaF include “does not close on command” (28.2%), “locking in open or closed position” (25.1%), “does not open on command” (16.4%), etc. These faults, originating from the complex kinematic chain of

the operating mechanism, can prevent the apparatus from safely performing its primary protection functions.

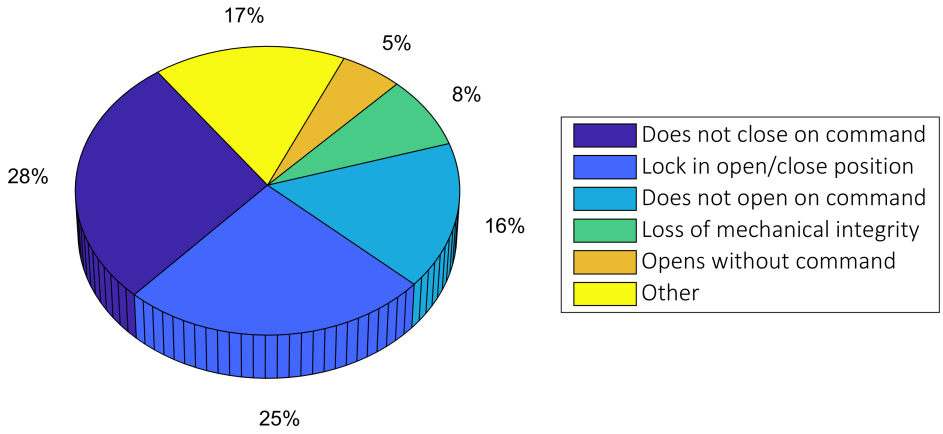


Figure 7: Failure modes of major failures for HVCB (data from [34])

For assets that are generally static, such as instrument transformers, mechanical failures are less frequent but not negligible. The CIGRE survey on instrument transformers identifies loss of mechanical integrity (mechanical damages of different parts like insulators, etc.) as a notable major failure mode, approximately 8% of cases [33].

1.3.2 Electrical and Dielectric Failures

Electrical and dielectric failures relate to the degradation of insulation systems and the disruption of current-carrying paths, compromising the fundamental dielectric and conductive functions of high-voltage equipment. While less dominant than mechanical issues, electrical integrity is also crucial for the switching apparatus. Based on the CIGRE survey, components at service voltage, i.e., arc-extinguishing medium, are responsible for 20% of major failures. Although less frequent than operational failures, electrical breakdowns across the poles or to earth represent a significant failure risk that can lead to catastrophic outcomes.

1.3.3 Auxiliary and Control System Failures

Failures in auxiliary systems, which provide the necessary power, control, and monitoring for the main component to function, are another source of unreliability. This is particularly true for switching apparatus, where the CIGRE data show that electrical control and auxiliary circuits are responsible for 30% of all major failures.

1.3.4 Summary

It is crucial to recognise that these failure modes are often highly interdependent. For instance, a mechanical degradation in the operating mechanism, such as increased friction or a stiff latch, can significantly reduce the contact separation speed. This prolongs the electrical arcing time, causing severe thermal erosion of the arcing contacts. Conversely, a purely electrical fault in the auxiliary control circuit, such as a degrading trip coil or a drop in supply voltage, prevents the delivery of the essential starting energy to the actuation mechanism, potentially leading to a catastrophic “does not open on command”

failure. To illustrate these critical vulnerabilities, the distribution of HVCB major failures per responsible component is presented in Fig. 8.

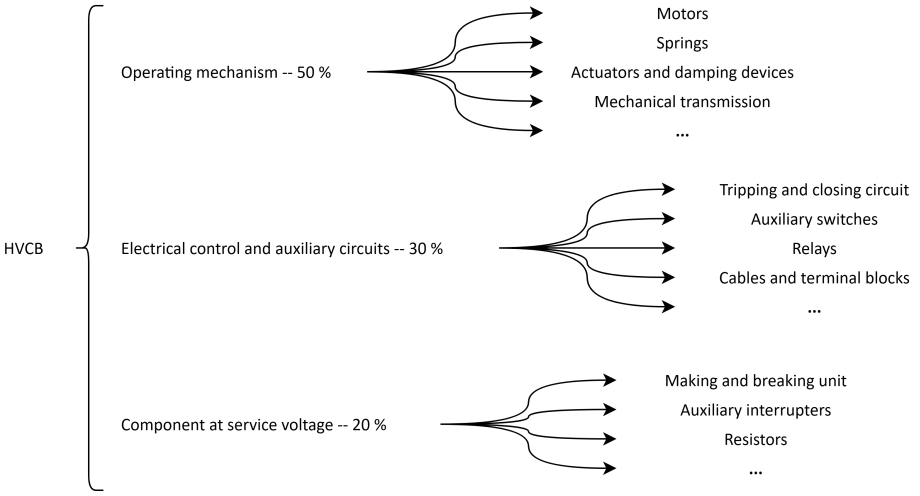


Figure 8: Distribution of HVCB failure per component responsible (data from [20])

1.4 Diagnostic Signals

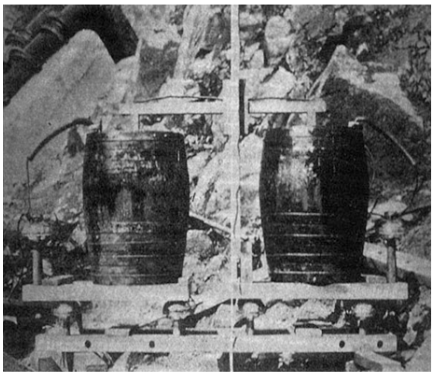
The selection of a diagnostic signal for condition monitoring is linked to the specific equipment and the failure mechanisms under investigation. An effective signal must be sensitive to the subtle physical changes that precede a failure, providing a measurable precursor to the fault. Because different components degrade in different ways, a variety of signals must be employed across substation assets to capture a holistic view of equipment health. This section reviews the prominent diagnostic signals used for monitoring HVCBs, which are foundational to the condition-monitoring strategies discussed previously.

HVCB is an electrical switch designed to protect power systems by interrupting fault currents and controlling power flow in transmission and distribution networks. Fig. 9 demonstrates various types of HVCBs. In 1907, the first oil circuit breaker was patented by J. N. Kelman in the United States [19]. Apart from oil, air-blast and vacuum interrupters have been utilised in the industry. However, currently, the majority of the HVCBs use SF_6 gas as the arc-extinguishing medium.

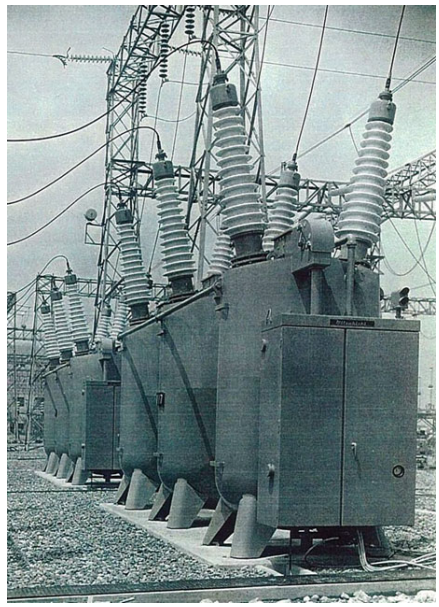
Various diagnostic signals could be employed to assess the condition of the circuit breakers under offline/online conditions. In this direction, the most important diagnostic signals have been presented to point out the research stream and the challenges.

1.4.1 Switching Number

In Fig. 10, an example of the maximum permissible switching number (MPSN) graph for an HVCB is provided, which is commonly given by the manufacturer. Based on that graph, it is possible to determine the maximum number of allowed switching operations. That number also depends on the interrupted current value at the moment of operation. If the current value is below the nominal current I_{lim} value, then this counts as one operation. In the case of higher current values, the remaining number of operations is scaled according to the current value. It is possible to calculate the breaking current influence to the number of operations using (1) [35]:



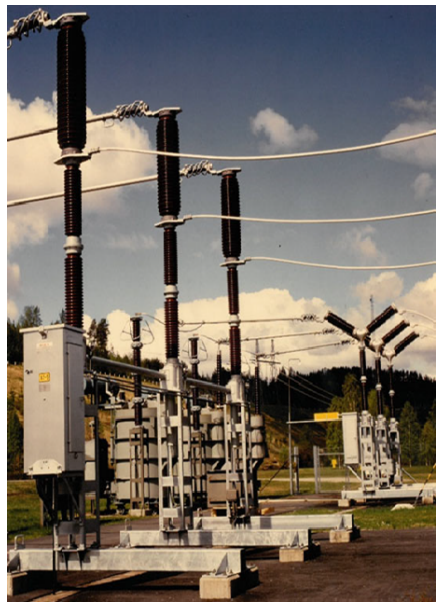
(a) Kelman's oil circuit breaker built in 1901 (40 kV, 300 A)



(b) 168 kV bulk-oil, dead tank oil circuit breaker, 1959



(c) 550 kV live-tank SF_6 gas circuit breaker



(d) 245 kV 50 kA double/single-break SF_6 gas circuit breakers

Figure 9: Different types of circuit breakers [19]

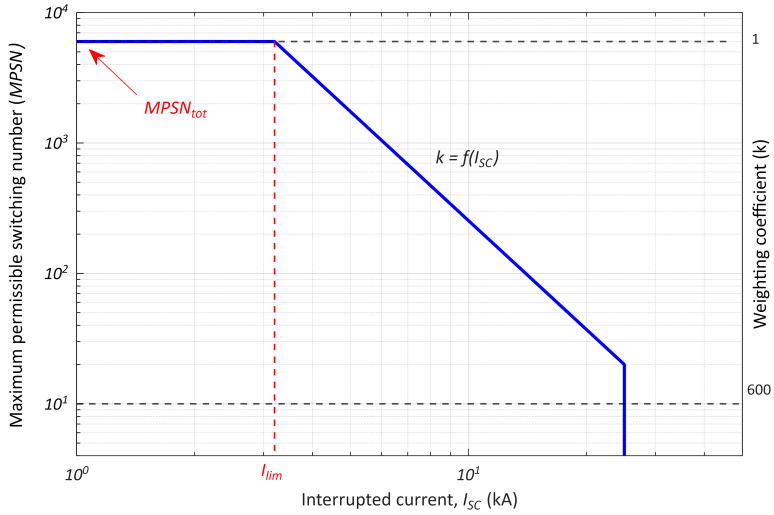


Figure 10: Sample of maximum permissible switching number graph for a 400 kV HVCB (data from [35])

$$MPSN_x = \frac{MPSN_{tot} - \sum_{i=1}^{m}(SN_i \times k_i)}{k_x} \tag{1}$$

where k_i and k_x are the weighting coefficient for interrupted current I_{SC} and $I_{SC,x}$, respectively; SN_i is the number of performed switching at current I_{SC}; $MPSN_x$ is the MPSN at current $I_{SC,x}$; $MPSN_{tot}$ is the total number of MPSN for this specific HVCB, which is equal to 6000; and m is total number of carried out interruptions. For each type of HVCB, the manufacturer shall provide a graph similar to Fig. 10.

1.4.2 SF_6 Gas Pressure

HVCBs mostly use pure SF_6 gas (also a mixture of gases or vacuum) to extinguish the electric arc. Pure SF_6 gas is an inert, thermally stable, non-flammable, colorless, and non-toxic gas. Under the influence of an electric arc, when the temperature rises above $2000\ K$, the SF_6 gas begins to decompose, resulting in the formation of toxic substances (SF_2 and SF_4). After the electric arc is extinguished, the resulting compounds are recombined again into non-toxic SF_6 gas.

According to the manufacturer's instructions, SF_6 gas leakage of up to 0.5% per year is permitted. Experience has shown that the annual gas leakage is about 0.1%. To prevent operation with an HVCB whose gas pressure has dropped to a critical limit, the switch is blocked and the resulting signal is sent to the control centre, which in turn responds to the situation. SF_6 gas pressure sensors are employed to detect leaks, triggering alarms or operational lockouts to prevent the HVCB from operating under compromised dielectric conditions.

1.4.3 Drive Motor Current

The operating mechanism of an HVCB includes the energy storage medium, actuating circuit and interlocking systems [36]. A spring drive mechanism is driven by the mechanical energy stored in springs. Typically, the closing spring is mechanically charged by a motor.

The characteristic values of the motor current are:

- Starting current of the motor: In general, the starting current is equal to the maximum current measured during a test;
- Operating current: Mean value of the motor current calculated over the defined evaluation period;
- Motor run time: Duration of motor operation during a test.

Failure in the drive mechanism can be identified by means of the spring charging motor current and voltage [36]. Fig. 11 shows a sample of recorded data (based on the experiments at Taltech's high-voltage laboratory) of a healthy spring charging motor current and voltage characteristic during the charging of the HVCB's closing spring. The current characteristic provides information on the electrical properties of the motor and the mechanical load.

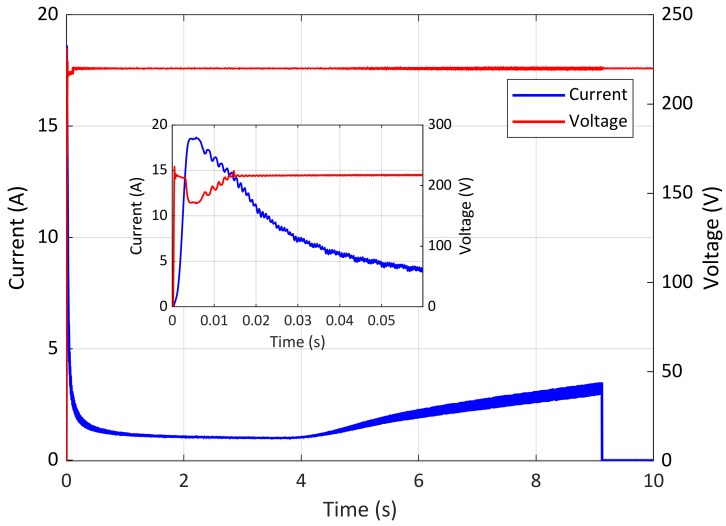
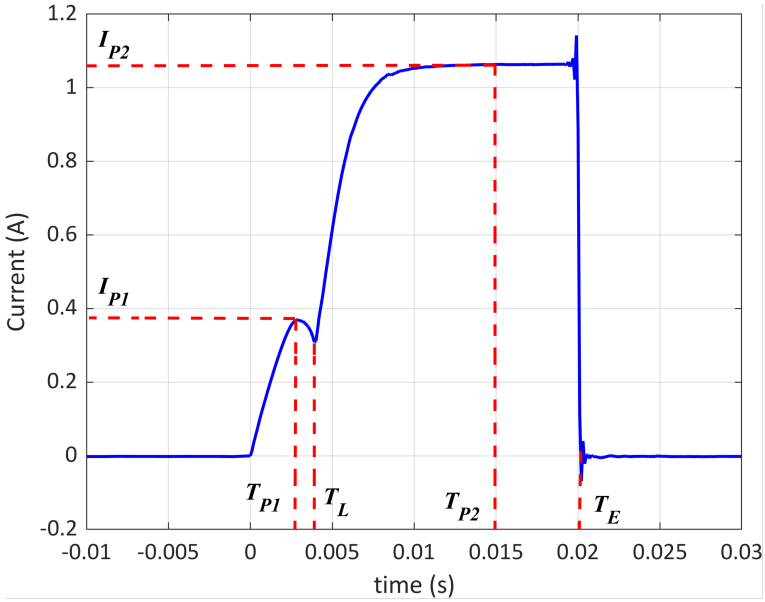


Figure 11: Circuit breaker's spring charging motor current and voltage characteristics

1.4.4 Trip/Close Coil Current

The control unit transforms the electrical command signal into the mechanical operation of the breaker switching mechanism. This section presents the correlation between the performance of HVCB operation and the characteristics of coil current waveform, as a straightforward diagnostic signal and compatible with real-time assessment. In order to assess the condition of the HVCB through its coil current waveform, six features reflecting the HVCB abnormalities are defined as illustrated on a typical measured waveform in Fig. 12 (based on the experiments at Taltech's high-voltage laboratory) [37].

Realising the fact that the characteristic parameters of coil current have a statistical nature, a large number of measurements are to be conducted to determine the statistical characteristics of these parameters. Based on the literature, malfunctioning of the HVCBs can be associated with failures in trip (also known as open) or close coil supply voltage, failures in trip/close coil, failures in latch operation, and failures in auxiliary contact performance. Taking the standard values for a corresponding HVCB's coil current features into account, the following principle can be used to detect the failure source:



I_{P1}	first peak current
T_{P1}	excitation time
I_{P2}	second peak current
T_{P2}	auxiliary contact operation time
T_L	start time of HVCBs operation (latching time)
T_E	total energization time

Figure 12: Coil current features on a healthy HVCB recorded pattern [20]

- **Data recording and calculation of features**
  Once the HVCB operation is completed, the coil current waveform is captured, and afterwards, the defined features are calculated to reveal the inconsistencies in the next step.

- **Determining the disparities of features and sorting**
  On the basis of the comparison between the calculated features in the previous step and the normal ones, the disparity of features ($\Delta\%$) is achieved. Subsequently, these disparities are sorted from the largest (most affected) to the smallest (least affected) absolute value.

- **Identification of failures and their causes**
  The mode of failure and its causes can be identified in this step.

1.4.5 Contact Travel Curve

Travel curve (TC) refers to the motion of the contacts against time, which is captured via a transducer that is connected to the main shaft. It indicates a close-open stroke time characteristic. The operation speed is calculated based on two predefined points on the curve. In addition, some timing characteristics could be obtained based on this curve.

Accordingly, TC is applied for the evaluation of the operation time of the HVCBs, as well as malfunctions in the operating mechanism [38]. A sample of TC for both closing and tripping the operation of a healthy HVCB is demonstrated in Fig. 13 (based on the experiments at Taltech's high-voltage laboratory).

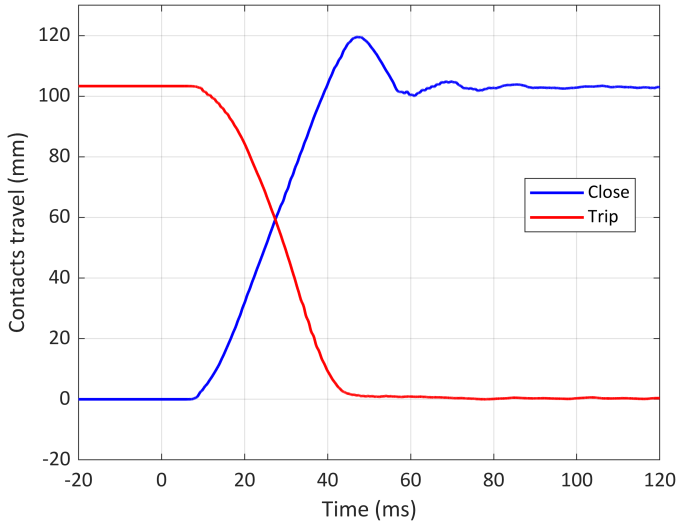


Figure 13: Circuit breaker contacts travel curve for trip/close operation [14]

The main advantage of TC is its ability to provide valuable information from the most common origin of failures in HVCBs, i.e., the operating mechanism. The disadvantage of using TC is the need for the installation of a transducer sensor, leading to the inapplicability of this method in online assessment for some HVCB designs.

1.4.6 Contact Resistance Measurement

Arc and main contacts are deteriorated during switching under normal and short-circuit currents in the life cycle of the HVCBs. In order to evaluate the condition of the contacts without dismantling of HVCBs, resistance measurements have been suggested. In this regards, once a DC current is injected, the voltage across the poles of the HVCB during the opening operation is recorded to find out the profile of the resistance versus motion.

In order to assess the condition of the contacts, static and dynamic resistance tests have been conducted on HVCBs. Once a DC is injected through a closed HVCB, the voltage drop across the HVCB is measured in a static resistance measurement test. In the dynamic resistance measurement (DRM) test, a DC is applied to the contacts, and the voltage drop can be measured against time or the position of the contact during the operation of the HVCB. Subsequently, the measured instantaneous voltage drop could be divided by the injected current to determine the resistance of the contact against time or the contact position.

The main advantage of using DRM is that it could provide helpful information associated with the condition of the arc and main contacts without any dismantling of the arc-extinguishing medium. The disadvantages are only applicability in offline mode of the HVCBs, the need for TC for the assessment of the arc contact length, and the sensitivity of the results to the injected current.

1.4.7 Other methodologies

Arc energy:

The estimation of the remaining lifetime of the contacts based on mass loss calculated through energy during the interruption/making of the currents has recently been addressed in the diagnosis of the HVCBs [39]. The main challenges or disadvantages of using arc energy for the assessment of contact wear is the low accuracy of the indices based on the transferred charge and the integral of current squared, owing to omitting the voltage.

Vibration:

The vibration signal generated during the opening and closing operation of the HVCBs has gradually become mainstream research owing to convenient data acquisition, as well as its suitability for non-intrusive and real-time evaluation, which could cover most origins of the failures occurring in the operating mechanism of the HVCBs [40]. The main disadvantage of this method is the dependency of its accuracy on the number of sensors and the post-processing techniques.

1.4.8 Summary

The primary focus of this thesis will be on the analysis of the coil current signal of the HVCB. This signal was chosen for several practical and technical advantages. It is a non-intrusive measurement that can be performed easily in the control cabinet without requiring an outage of the high-voltage primary equipment. The required sensors are simple and cost-effective, making the method highly scalable. Most importantly, the coil current signature is an informative signal that encapsulates the performance of both the electrical control circuits and the mechanical operating mechanism, making it an appropriate choice for condition assessment.

1.5 Health Index Evaluation Techniques

The central goal of condition monitoring is to translate diverse streams of measurement data into a clear and actionable assessment of an asset's overall health. As noted in the literature, maintenance approaches that only rely on asset age should be used with caution, as advanced age does not always equate to poor technical condition if the asset has been well-maintained [41]. A direct approach would be the dynamic adjustment of maintenance schedules, moving from fixed-interval overhauls to condition-based interventions triggered when an asset's health status crosses a predetermined threshold [28]. To achieve this, an HI is often formulated. The HI is a commonly used composite indicator implemented in power systems to represent the technical condition of a complex asset as a single, intuitive value [32]. It serves to quantify an asset's condition on a scale from good to bad and can be used to estimate its remaining fault-free service life. While there are multiple ways to represent the HI, the most common approaches use a linear numerical scale, such as 0–100 or 0–5, or qualitative colour codes based on a traffic light system [41]. A variety of methodologies have been developed to calculate the HI for high-voltage assets by aggregating diagnostic data with operational and historical information.

One of the most common approaches for HI calculation involves scoring and weighting methods. These models combine multiple parameters into a single score using weighted factors that reflect the relative importance of each input. For HVCBs, an HI model can be constructed as a weighted sum of features extracted from coil current measurements, along with operational and maintenance records, where the weights are determined through expert judgment [42]. A similar approach employs the analytical hierarchy process, which uses expert interviews and surveys to systematically determine the weights for combining condition measurements, such as contact resistance, with operational factors like the

HVCB's age [43].

More advanced, data-driven techniques have also been proposed. Neural network-based models, for instance, can be trained to produce an HI by using various measurements, such as coil current features, SF_6 gas pressure, and operation time, as feature indicators. In such models, the inputs are typically normalised to a common scale before being processed by the network, with the final HI output being categorised based on expert-defined thresholds [44]. Other mathematical methods have also been explored, such as formulating the HI using the geometric concept of a hyper-ellipse, where various parameters define the shape and boundaries of the state of health [45].

Once calculated, the HI becomes a critical input for asset management decisions, primarily for estimating failure risk and optimising maintenance. Several studies focus on translating the HI into a quantitative, condition-dependent failure rate. This can be achieved by incorporating the HI as a dynamic covariate in statistical lifetime models, such as the Cox proportional hazard model, to reflect the asset's real-time condition [46, 47]. Other approaches link the HI directly to the PoF using statistical distributions like the Weibull curve.

It is to be noted that the mentioned methodologies are broadly applicable to other critical assets, such as instrument transformers, by using their specific diagnostic inputs, e.g., dissolved gas analysis, partial discharge results, etc. [30].

1.6 Remarks

This chapter has established the foundational principles of condition monitoring for critical high-voltage substation assets. It began by reviewing the evolution of maintenance philosophies. Moreover, through an analysis of international survey data, the dominant failure mechanisms for key equipment were identified. For circuit breakers, in particular, the susceptibility to mechanical failures was underscored. Consequently, a range of diagnostic signals targeting these failure modes was presented, culminating in the selection of the coil current signature as the primary focus for this research due to its non-intrusive nature and rich diagnostic information. Finally, the concept of the HI was introduced as the primary tool for translating raw diagnostic data into actionable asset management intelligence.

Building upon the provided literature review, the subsequent chapters of this thesis will present a detailed methodology for processing and analysing the HVCB coil current signal. The aim is to develop a model capable of detecting the incipient defects and to formulate a quantitative HI for improved maintenance and reliability.

2 Condition Monitoring of High-Voltage Circuit Breaker

Following the establishment of condition monitoring principles in the previous chapter, it is necessary to delve into the specific operational characteristics and failure behaviours of the HVCB. This chapter begins by dissecting the HVCB into its critical subsystems, specifically focusing on the physics of SF_6 gas arc extinction, the kinematics of spring operating mechanisms, and the logic of control circuits. Subsequently, a statistical analysis of failure rates based on the CIGRE survey is presented, with a specific focus on the varying service applications for which the HVCBs are utilised. Finally, a Gaussian function-based methodology for estimating the RUL is proposed, and it is incorporated in the implementation of a computational tool. This chapter is based on publications II and III.

2.1 Architecture and Operational Principles of SF_6 Gas Circuit Breakers

To accurately model degradation, initially, the processes governing current interruption must be understood. The modern HVCB is a complex integration of mechanical and electrical subsystems, defined primarily by the technology used to extinguish the electric arc. Fig. 14 and Fig. 15 demonstrate a generic component-oriented model of HVCB and an HVCB under operation installed in the substation, respectively.

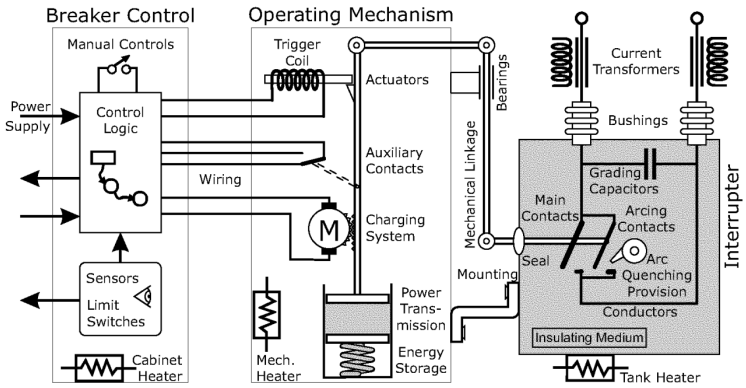


Figure 14: Generic model of HVCB components [48]

2.1.1 The SF_6 Gas Arc Extinguishing Medium

Sulphur hexafluoride (SF_6) gas has become the dominant medium for high-voltage interruption due to its exceptional dielectric and thermodynamic properties. SF_6 gas is electronegative, possessing a high tendency for capturing free electrons to form heavy negative ions. This characteristic is critical during the arcing phase, as it facilitates the rapid removal of conducting electrons from the arc plasma, thereby increasing the rate of conductance decay as the current approaches zero [18].

Furthermore, the decomposition temperature of SF_6 gas is relatively high (approx. 2000 K), and its thermal conductivity exhibits a marked peak at this dissociation temperature. This property allows for efficient radial heat transport from the arc core to the surrounding cool gas, effectively cooling the arc channel. Crucially, the decomposition of SF_6 gas is reversible, i.e., after the arc is extinguished, the constituent by-products (SF_4, SF_2, etc.) recombine to form stable SF_6 gas, ensuring the longevity of the insulating medium [19].

By the early 1990s, the industry recognised that the specific physical characteristics of

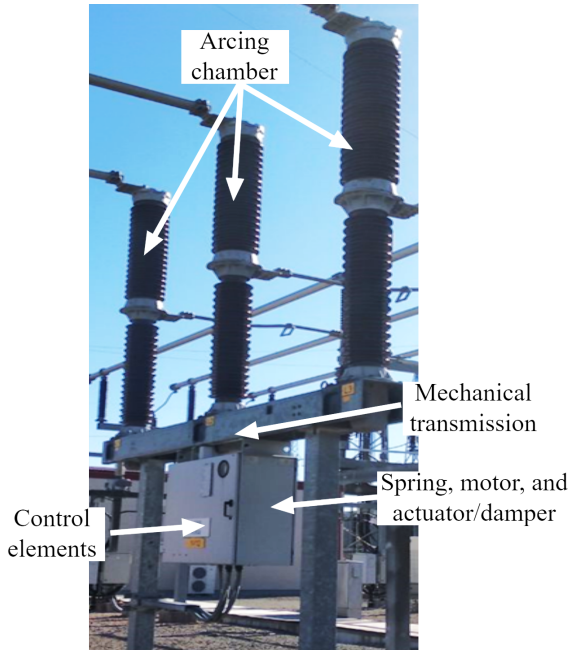


Figure 15: Component specification of a 110 kV HVCB

SF_6 gas categorise it as a highly powerful greenhouse gas, meaning that any atmospheric leakage directly facilitates global warming. To replace the insulation and arc quenching capabilities of SF_6 without its extreme global warming potential, the industry is adopting several alternative gas technologies. These include natural gases such as dry air (a nitrogen and oxygen mix), nitrogen, and carbon dioxide (CO_2), as well as advanced synthetic mixtures. One of the most prominent synthetic alternatives involves fluoronitrile-based gas blends (often referred to as C_4-FN), which can be mixed with CO_2 or oxygen to achieve dielectric properties similar to SF_6 while significantly reducing the environmental impact. These alternatives allow for the continued use of compact GIS designs while aligning with global sustainability goals [49].

Vacuum circuit breakers are a well-established and highly effective alternative to SF_6 technology, particularly within the medium voltage range. They operate by extinguishing the electrical arc in a high-vacuum environment, which offers excellent dielectric recovery and requires minimal maintenance compared to gas-insulated systems. However, their application in high-voltage transmission (above 36 kV) has historically been limited by the dielectric strength of a single vacuum gap. Nevertheless, recent advancements in multi-break designs and optimised contact geometries have enabled them to reach higher voltage levels, making them a viable, environmentally friendly replacement for SF_6 in many modern grid applications [49].

It is to be noted that the European Union (EU) has formalised the phase-out of SF_6 through regulation (EU) 2024/573, which entered into force in March 2024. This directive sets a rigorous timeline for banning the commissioning of new electrical switchgear that relies on fluorinated gases with high global warming potential. The phase-out begins on 1 January 2026, for new medium-voltage equipment up to 24 kV, followed by high-voltage equipment between 52 kV and 145 kV in 2028, and finally encompassing all new installations above 145 kV by 2032. Additionally, from 2035, the use of newly synthesised

SF_6 for maintaining existing equipment will be prohibited, mandating the use of only reclaimed or recycled gas to further mitigate atmospheric leakage [50].

Interrupter Technologies

In interrupters where SF_6 gas serves as the medium, arc extinction is achieved by generating a gas flow across the arc channel, thereby facilitating cooling through thermal exchange. The evolution of the interrupting chamber has moved from double-pressure systems to the more reliable single-pressure designs. Fig. 16 depicts several common configurations used to achieve this quenching effect:

- Plain Break: This configuration does not employ a forced gas flow mechanism. Instead, it relies on natural convection induced by gravity and the thermal or density gradients created by the arc itself to alter the temperature distribution and eventually extinguish the arc (Fig. 16-a).
- Self-blast: In this design, the thermal energy of the arc is harnessed to generate pressure within a fixed volume chamber. This localised pressure rise drives a gas flow back across the arc, effectively cooling and interrupting it (Fig. 16-b).
- Double-pressure blast: This structure employs an external mechanism, such as a compressor, to generate a reserve of high-pressure SF_6 gas. To extinguish the arc, this pre-compressed gas is blasted directly across the arcing zone (Fig. 16-c).
- Puffer blast: This arrangement generates the necessary gas flow through the mechanical action of contact separation itself. As the contacts open, a cylinder compresses the gas, forcing it across the arc (Fig. 16-d).

This single-pressure puffer concept forms the basis for most modern HVCB designs. Crucial to the interruption process are the thermodynamic energy exchange within the arcing zone and the pressurisation of the puffer chamber. It is noted that the physical presence of the arc influences the mechanical motion of the arcing contact, particularly in puffer designs, due to the interaction between the arc current and the pressure building within the cylinder.

The interrupters consist of two parts – a fixed part and a moving part. When the interrupter is closed, these two parts are connected together. The part that moves traps the SF_6 gas, which, upon the separation of the two parts, is propelled through the created gap, forcing the arc to be extinguished. The interrupters are physically linked to an operating mechanism. Fig. 17 specifies various components of an interrupter.

2.1.2 Operating Mechanisms and Control Circuits

While the interrupter performs the electrical isolation, the operating mechanism and control circuits provide the necessary kinetic energy and intelligence. As mentioned in the previous chapter, reliability surveys indicate that these subsystems are the most frequent contributors to major failures.

Spring Charging Mechanisms

Various operating mechanisms have been developed to provide the necessary kinetic energy for contact movement, including pneumatic, hydraulic, and spring systems, as well as hybrid configurations such as hydraulic-spring or pneumatic-spring designs [19]. While pneumatic and hydraulic mechanisms were historically utilised for their high energy output suitable for older interruption technologies, the spring mechanism has become

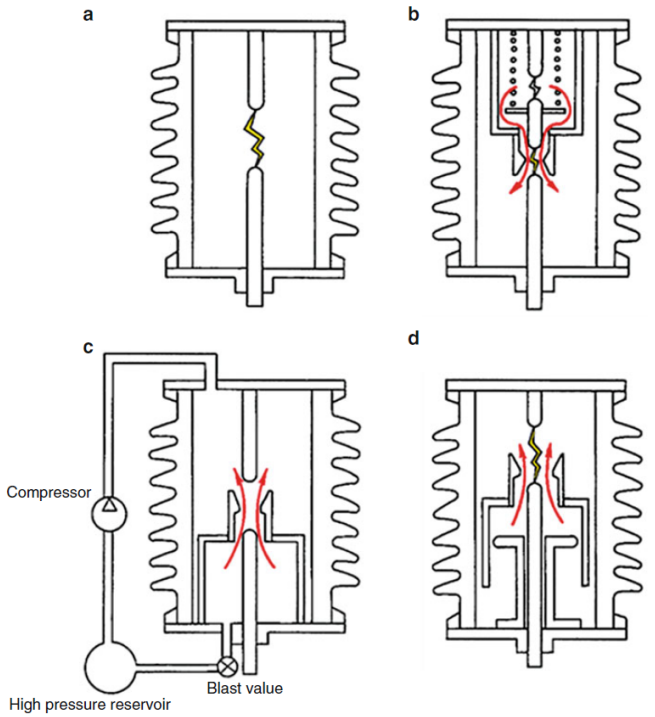


Figure 16: Cross-section comparison of SF_6 gas Interrupters: a) Plain break, (b) Self blast, (c) Double pressure blast, (d) Puffer blast [19]

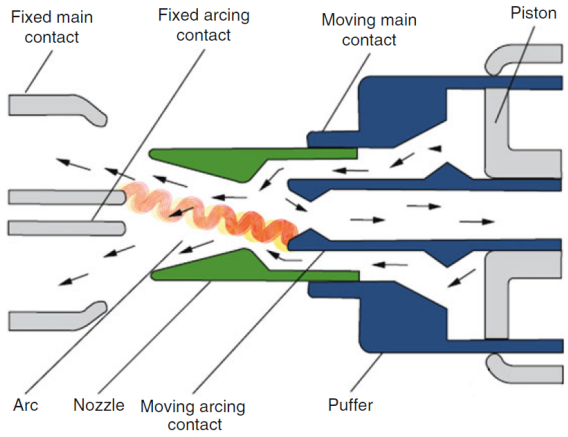


Figure 17: Interrupter principle [19]

the dominant technology for modern HVCBs due to its mechanical reliability and stability across temperature variations.

In the spring mechanism, the energy required for the opening and closing strokes is stored in helical or torsion bar springs. The kinematic chain is typically designed such that the closing operation releases potential energy to close the interrupter contacts while simultaneously recharging the opening spring. This configuration ensures that the breaker

remains primed for immediate tripping operations, even in the event of auxiliary power loss, thereby satisfying the standard Open-Close-Open duty cycle requirement. The charging of the closing spring is typically accomplished by an electric motor acting through a reduction gear system, which compresses the spring until it is secured by a latching mechanism.

As illustrated in Fig. 18, the mechanical linkage system translates the stored potential energy into the linear motion required by the interrupter. Central to the interface between the electrical control system and the mechanical drive are the trip and close coils. These solenoid devices act as the primary actuators. Upon receiving a command signal from the protection relay or control centre, the respective coil is energised to release the mechanical latches holding the compressed springs.

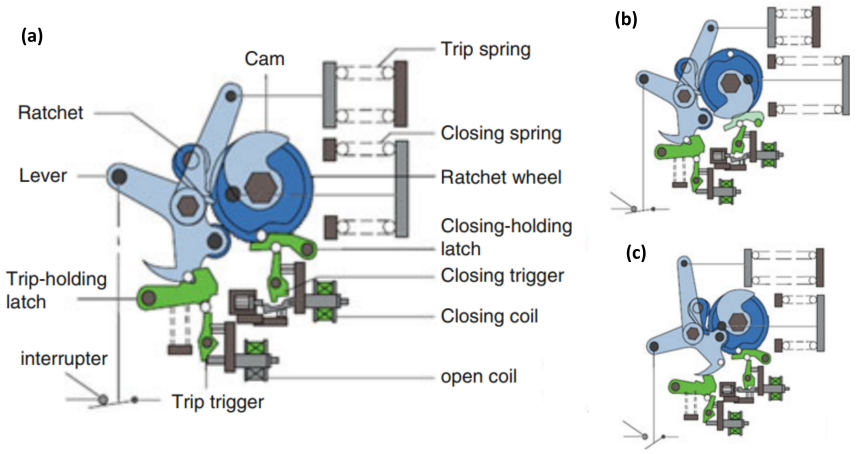


Figure 18: Schematic configuration of a spring operating mechanism: (a) components (b) close (c) trip [18]

Auxiliary and Control Circuits

The control circuits serve as the interface between external commands and the physical operation of the HVCB, ensuring that actions are performed correctly, safely, and reliably. In other words, it acts as the nervous system of the HVCB, managing the flow of commands and monitoring vital parameters. These circuits have two primary functions: executing control commands and monitoring the condition to ensure the safe operation of the HVCB. Upon receiving an open or close signal, the control system first verifies that the HVCB is capable of the manoeuvre by checking critical parameters such as stored energy levels and gas density. If the conditions are unsafe, the system will block the operation and alert the operator.

The core of the actuation system involves trip and close coils, which are solenoids that release the operating mechanism's stored energy to move the main contacts. To ensure redundancy, two independent trip coils are typically provided. The system also includes an energy-charging component, such as a motor, which recharges the mechanism's spring, and is supervised by limit switches that lock out operations if insufficient energy is available. Density monitors are crucial for gas-insulated HVCBs, providing alarms or locking-out controls if the SF_6 gas density drops below the levels required for insulation and arc interruption. Additional safety features include anti-pumping logic, which prevents the HVCB from cycling continuously if a close command persists during a trip event, and

pole discrepancy circuits for independent pole-operated HVCBs, which trip all phases if they do not operate simultaneously. For maintenance purposes, the circuitry includes local/remote selector switches and disconnects elements to isolate power to the control system. Fig. 19 presents a generalised framework of an HVCB.

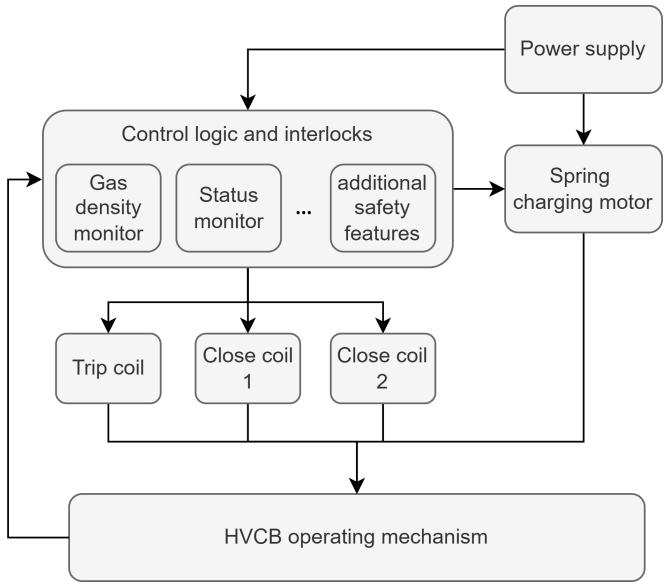


Figure 19: Schematic of a generalised HVCB control circuit

2.2 Failure Analysis Based on Service Application

The failure of an HVCB is not solely intrinsic to its design; it is heavily contingent upon the environmental and operational stresses it endures. A critical variable, often overlooked in general failure rate calculations, is the service type, or the specific functional application of the HVCB within the substation topology.

There are several types of circuits in which HVCBs are connected, and the duty imposed on the HVCB varies depending on the type of circuit being controlled, e.g., overhead line circuit, power cable, power transformer, capacitor bank, series or shunt reactor (inductive/reactive), etc. When the current and voltage are out of phase (lagging or leading), the interrupter faces significantly higher electrical stress, as it must withstand peak recovery voltages at the exact moment of arc interruption.

The specific service application of an HVCB has an apparent impact on its failure frequency, with devices used for reactive power switching demonstrating significantly higher failure rates than those used for transmission or distribution tasks. HVCBs assigned to the shunt reactor service exhibit the highest frequency of major failures, recorded at 2.46 failures per 100 HVCB-years, followed by those used for capacitor switching at 1.04 failures per 100 HVCB-years [34]. These rates are considerably higher than the failure frequencies for more common applications such as overhead line switching (0.25), transformer switching (0.22), and cable switching (0.09). The above-mentioned failure frequencies are summarised in Fig. 20.

The statistical diversity, which is demonstrated in Fig. 20, can be attributed to the high frequency of operation required for reactive power management compared to the

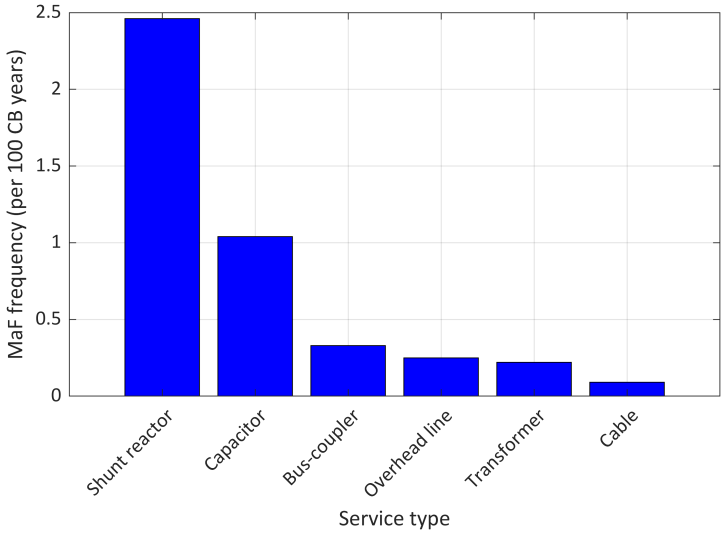


Figure 20: Major failure of HVCB according to the service type based on CIGRE survey [34]

relatively static operation of the transmission line or cable HVCBs. The mechanical and electrical stresses imposed by daily switching operations accelerate wear mechanisms significantly faster than in assets that only operate during fault clearance or rare topology changes.

As illustrated in the failure frequency distributions, HVCBs employed for shunt reactors exhibit a major failure frequency that is significantly higher than those deployed for overhead lines or cables. For instance, while overhead line breakers are the most common, their failure rate per unit is considerably lower than that of reactor breakers, which are subjected to frequent transient recovery voltages and high mechanical cycle counts.

2.3 Theoretical Framework of Equipment Failure

To translate statistical failure data into predictive maintenance schedules, mathematical modelling of the failure process is required. In reliability engineering, the stochastic nature of equipment breakdown is typically represented by the hazard rate function, denoted as $\lambda(t)$.

2.3.1 The Bathtub Curve Concept

The lifecycle of an HVCB generally may follow a distinct trajectory known as the bathtub curve [19, 51], as shown in Fig. 21. This curve segments the asset's life into three discrete phases, each governed by different failure mechanisms [52, 53, 54]:

1. **Early stage failure (Infant mortality):** This initial phase is characterised by a decreasing failure rate. Failures here are typically attributable to manufacturing defects, material flaws, or improper installation.

2. **Random failure (Constant rate):** Following the stabilisation of the equipment, the failure rate becomes approximately constant. During this phase, failures are generally stochastic in nature, caused by external random events rather than internal degradation.

3. **Ageing failure (Wear out):** In the final stage, the failure rate rises exponentially. This increase is driven by the irreversible physical and chemical deterioration of the insulation, contact wear, and mechanical fatigue.

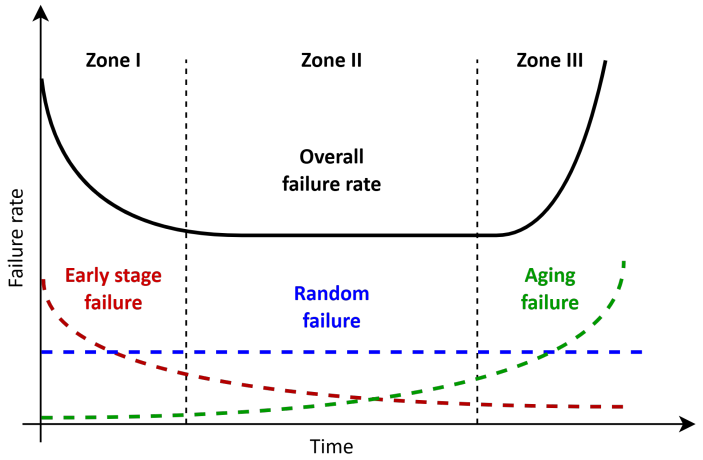


Figure 21: Typical time-varying failure rate for the power system equipment throughout the lifetime

2.3.2 Weibull Distribution Limitations

Conventionally, the Weibull distribution has been the standard tool for modelling these phases due to its mathematical flexibility [55]. The failure rate $\lambda_W(t)$ and the mean time to failure $MTTF_W(t)$ in the Weibull model are defined as:

$$\lambda_W(t) = \frac{\nu}{\eta}\left(\frac{t}{\eta}\right)^{\nu-1} \tag{2}$$

$$MTTF_W(t) = \frac{\eta}{\nu}\left(\frac{t}{\eta}\right)^{1-\nu} \tag{3}$$

where t represents time, ν is the shape parameter, and η is the scale parameter. While the Weibull distribution can approximate the bathtub curve by varying the shape parameter ($\nu < 1$ for early failures, $\nu \approx 1$ for random failures, and $\nu > 1$ for ageing). In another word, it does not provide a single continuous function that accurately fits empirical data across all three transition zones simultaneously [56].

2.4 Proposed Methodology for Remaining Useful Life Estimation

To address the limitations of standard Weibull approaches, this thesis utilises a model based on a Gaussian function. Furthermore, the influence of operational service types discussed in Section 2.2 is subsequently integrated into the broader calculation framework.

2.4.1 Gaussian Function-Based Ageing Model

Curve-fitting techniques allow for the development of mathematical functions that expose the fundamental pattern of the empirical data. In this research, a Gaussian function-based model is utilised to fit the MTTF data derived from [34]. This data is presented in Table 2, and it indicates the failure rate and MTTF with respect to the HVCB operational lifetime.

Table 2: MTTF and λ values for HVCB based on third CIGRE survey (data from [34])

Age (years)	λ (failure/100HVCB-years)	MTTF (years)
2	0.14	714.3
6	0.25	400
10	0.25	400
14	0.26	384.6
18	0.36	277.7
22	0.49	204.1

The proposed model utilises a summation of two Gaussian functions to capture the complex nonlinear behaviour of the HVCB lifecycle. The general form of the probability density function $P(x)$ for a random variable x in a Gaussian distribution is given by:

$$P(x) = \frac{1}{\sigma\sqrt{2\pi}} e^{-(x-\mu)^2/2\sigma^2} \tag{4}$$

where μ is the mean, and σ is the standard deviation. Adapting this for the ageing profile, the proposed function for the estimated mean time to failure, $MTTF'_{base}(t)$, is formulated as:

$$MTTF'_{base}(t) = \frac{1}{a_1} e^{-\left(\frac{t-b_1}{c_1}\right)^2} + \frac{1}{a_2} e^{-\left(\frac{t-b_2}{c_2}\right)^2} \tag{5}$$

in which, a_1, a_2, b_1, b_2, c_1, and c_2 serve as the tunable parameters of the model. The selection of a sum of Gaussian functions to model the ageing trajectory of HVCBs is driven by the need to reflect distinct stages of the equipment lifecycle. A superposition of Gaussian distributions provides the mathematical flexibility required to approximate the different phases of the conventional bathtub curve. Because the MTTF is inversely proportional to the failure rate λ, the proposed ageing model seeks an analogy to the inverse of the conventional bathtub curve.

Three mathematical models are fitted to the scattered data in Table 2, which are Exponential, Weibull, and the proposed sum of Gaussian. The fitting accuracy of the models is presented in Table 3, and the MTTF of the HVCB based on the proposed model in comparison with the conventional ones is demonstrated in Fig. 22. To ensure the reproducibility of the proposed ageing models and to facilitate future comparative studies, the specific mathematical parameters derived for each distribution are detailed in Table 4. These parameters were obtained utilising a nonlinear least squares optimisation algorithm within MATLAB.

Table 3: R-squared values of the applied models

Method	Weibull	Exponential	Proposed
Value	0.9024	0.8583	0.9977

2.4.2 Data Limitations and the Bathtub Curve Analogy

The proposed six-parameter Gaussian ageing model effectively captures the variance in MTTF for the provided CIGRE dataset. However, an objective evaluation of the model's

Table 4: Estimated parameters of the applied ageing models for reproducibility.

Distribution Model	Mathematical Formulation	Fitted Parameters
Gaussian	$y = \frac{1}{a_1} e^{-\left(\frac{x-b_1}{c_1}\right)^2} + \frac{1}{a_2} e^{-\left(\frac{x-b_2}{c_2}\right)^2}$	$a_1 = 0.0021, a_2 = 0.0025$ $b_1 = 2.7343, b_2 = 9.9926$ $c_1 = 1.9227, c_2 = 14.1496$
Weibull	$y = \frac{\eta}{\nu} \left(\frac{x}{\eta}\right)^{1-\nu}$	$\nu = 1.4163, \eta = 161.4659$
Exponential	$y = ae^{bx}$	$a = 726.7028, b = -0.0569$

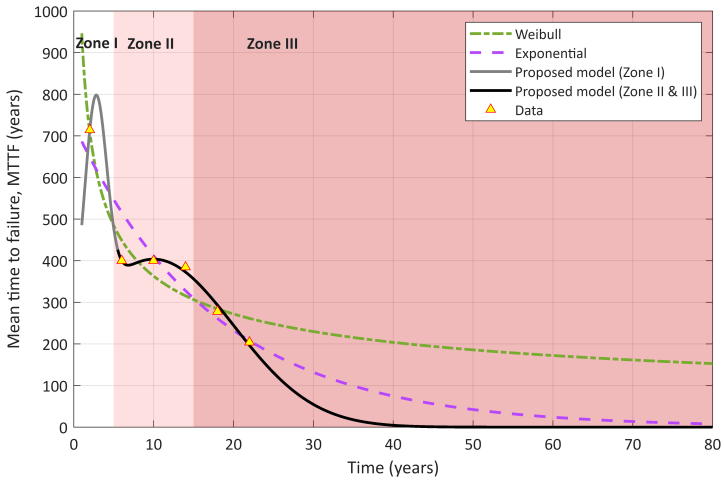


Figure 22: Comparison of the proposed model to Weibull and exponential models in analogy to the bathtub curve zones, shown in Fig. 21; Due to a lack of data in Zone I, the proposed model cannot be fully validated in this region, and this unvalidated section is denoted by the solid gray line.

constraints is necessary to define its applicable boundaries. The classical reliability bathtub curve comprises three distinct phases: infant mortality (Zone I), random failures (Zone II), and wear-out (Zone III). The empirical dataset utilized for this model spans operational ages from 2 to 22 years, predominantly capturing the transition from Zone II into the early stages of Zone III. Although not supported by sufficient empirical evidence for validation, the initial volatility exhibited by the Gaussian-based formulation may correspond to the early-stage failure behaviour (infant mortality). Confirmation of this interpretation will require high-resolution failure data covering the initial years of operation.

It is to be noted that fitting a function governed by six parameters ($a_1, b_1, c_1, a_2, b_2, c_2$) to a dataset containing exactly six observation points inherently creates a perfect fit for the historical data, but limits the model's unconstrained predictive capability. Consequently, the rapid decline of the MTTF curve toward zero after 40 years must be interpreted as a mathematical characteristic of the Gaussian function, rather than a definitive physical boundary of the HVCB.

2.4.3 Interpolation of the Data and Sensitivity Analysis

To address the limited number of empirical data points, a standard shape-preserving interpolation technique is applied. This expands the dataset to 60 synthetic points between

ages 2 and 22, maintaining the underlying trend of the data. Moreover, in order to evaluate the sensitivity of the proposed framework against real-world data scatter, a sensitivity analysis was conducted. Synthetic variance (up to 7%) was introduced to the interpolated MTTF values across 100 iterations. Fig. 23 presents one iteration of the sensitivity analysis. The triangular markers indicate the six original values derived from the CIGRE statistics, while the blue markers represent the interpolated values after introducing synthetic variation. The curves show the proposed, Weibull-based, and exponential models fitted to this perturbed dataset. This example illustrates an individual fitting result, whereas Table 5 summarises the average performance across all 100 iterations.

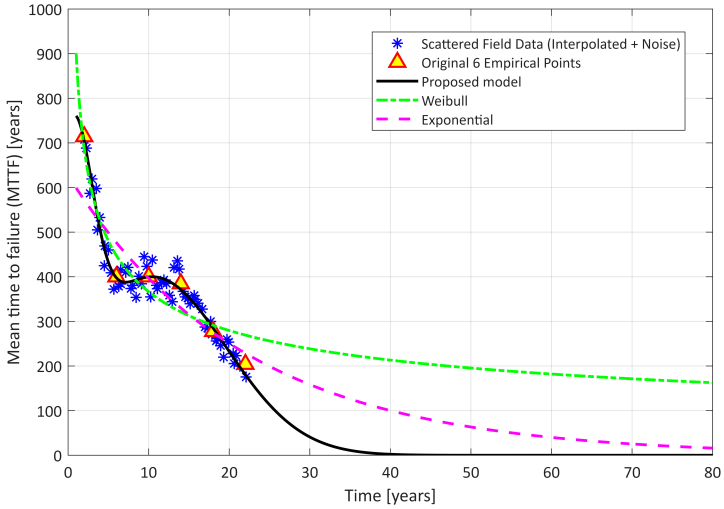


Figure 23: Example of one sensitivity-analysis iteration showing the original data, perturbed interpolated values, and fitted models.

Although simpler models mitigate overfitting, but based on the results in Table 5, they inadequately describe the mechanical degradation occurring during the HVCB transition from Zone II to Zone III. The Gaussian model demonstrates superior statistical stability within the known data boundaries, maintaining a high correlation despite the introduced variance.

Table 5: Model Sensitivity Evaluation Under Simulated Data Variance

Model Type	**Average R^2**	**Average RMSE (years)**
Exponential	0.7729	53.65
Weibull	0.8038	49.76
Proposed model	0.9415	28

A comparative test was conducted by fitting the Gaussian model to a truncated dataset (up to 14 years, marked by the boundary point in Fig. 24) versus the full dataset (up to 22 years). Fig. 24 illustrates that excluding data beyond 14 years causes the predictive tail of the model to diverge. This demonstrates that incorporating additional data points significantly refines the model's trajectory. Although, the proposed model effectively maps degradation trajectories within the observed period (years 2–22), however, extrapolating beyond the known year range still requires boundary limits to prevent unrealistic trends.

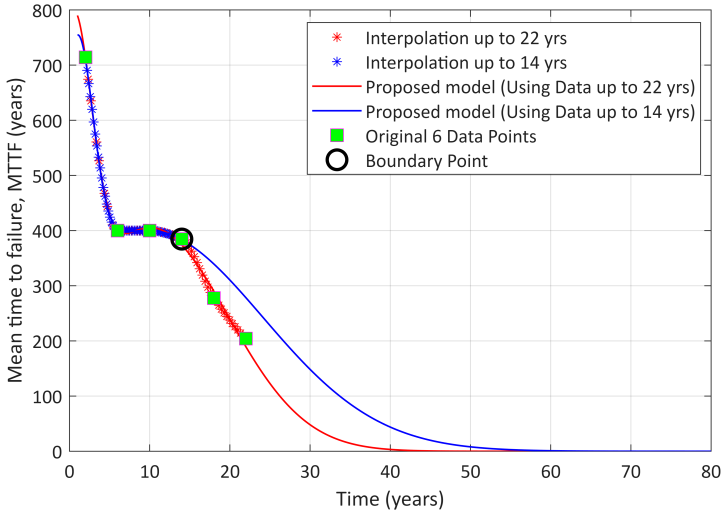


Figure 24: Comparison of Gaussian model extrapolation trajectories when fitted on data truncated at 14 years versus 22 years.

2.4.4 Integration of Service Type via Normalisation

A key feature of this proposed framework is the integration of service-type parameters as a weighting factor in the RUL calculation. Since raw failure frequency data for different applications (e.g., shunt reactor vs overhead line) exist on different scales, a normalisation process is required. The z-score normalisation technique is employed to standardise the major failure (MaF) frequencies of various service types. For a dataset x with mean $\overline{X}$ and standard deviation S, the normalised value ζ is calculated as:

$$\zeta = \frac{x - \overline{X}}{S} \tag{6}$$

This normalised parameter, ζ, is then inversely applied to the base MTTF to derive a service-dependent ageing curve. To ensure that the proposed framework remains adaptable to diverse asset classes and varying operational environments, the modification of the MTTF is formulated through a generalised function that is influenced by service type, denoted as $\phi(\zeta)$. The modified life expectancy, $MTTF_{mod}$, is expressed as:

$$MTTF_{mod} = MTTF_{base} \cdot \phi(\zeta) \tag{7}$$

In this research $\phi(\zeta)$ is implemented using a linear scaling approach, defined as:

$$\phi(\zeta) = 1 - q \cdot \zeta \tag{8}$$

The sensitivity coefficient q determines the magnitude by which the operational stress impacts the remaining technical life. For the purposes of this study, q is selected as 0.1, representing a 10% adjustment per unit of normalised deviation. In practical TSO implementation, q may be calibrated using historical asset population data or aligned with empirical degradation metrics specified by manufacturers and industry standards. While linear scaling provides a computationally efficient model for utility operators, the framework can accommodate other functional forms depending on the physics of failure, such as exponential decay for transient stresses. This adjustment ensures that HVCBs

operating in high-stress environments, such as those connected to shunt reactors, exhibit a steeper ageing trajectory in the model, thereby preventing the overestimation of their useful life. By utilising this generalised approach, the transmission system operator (TSO) can calibrate the influence of service types to align with specific maintenance philosophies.

Fig. 25 demonstrates the application of service-type integration, considering the major failure rates across service types that is shown in Fig. 20.

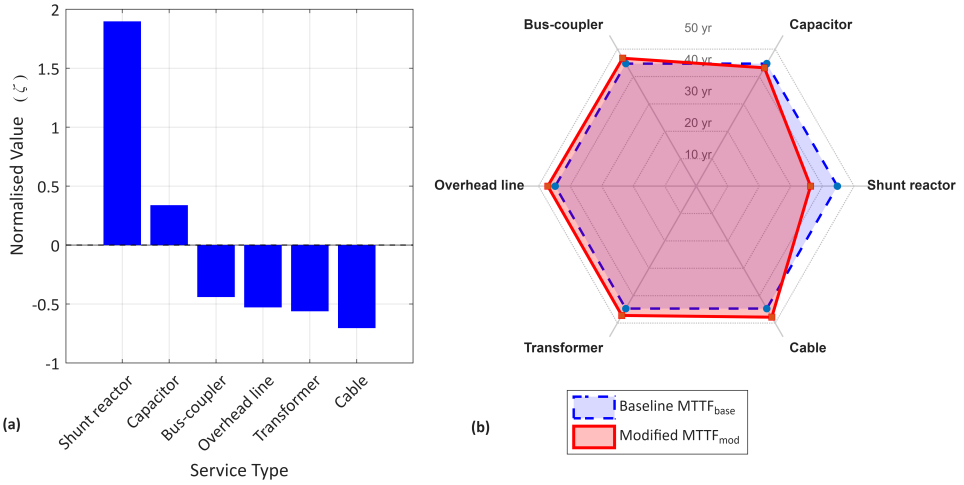


Figure 25: Impact of normalized service-type integration on HVCB life expectancy: (a) normalised failure rates (ζ) per service-type; (b) comparison between $MTTF_{base}$ and $MTTF_{mod}$.

As illustrated in Fig. 25-(a), applying (6) standardises these failure rates into relative deviations, producing positive scores for high-duty applications and negative scores for less severe duties. Fig. 25-(b) presents the resulting effect on life expectancy compared against an unweighted baseline lifespan of $MTTF_{base} \approx 45$ years, considering that the MTTF based on proposed model reaches to one year. Assuming $q = 0.10$, the scaling factor derates the life expectancy of shunt reactor HVCB to 36 years (19% reduction), whereas cable HVCB exhibit an extended expected lifespan of 48 years (7% increase). This quantitative shift confirms that the normalisation framework systematically captures application-specific degradation drivers without distorting baseline metrics across less demanding assets.

2.4.5 Computational Implementation

To facilitate the practical application of the proposed Gaussian ageing model and service-type adjustments, a computational tool was developed within the MATLAB environment, as shown in Fig. 26. This graphical user interface can serve as a decision support mechanism for asset managers. The computational framework operates by processing three primary categories of input data:

1. **Voltage level:** To select the failure rates corresponding to that specific voltage level.

2. **Service type:** The specific service type (e.g., shunt reactor, overhead line, etc.) which triggers the relevant ζ weighting factor derived in (6).

3. **Historical data:** Fit the proposed Gaussian model on aggregated failure rates from the CIGRE database corresponding to the specified voltage class and service type.

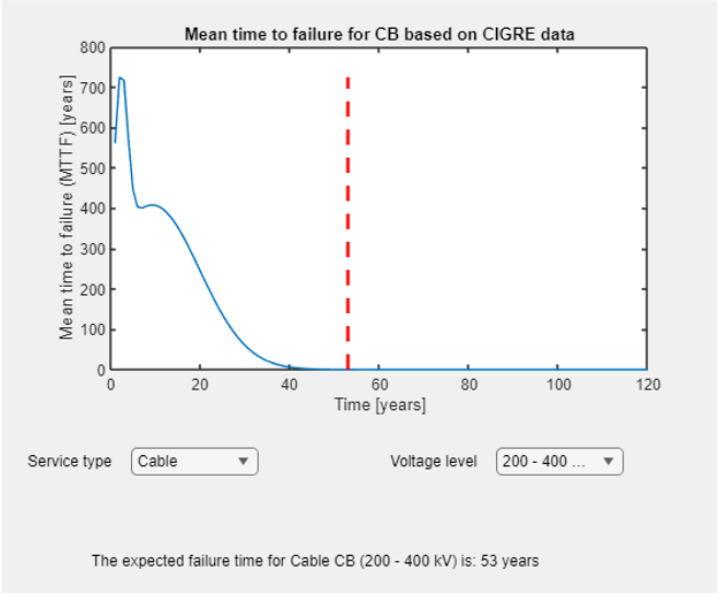


Figure 26: An output sample from the designed graphical user interface

The algorithm processes these inputs through the Gaussian function described in (5). The output is a visualised ageing curve that projects the MTTF over the asset's lifespan. By adjusting the input parameters, the user can simulate different scenarios, for example, observing how re-deploying a breaker from a transmission line to a capacitor bank reduces its projected time to failure.

2.5 Remarks

This chapter reviewed the principal HVCB subsystems and used aggregated CIGRE data to formulate a Gaussian function-based ageing model. The service-type adjustment illustrates how the application-specific failure rates may alter the baseline trajectory. Given the limited data and the assumed scaling coefficient, these results should be interpreted as relative population-level adjustments rather than quantified degradation rates for individual HVCBs.

While the probabilistic models presented herein offer a framework for estimating the RUL of the asset population, they rely inherently on historical failure data. Consequently, these statistical approaches provide a baseline expectation of performance rather than a precise diagnosis of a specific unit's instantaneous health. To achieve the higher precision required for predictive asset management, it is necessary to move beyond population-based statistics to individual asset diagnostics. The next chapter will therefore focus on condition monitoring techniques, utilising the signal-processing of coil current waveforms to capture the actual physical state of the equipment.

3 Condition Monitoring of HVCB Based on Coil Current Measurements

Building upon the theoretical frameworks and failure mechanisms discussed in Chapters 1 and in Chapter 2, this chapter focuses on the practical implementation of condition monitoring methodologies for HVCBs. As identified in the previous chapter, the trip/close coil current signatures provide a wealth of diagnostic information regarding the condition of the operating mechanism and the control circuitry. These components are responsible for a significant portion of major failures in HVCBs. Consequently, developing a cost-effective monitoring system based on coil current signals is of importance for modern power systems.

This chapter details the experimental and analytical methodologies developed to assess an HVCB condition. It begins by contrasting commercial measurement solutions with the cost-effective experimental setup designed for this research. Subsequently, it presents a comprehensive mathematical framework for calculating an HI, explicitly accounting for measurement accuracy and signal preprocessing. The chapter further explores the integration of this HI into RCM scheduling. Finally, an automated online condition monitoring framework is proposed, utilising signal processing techniques such as the Savitzky-Golay filter and DTW, combined with ML algorithms for classification of the investigated emulated conditions. This chapter is based on publications IV, V, and VI.

3.1 Commercial Measurement Equipment

Within the domain of asset management, data acquisition is an important factor of any diagnostic algorithm. Commercial measurement equipment for HVCBs is typically engineered for high-precision and electromagnetic compatibility to withstand the harsh environment of a substation. These devices are standard for factory acceptance tests, site commissioning, and periodic maintenance intervals. Commercial analysers are capable of recording a multitude of signals simultaneously, including coil currents, contact travel, auxiliary contacts status, main contacts resistance, etc. They utilise high-resolution analogue-to-digital converters to capture the coil current data with minimal noise and high accuracy.

The CIBANO 500, manufactured by OMICRON electronics, is a comprehensive test system specifically engineered for the maintenance and diagnostic testing of high- and medium-voltage circuit breakers [57]. Its main feature is the integration of three typically separate instruments: a micro-ohmmeter for resistance, a timing analyser for operation speed, and a high-power 2.4 kW AC/DC voltage supply. This consolidation allows engineers to carry fewer devices to the field while retaining the ability to perform a full set of standard tests. Fig. 27 displays the CIBANO 500 test system with its key accessories, including the main contact modules and the primary test manager software interface. Moreover, a typical field application setup showing the CIBANO 500 connected to a live-tank HVCB, is demonstrated in Fig. 28.

A primary operational advantage of this system is its one-time connection, meaning that once the engineer connects the cables to the HVCB, they can perform all the necessary tests sequentially without having to alter the wiring setup for different measurements. Because the device includes its own powerful integrated power supply, it can drive the breaker's coils and motors directly. In terms of diagnostic capabilities, the CIBANO 500 is highly versatile. It measures the precise timing of opening and closing sequences and performs static contact resistance checks to identify potential overheating issues. For more advanced analysis, it conducts DRM to diagnose wear on arcing contacts and utilises transducers to map the physical motion, velocity, and damping of the breaker mechanism.



Figure 27: The CIBANO 500 HVCB test system [58]

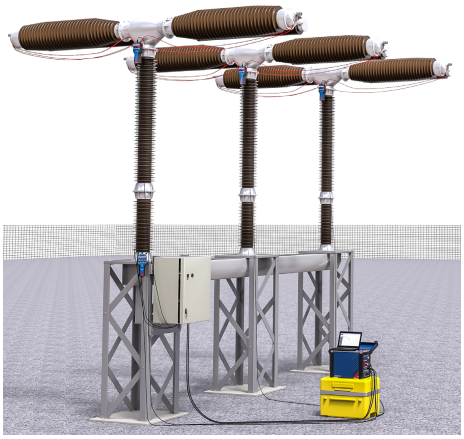


Figure 28: CIBANO 500 connected to a live tank HVCB (a typical field application) [58]

It also performs minimum pick-up tests to ensure that the breaker operates at lower voltage levels and analyses coil and motor currents. It is compatible with a wide range of breaker types, including live tank, dead tank, and GIS. Fig. 29 illustrates a typical test report produced by CIBANO 500. Apart from graphical representation, it is possible to extract numerical data for further analysis.

For routine testing, the system is designed to reduce the need for an expert on-site. The software automates much of the process. It compares the measured results against standard limits, e.g., IEEE/IEC or manufacturer's specifications, and provides an immediate "Pass/Fail" assessment (often visualised as green/red indicators). A trained technician can perform the test and identify whether the HVCB is within acceptable limits without being a switchgear engineer. However, if a test fails or shows a marginal result, an expert is absolutely required to specify the actual status or root cause. The most significant drawback from a condition monitoring perspective is that the CIBANO 500 is an offline test set. It cannot monitor the HVCB continuously while it is in service (online). It only provides a snapshot of the HVCB's health at the specific moment of testing. Consequently, it cannot detect transient faults or developing issues that occur between maintenance intervals, unlike online monitoring systems installed permanently on the HVCB.

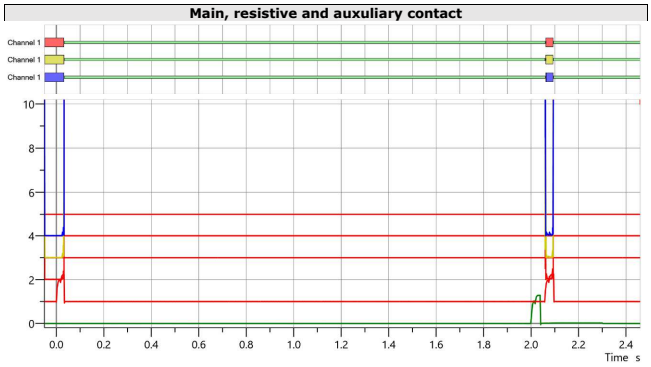
However, the deployment of such high-precision equipment for continuous online monitoring on every HVCB in a grid is often economically prohibitive. The cost of installation, coupled with the complexity of integrating these devices into legacy infrastructure, necessitates the exploration of more cost-effective solutions. However, the trade-off is often a reduction in SNR and measurement precision. This chapter of the thesis addresses this gap by evaluating diagnostic algorithms on data acquired from low-cost sensors, which inherently exhibit higher noise levels, thereby simulating a realistic, large-scale internet of things (IoT)-based monitoring scenario.

3.2 Coil Current Measurement Experimental Setup

To develop and validate data-driven diagnostic algorithms, a substantial dataset representing both healthy and defective operational states is required. Due to the scarcity of publicly available fault data from operational HVCBs, an experimental emulator was designed and constructed. This setup allows for the controlled simulation of specific mechanical and

O-CO Dynamic Contact Resistance	
Execution date/Time	06.05.2021 15:54:38
Sequence	O-CO
Coil supply	220 V DC
Time calculation	According to IEC 62271-100
CB MC2 settings	
Test current	100 A
V DC range	10 V
Sample rate	40 kHz

Main, resistive and auxuliary contact



Label	Unit/div.	Y-Axis pos.
Close coil (A)	1 A	0
Trip coil (A)	2,5 mΩ	1

Label	Unit/div.	Y-Axis pos.
Channel 1 (Ω)	2,5 mΩ	2
Channel 1 (Ω)	2,5 mΩ	3
Channel 1 (Ω)	2,5 mΩ	4

Operating times

Measured	Opening time (ms)	Opening sync. (ms)	Closing time (ms)	Closing sync. (ms)	Open-Close time (ms)	Close-Open time 1 (ms)	Assessment
Breaker	33,02	0,60	60,78	1,53	26,23	34,63	Not assessed
A	32,42		60,10		27,68	33,50	Not assessed
B	33,02		59,25		26,23	33,75	Not assessed
C	32,55		60,78		28,22	33,10	Not assessed

Coil characteristics

	Peak current (A)	Average current (A)	Average voltage (V)	Resistance (Ω)	Assessment
Close	1,28	-	-	-	Not assessed
Trip A	1,26	-	-	-	Not assessed

Figure 29: HVCB test report by CIBANO 500 [59]

electrical defects, facilitating the training of ML models.

3.2.1 Emulator Architecture

The experimental setup aims to emulate the inductive and resistive characteristics of an HVCB's trip/close coil mechanism. The core of the data acquisition system is built around cost-effective hardware to demonstrate the feasibility of low-cost monitoring. Fig. 30 presents the schematic and physical realisation of the experimental setup. The setup comprises the following key components:

- **Coil emulator circuit:** A circuit designed to replicate the inductive and resistive characteristics of a standard HVCB coil that produces a similar current level and waveform (Fig. 31).
- **Data acquisition unit:** An Arduino NANO microcontroller is utilised for controlling

the emulator circuit and digitizing the analogue current sensor readings.

- **Current sensor:** An ACS712 current sensor (5 A model) is employed to measure the coil current. While this sensor is affordable and easy to interface, it introduces a realistic level of measurement noise which allows the denoising and feature extraction algorithms to be evaluated under the investigated measurement conditions.

The ACS712 was selected for its low cost, DC-current measurement capability, and straightforward integration with IoT devices. The ±5 A version provides a nominal sensitivity of 185 mV/A, suitable for the current range investigated. Its analogue output, 5 V supply, and galvanic isolation between the current path and measurement circuitry simplify implementation of the laboratory setup.

Conventional current transformers and Rogowski coils cannot directly measure steady DC current. A shunt-based solution can measure DC but requires additional circuitry to provide electrical isolation. Other DC-capable Hall-effect sensors could also meet the measurement requirements; the ACS712 was therefore a practical choice for the laboratory prototype, without claiming superiority over all alternative sensors.

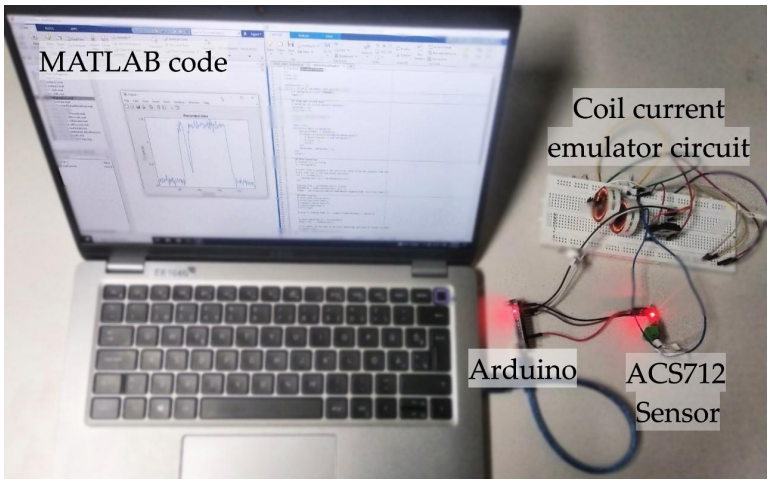


Figure 30: Schematic representation of the experimental setup for emulating HVCB coil current behaviour and defects.

The Arduino NANO was used to control the emulator and to digitise the ACS712 output during the emulator experiments. In addition to this setup, a separate measurement arrangement was implemented for acquiring the coil current of a real 110 kV HVCB in TalTech's high-voltage laboratory. In this arrangement, an ACS712 sensor was interfaced with a Raspberry Pi. The Raspberry Pi acquisition configuration was operated at a higher effective sampling frequency than the Arduino-based acquisition used for the emulator. Fig. 32 compares trip/close coil current waveforms obtained using three measurement configurations under baseline operating conditions. The waveform in Fig. 32-(a) was recorded from a real HVCB using the CIBANO 500 commercial test system. It provides a comparatively clean reference for the general waveform and for the locations of the peak-current and timing features shown in Fig. 12. Fig. 32-(b) presents a measurement obtained from the HVCB same as Fig. 32-(a), but using an ACS712 current sensor and a Raspberry Pi data acquisition unit. This measurement provides a practical assessment of whether the low-cost measurement chain can capture the principal characteristics of an

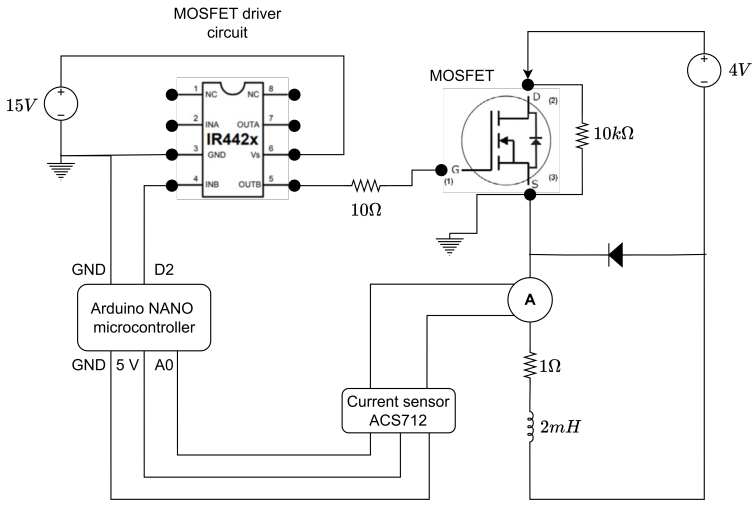


Figure 31: Coil current emulator circuit diagram

actual HVCB coil current waveform. The same measurement is subsequently processed in Fig. 52 to evaluate the feature extraction procedure using a real coil current signal. Fig. 32-(c) shows the baseline current generated by the coil current emulator and measured using the same type of ACS712 sensor, with an Arduino NANO used for data acquisition. The higher sample density visible in Fig. 32-(b) results from the higher sampling frequency used in the Raspberry Pi acquisition configuration. Therefore, differences in waveform detail and apparent noise between Fig. 32-(b) and Fig. 32-(c) should not be attributed solely to differences between the real HVCB and the emulator.

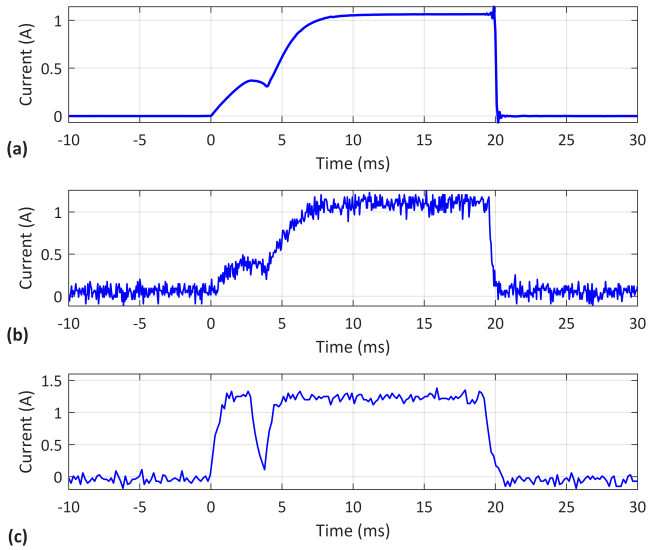


Figure 32: Trip/close coil current signal and related diagnostic features. (a) Real HVCB coil current measured with CIBANO 500. (b) Real HVCB coil current measured using Raspberry Pi. (c) Emulator circuit current measured using an inexpensive sensor.

The comparison in Fig. 32 is intended to illustrate the waveform obtained from the different measurement configurations. The quantitative comparison of the ACS712 sensor against a laboratory reference instrument is presented separately in Section 3.2.2. In this chapter, the term "normal" refers to a baseline operating condition in which no defect was deliberately introduced.

3.2.2 Comparative Analysis of Current Sensors

To evaluate the performance of low-cost current measurement solutions against laboratory-standard instrumentation, two distinct measurement devices were employed to capture the current waveform of the coil current emulator circuit:

- **Reference instrument (Tektronix TCP0030A):** The primary reference signal was acquired using a Tektronix TCP0030A AC/DC current probe. This device provides high-bandwidth (up to 120 MHz) and high-accuracy measurements. It represents the ground truth for this analysis, characterised by minimal noise and high signal fidelity.

- **Device under test (ACS712):** The secondary signal was acquired using the ACS712. Due to its internal operational amplifier structure and lower bandwidth (80 kHz), it is expected to exhibit higher noise levels and a lower transient response compared to the reference probe.

The coil current signals were recorded simultaneously over an active period of $T = 20$ ms. Post-acquisition analysis revealed a discrepancy in the sampling density between the two recording channels, necessitating a calculation of their respective effective sampling frequencies (f_s).

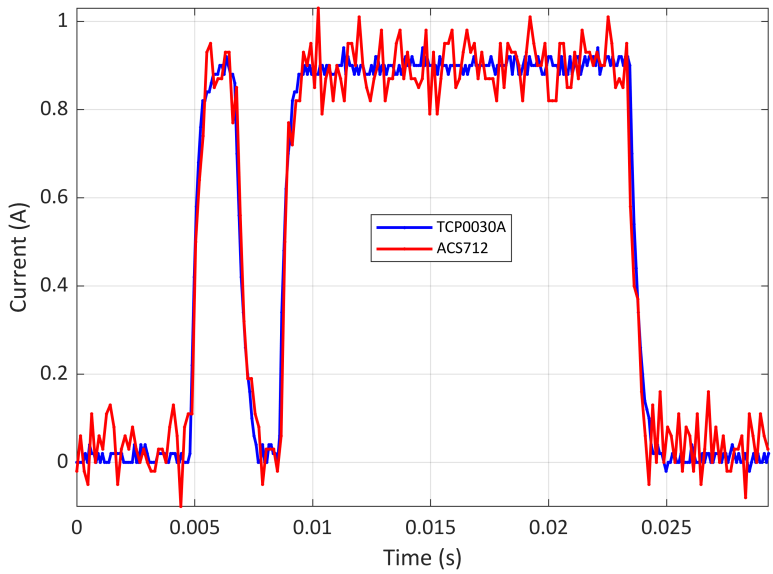


Figure 33: Time-domain comparison of signals captured by TCP0030A and ACS712

The sampling frequency for each signal was derived using the relationship $f_s = N/T$, where N is the number of samples acquired.

- **TCP0030A:** With $N_A = 220$ samples, the sampling frequency was calculated as:

$$f_{sA} = \frac{220}{0.02\ \text{s}} = 11{,}000\ \text{Hz} \quad (11\ \text{kHz}) \tag{9}$$

- **ACS712:** With $N_B = 122$ samples, the sampling frequency was calculated as:

$$f_{sB} = \frac{122}{0.02\ \text{s}} = 6{,}100\ \text{Hz} \quad (6.1\ \text{kHz}) \tag{10}$$

This variance in sampling rates necessitated digital signal-processing techniques to synchronise the datasets for direct comparison. To quantify the performance degradation of the ACS712 relative to the TCP0030A, the SNR is selected as the primary metric. In this context, the SNR is not a measure of the signal strength relative to environmental background noise, but rather a measure of the accuracy of the ACS712 (noisy signal) relative to the TCP0030A (clean reference). The objective is to isolate the error vector, i.e., the difference between the cheap sensor's output, and the professional probe's output and define this deviation as the noise component. The comparative analysis was performed in MATLAB using a four-stage signal-processing pipeline:

1. **Uniform resampling:** Since the signals possessed different time bases (11 kHz vs 6.1 kHz), direct subtraction was impossible. The signal from the ACS712 was digitally resampled to match the higher sampling rate of the reference signal (11 kHz). To preserve the accuracy of the waveform during interpolation, a low-pass filter was used to smooth the newly generated data points.

2. **Temporal alignment:** Hardware latencies often introduce phase shifts between measurement channels. A cross-correlation analysis was performed to determine the delay between the two signals. The signals were then shifted in time to maximise synchronisation.

3. **Amplitude scaling (gain correction):** To decouple gain errors (calibration differences) from noise, a linear least squares regression was applied. This calculated a scalar scaling factor (k_{scale}) that minimised the squared difference between the reference (Ref) and the noisy signal ($Meas$).

   The outcome of the above-mentioned modification stages is demonstrated in Fig. 34, where the resampled and gain-corrected signals are superimposed, demonstrating the precise alignment achieved prior to noise extraction.

4. **Residual noise extraction and SNR calculation:** The noise component (n) was isolated by subtracting the scaled reference from the measured signal:

$$n(t) = Meas(t) - (k_{scale} \times Ref(t)) \tag{11}$$

   Finally, the SNR was computed using the root mean square (RMS) power of the scaled signal and the extracted noise:

$$\begin{aligned} SNR_{dB} &= 10\log_{10}\left(\frac{P_{signal}}{P_{noise}}\right) \\ &= 20\log_{10}\left(\frac{RMS_{signal}}{RMS_{noise}}\right) \\ &= 20\log_{10}\left(\frac{0.668}{0.0658}\right) \\ &= 20.14 \end{aligned} \tag{12}$$

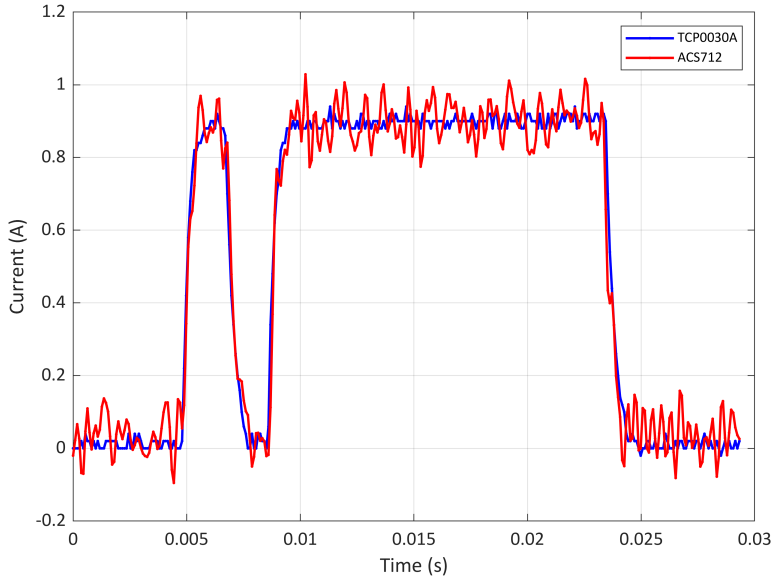


Figure 34: Demonstration of the reference (TCP0030A) and modified signal (ACS712)

To summarise, the analysis yielded an SNR of 20.14 dB for the ACS712 sensor. Physically, this result implies that the amplitude of the noise and distortion artefacts present in the ACS712 output is approximately 10% of the fundamental signal amplitude ($10^{-20/20} = 0.1$). This confirms that while the ACS712 is sufficient for general-purpose monitoring, where $\approx 10\%$ total error margin is acceptable, it lacks the fidelity required for high-precision analysis or transient characterisation. To compensate for the inherent noise and ensure the geometric integrity of the waveform for feature extraction, a digital filtering stage is strictly required.

3.2.3 Comparison of Denoising Algorithms

The raw output from the ACS712 sensor exhibits significant stochastic noise, which introduces variance in peak detection algorithms and may mask subtle temporal characteristics essential for detecting the coil's behaviour. To facilitate the accurate extraction of critical signal features, specifically the peak current amplitude and the precise timing of transient events within the coil current waveform, a denoising stage must be implemented. Consequently, a comparative analysis of various digital signal-processing denoising techniques was conducted. The primary objective was to identify an algorithm capable of suppressing high-frequency noise without attenuating peak magnitudes or inducing phase shifts that would distort the time domain analysis. Four distinct filtering methodologies were evaluated:

- **Moving average filter:** A linear convolution filter that smooths data by averaging adjacent samples within a sliding window. While computationally efficient, it tends to attenuate high-frequency transients and can degrade the accuracy of peak value estimation.
- **Gaussian filter:** A weighted averaging method that applies a Gaussian kernel, assigning higher significance to central data points. This approach reduces the edge distortion common in simple moving averages, but may still smooth out sharp signal

transitions.

- **Butterworth low-pass filter:** A frequency domain infinite impulse response filter configured with a cutoff frequency of 500 Hz. However, this method is prone to distorting the true shape of the waveform by shifting it in time and adding artificial ripples at sharp peaks, thereby reducing the accuracy of the extracted timing features.

- **Savitzky-Golay filter:** A polynomial-based smoothing filter that fits a low-degree polynomial (in this thesis, the polynomial has the degree of 3) to subsets of adjacent data points using the method of linear least squares. This technique is specifically selected for its renowned ability to preserve high-frequency signal features, such as peak height and width, which are critical for the subsequent feature extraction phase.

Fig. 35 shows the comparison of the raw ACS712 signal against some of the applied denoising algorithms together with the reference signal obtained from the TCP0030A probe. Moreover, the performance of each algorithm was quantified by calculating the root mean square error (RMSE) against the reference signal. It is to be noted that the filtering window size has been set to 15, if applicable. Table 6 summarises the error metrics for each technique. Among the evaluated configurations, the Savitzky-Golay filter produced the lowest RMSE against the reference signal and was therefore selected for the subsequent feature extraction analysis.

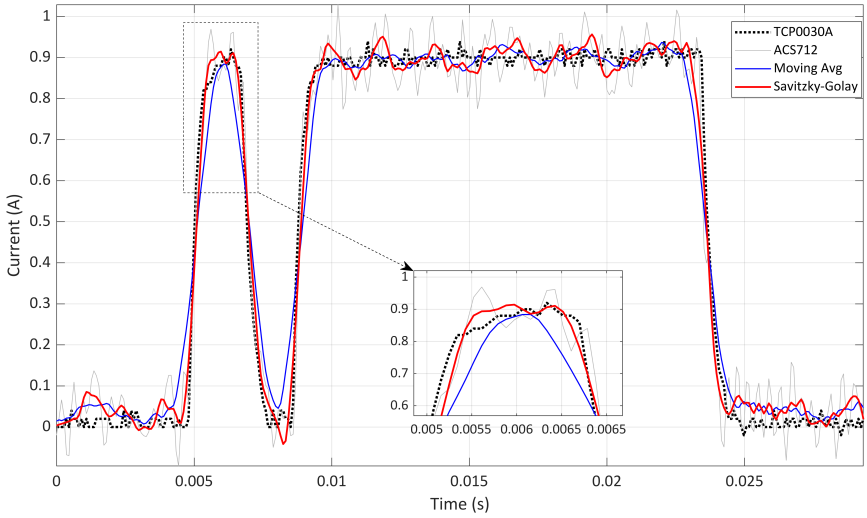


Figure 35: Time-domain comparison of denoising techniques.

It is important to acknowledge that in certain parameter configurations, linear averaging techniques such as the moving average may result in RMSE values that are comparable to, or marginally lower than, the Savitzky-Golay filter. This phenomenon occurs because averaging filters are highly effective at suppressing variance in the quasi-static regions of the signal, which constitute the majority of the data points, thereby lowering the global error score. However, the selection of the optimal denoising strategy cannot rely solely on global error metrics. A critical limitation of the moving average and Gaussian filters is their tendency to introduce systematic bias, specifically, amplitude reduction at local maxima

Table 6: Comparison of root mean square error across denoising techniques.

Denoising Method	RMSE
Moving average	0.0663
Gaussian	0.0485
Butterworth low pass	0.0543
Savitzky-Golay	0.0448

(peak clipping) and time domain degradation of transient edges. Given the fact that the primary objective of this research involves the precise extraction of coil current features, preserving the signal's geometric integrity is essential.

The Savitzky-Golay filter is selected because it minimises the least squares error in fitting a local polynomial to each selected window of data. Unlike linear averaging, which acts as a low-pass filter that degrades high-frequency signal components (corners and peaks), the Savitzky-Golay method preserves the higher-order moments of the waveform. Consequently, it retains the true vertical amplitude of current peaks and the steepness of transient slopes, ensuring that the subsequent feature extraction stage is not compromised by filtering technique.

The comparison focused on waveform reconstruction before feature extraction. RMSE provided a common measure of agreement with the reference signal without depending on the segmentation and feature-detection procedure. A separate quantitative comparison of extracted features was not performed. Consequently, the results support the selection of Savitzky–Golay based on waveform agreement among the tested configurations, while its comparative accuracy for estimating individual peak currents and event timings remains unverified.

3.2.4 Defect Emulation Scenarios

To train the supervised learning ML models discussed in Section 3.5, specific classes of defects were implemented in the emulator. Fig. 36 demonstrates the comparative waveforms for these defect scenarios against a healthy baseline signal. The following defect categories were implemented based on common failure modes identified in the literature [14]:

1. **Supply voltage deviations:** The DC supply voltage to the coil was varied to simulate substation battery issues or loose connections in the supply circuit. Tests were conducted at voltage levels of $\pm 10\%$ and $\pm 20\%$ relative to the nominal voltage.

    - *Effect:* Voltage variations directly impact the electromotive force, shifting the current curve and altering peak magnitudes and timing parameters (T_{P1}, T_L,I_{P1}, and I_{P2}). In the signals generated by the emulator, the induced changes across these parameters are approximately up to 22 percent in comparison to the normal scenario.

2. **Latch mechanism defects:** Mechanical issues within the latching system, such as friction (stiffness), were simulated.

    - *Effect:* A stiff latch delays the plunger movement, increasing the excitation time (T_{P1}), latching time (T_L) and the total energising time (T_E). Conversely, a soft latch may lead to premature actuation. In the signals generated by the

emulator, the induced changes across these parameters approximately up to 10 percent in comparison to the normal scenario.

3. **Auxiliary contact malfunctions:** Issues with the auxiliary switch, which cuts off the coil current once the operation is successfully initiated, were emulated. This includes contact bouncing or delays in actuation.

    - *Effect*: These defects manifest primarily in the tail of the current waveform, affecting the cut-off timing (T_{P2}) and the decay profile (T_E). In the signals generated by the emulator, the induced changes across these parameters approximately up to 12 percent in comparison to the normal scenario.

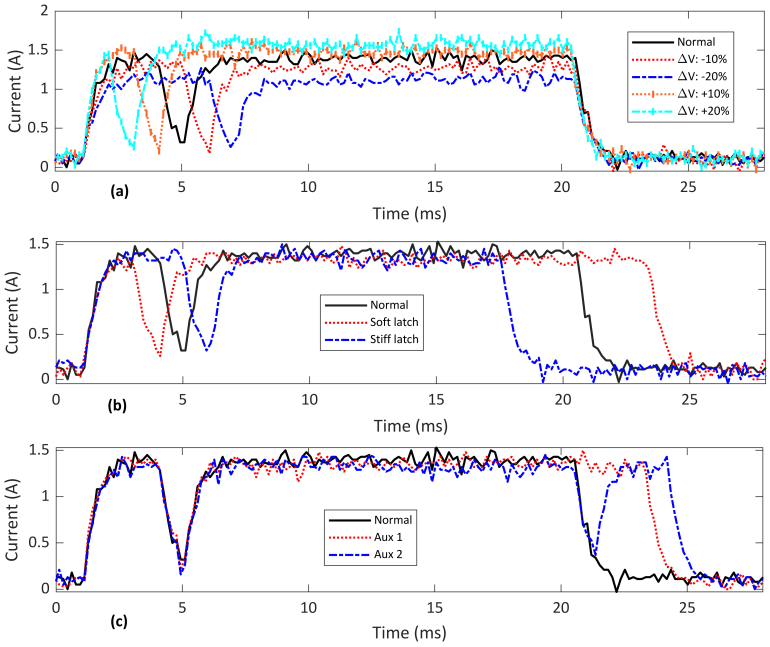


Figure 36: Illustration of the effects of various defects on the coil current waveform: (a) supply voltage, (b) latch operation, (c) auxiliary contact.

3.3 Feature Extraction Framework

The extraction of diagnostic features from the coil current signature is a critical step in the proposed condition monitoring framework. While the Savitzky-Golay filter effectively suppresses noise, the automated identification of key kinematic points (e.g., plunger actuation, latching, buffer impact) requires a segmentation algorithm. The feature extraction process utilises a segmentation strategy driven by cumulative maximums and percentage changes. This approach is designed to be resilient to the signal fluctuations inherent in low-cost sensors. The feature extraction workflow processes the digitised signal $x(t)$ through the following sequential stages:

- **Savitzky-Golay filtering:** To smooth the signal without distorting the peaks, a Savitzky-Golay filter is applied. The core of the extraction logic relies on the cumulative maximum vector, $C_{max}(t) = \max(x(1), \ldots, x(t))$, which at any given time point t,

$C_{max}(t)$ holds the highest current value observed in the signal up to that moment. By calculating the relative percentage change of C_{max}, the algorithm identifies stable plateaus and rising edges. The signal is mapped into 6 critical points (see Fig. 37 (d)).

- **Excitation phase (points 1-2):** Point 1 represents the start of the current rise, detected as the first non-zero percentage change in C_{max}. Point 2 marks the end of the first rise (First Peak I_{P1}), identified where the percentage change returns to zero.
- **Plunger movement (point 3):** The local minimum between the two peaks is found by searching for the minimum value in a defined search window (approx. 100 samples) following point 2.
- **Latching and saturation (points 4-5):** The second rise (I_{P2}) is detected using a renewed cumulative max search starting from point 3. Point 5, representing the end of the saturation plateau (Auxiliary contact cutoff), is identified using a reverse-time search on the flipped signal to detect the sharp drop off.
- **De-energisation (point 6):** This point marks the instant that the current returns to zero, detected via the reverse cumulative maximum of the falling edge.

Fig. 37 illustrates the above mentioned stages of the feature extraction. Physically, these discrete points represent a highly specific sequence of electromechanical events. The excitation phase begins at Point 1 when the coil is energised. The current rises to the first peak at Point 2 (I_{P1}, T_{P1}), marking the exact moment the magnetic force overcomes mechanical inertia and the plunger begins to move. As the plunger travels, the changing magnetic reluctance induces a back electromotive force, causing the current to dip to a local minimum at Point 3 (T_L), which indicates the completion of the plunger's stroke and operation of the latching mechanism. The current then rises to a steady-state saturation plateau beginning at Point 4. Point 5 marks the operation time of the auxiliary contact, which cuts off the circuit to protect the coil from overheating (T_{P2} is the amplitude at median of point 4 and 5). Finally, Point 6 (T_E) corresponds to the complete de-energisation of the circuit when the current returns to zero.

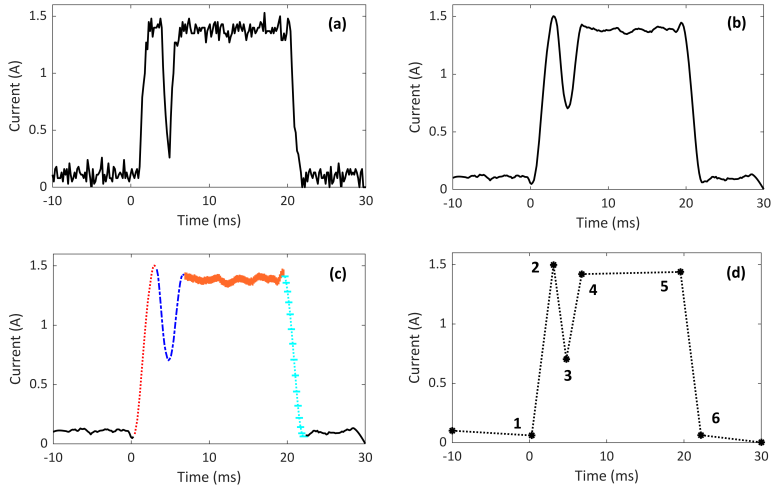


Figure 37: Trip/close coil current signal feature extraction process. (a) Raw measurement. (b) Filtered signal. (c) Segmentation. (d) Extracting critical points.

3.4 Selection of Savitzky-Golay Parameters

The performance of the Savitzky-Golay filter is sensitive to its hyperparameters, namely the polynomial degree (p_{deg}) and the window length (W_{len}). Improper selection can lead to either insufficient noise rejection (under smoothing) or the attenuation of critical diagnostic features (over smoothing). To determine the optimal parameters, a sensitivity analysis is conducted using a coil current signal containing an auxiliary contact defect. The results in Fig. 38 indicate that while a first-degree polynomial oversimplifies the data, excessively high degrees can lead to overfitting, introducing artificial oscillations and amplifying the noise. Consequently, a third-degree polynomial is selected as it provides the most effective compromise between capturing transients and reducing noise. Moreover, the impact of window size is examined, noting that while smaller windows preserve finer details, they fail to sufficiently eliminate noise. Conversely, large windows, such as those spanning 40 samples, tend to over-smooth the data and hide essential transitions.

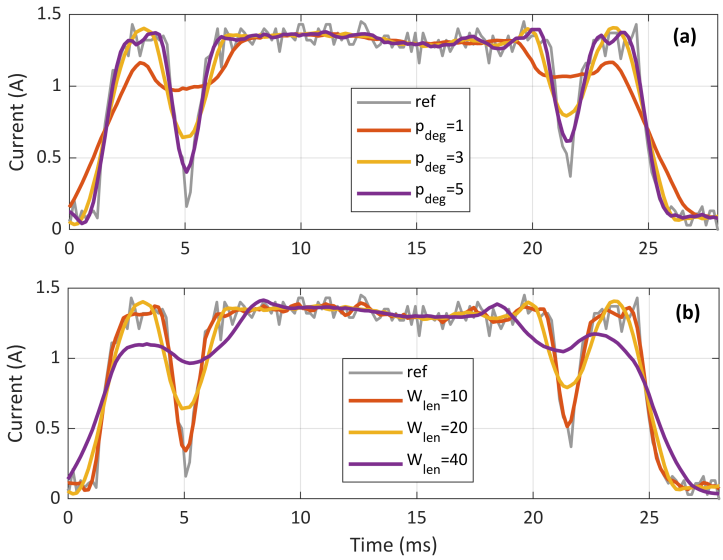


Figure 38: Sensitivity analysis of the Savitzky-Golay parameters. (a) Effect of polynomial degree variation by constant window size (W_{len} = 20). (b) Effect of window size variation by constant polynomial degree (p_{deg} = 3).

By testing various configurations, it is determined that a sample window of 20, paired with a third-degree polynomial, offers the ideal balance for this specific signal. However, because these settings are derived empirically, they may need to be calibrated for other datasets if there are notable changes in the sampling rate, noise levels, etc.

3.5 Machine Learning Classification Methodology

Once the features ($I_{P1}, T_{P1}, I_{P2}, T_{P2}, T_L, T_E$) are extracted, they serve as the input vector for defect classification. In this thesis, a supervised learning approach has been utilised to categorise the breaker's condition into four classes: normal, supply voltage defect, latch defect, and auxiliary contact defect. To classify the condition of the HVCB into the aforementioned states, four supervised learning algorithms are evaluated. In supervised learning, the model is trained on a labelled dataset, learning the mapping between input features and known output classes to predict the category of new, unseen data.

The specific methods are briefly described as follows:

- **K-nearest neighbours (KNN):** KNN is a simple, instance-based algorithm that classifies a new data point based on the majority class of its neighbours. It calculates the distance between the new point and all points in the training set, selects the k closest neighbours, and assigns the most common class among them to the new point.
- **Decision trees:** This method splits the data into subsets based on the value of the input features. It creates a tree-like structure where each internal node represents a test on a feature, each branch represents the outcome of the test, and each leaf node represents a final class label.
- **Logistic regression:** Despite its name, this is a classification algorithm used to estimate the probability that a given instance belongs to a particular class. It models the relationship between the features and the categorical outcome using a logistic function, outputting a value between 0 and 1, where a threshold is then set to assign a class label.
- **Support vector machines (SVM):** SVM finds the optimal boundary (hyperplane) that best separates the different classes in the feature space. The algorithm aims to maximise the margin, which is the distance between the boundary and the nearest data points of each class, to improve the classification accuracy on future data.

The results of the supervised classification models, decision trees, logistic regression, KNN, and SVM, are presented in this section [6]. The models were evaluated based on their ability to classify coil current signals into normal and defective states, as well as to distinguish between different defect categories. The performance of each model is summarised using accuracy and a confusion matrix. The accuracy points out the percentage of observations that are correctly classified. Additionally, the true positive ratio (TPR) and false negative ratio (FNR) for each class of defects are presented next to the confusion matrices, Fig. 39 to Fig. 42. The dataset consisted of 112 measurement signals obtained from the coil current emulator. The data has been split into $\approx$80% for training (90 signals) and $\approx$20% for testing (22 signals).A five-fold cross-validation scheme was used during training to assess generalisation within the emulator dataset and reduce dependence on a single data split.

Table 7 summarises the training and testing accuracy of the four algorithms. The comparative analysis of the models highlights the strengths and weaknesses of each approach, considering their accuracy and training time. The logistic regression and SVM provided were not able to perform classification at an acceptable level, considering their high training time. KNN outperformed the other models in terms of accuracy. The KNN algorithm effectively groups the multi-dimensional feature vectors based on Euclidean distance, making it highly suitable for the distinct clusters formed by the different HVCB defect types in the feature space. However, as expected, its training time is slightly higher than the rest of the models. It is assumed that the training process occurs offline in this study. Therefore, accuracy has a higher priority than the training time.

3.6 Feature Importance Specification via SHAP

To examine the contribution of individual features to the KNN classifier outputs, Shapley additive explanations (SHAP) were employed. Fig. 43 presents the resulting global feature importance plot, which quantifies the mean absolute SHAP value for each feature, broken down by its contribution to detecting specific classes (Auxiliary, Latch, Normal, and Voltage).

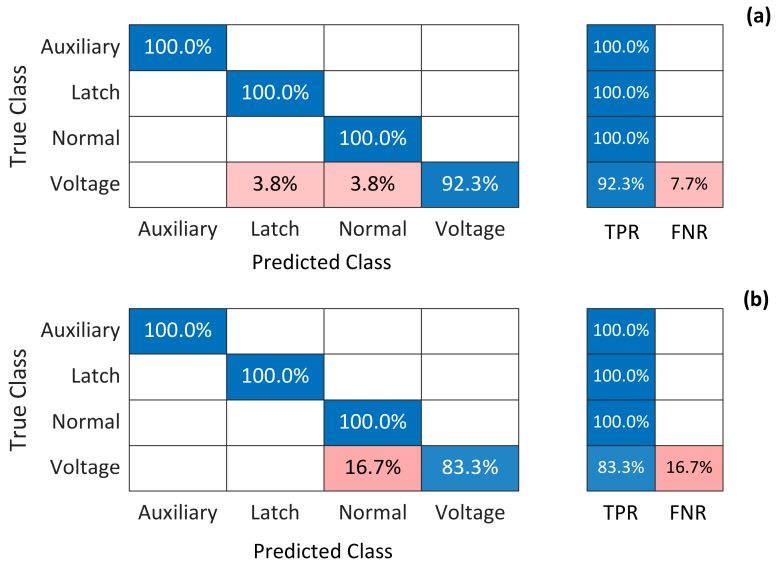


Figure 39: Confusion matrix, TPR, and FNR of the kNN model: (a) Training validation, (b) Testing

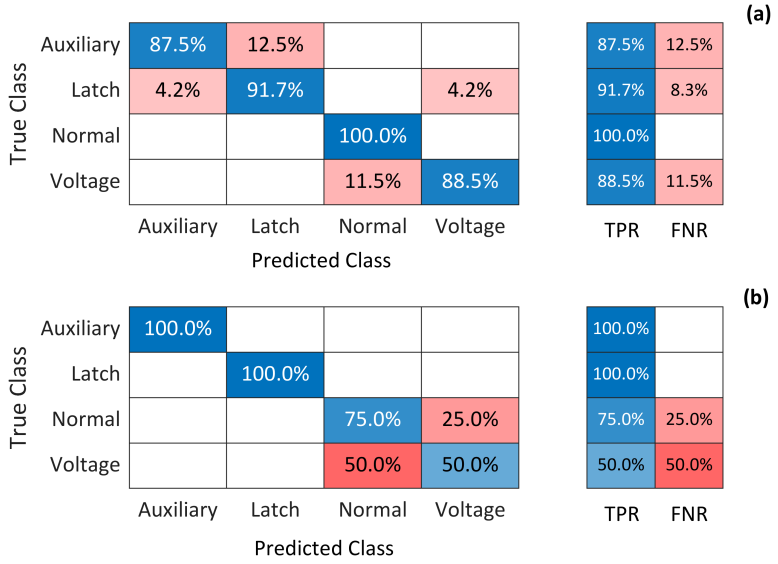


Figure 40: Confusion matrix, TPR, and FNR of the decision tree model: (a) Training validation, (b) Testing

As observed in the SHAP analysis results, the timing parameters exhibit the highest global influence on the model's predictions. Specifically, the excitation time (T_{P1}), followed by the auxiliary contact operation time (T_{P2}) and the total energising time (T_E), are the most significant features. This dominance suggests that temporal shifts are the primary indicators of mechanical degradation in the coil assembly rather than purely current amplitude variations. Moreover, the stacked bar chart reveals distinct correlations between specific features and defect types, confirming that the model has learnt the physically relevant diagnostic rules:

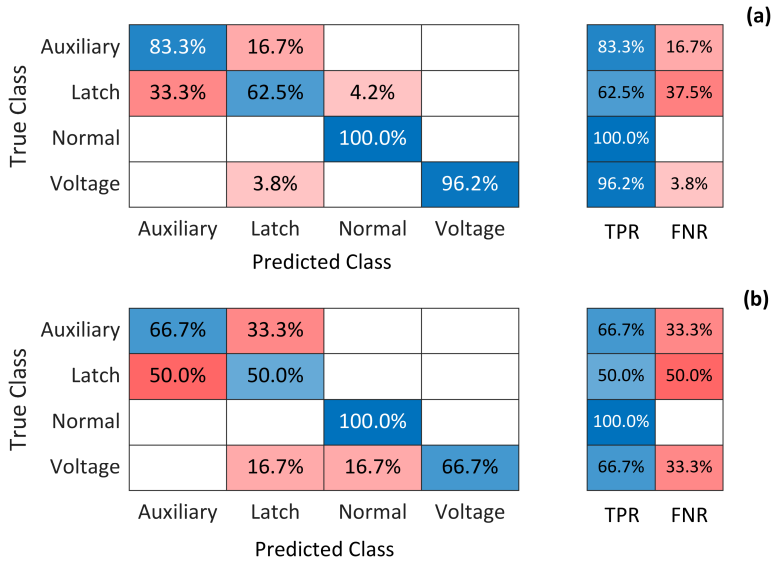


Figure 41: Confusion matrix, TPR, and FNR of the logestic regression model: (a) Training validation, (b) Testing

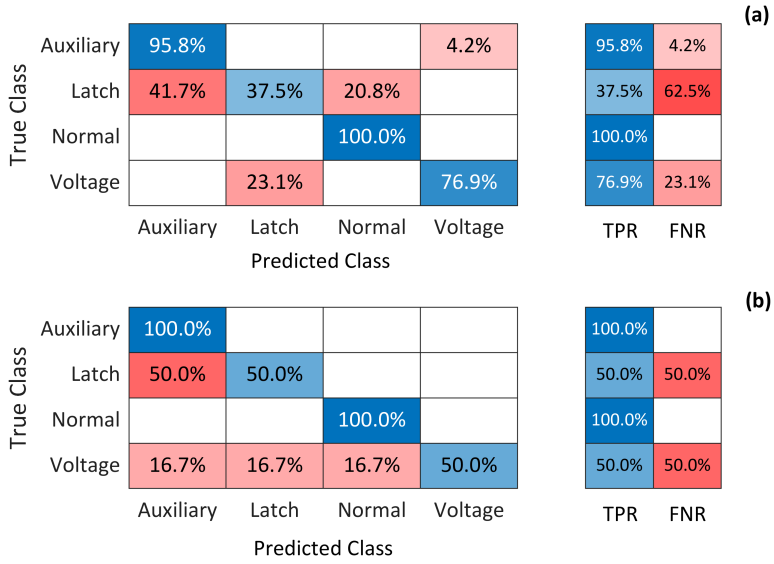


Figure 42: Confusion matrix, TPR, and FNR of the SVM model: (a) Training validation, (b) Testing

- **Auxiliary contact defects:** The detection of auxiliary defects (represented by the blue segments) is overwhelmingly driven by T_{P2} and T_E. This aligns perfectly with the physical reality, as defects in the auxiliary switch or linkage directly alter the moment of current cutoff (T_{P2}) and the overall duration of the coil current signal (T_E).

- **Supply voltage defects:** While timing remains important, the supply voltage defects (represented by the purple segments) show a comparatively higher reliance on

Table 7: Comparison of ML-based algorithms for classification of coil current defects

Model	Training accuracy (%)	Test accuracy (%)
KNN	97.78	95.46
Decision tree	91.11	81.82
Logistic regression	84.44	68.18
SVM	75.56	72.73

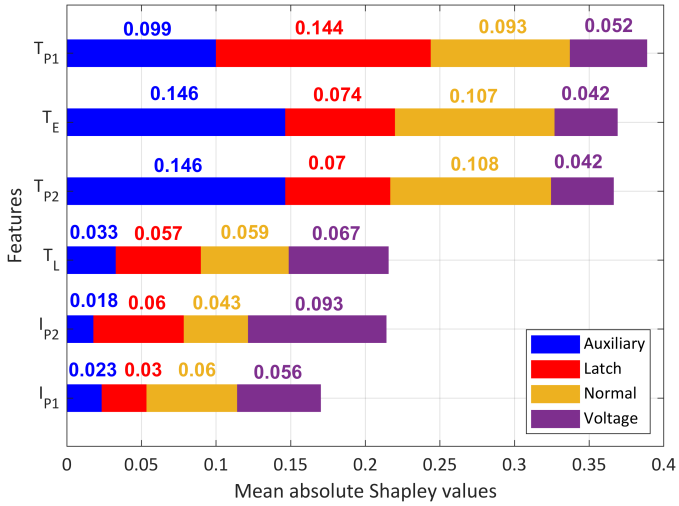


Figure 43: Global feature importance plot showing the mean absolute Shapley values for each class

current amplitude features such as the first peak current (I_{P1}) and second peak current (I_{P2}) compared to other defect types.

- **Latch mechanism defects:** The classification of latch defects (represented by the red segments) is notably influenced by T_{P1} (excitation time) and T_E (total energising time). Since latch friction or stiffness retards the plunger's initial movement, it logically impacts the time required to reach the first peak.

This analysis confirms that the automated system relies on physically meaningful variations in the coil signature rather than fitting to noise artefacts.

3.7 Signal Comparison via Dynamic Time Warping

The Euclidean distance serves as a fundamental metric for quantifying the similarity between discrete time-series datasets. This method operates on the premise that the compared sequences possess identical lengths and are strictly synchronised in the time domain. For two given time series, $X = [x_1, x_2, \ldots, x_n]$ and $Y = [y_1, y_2, \ldots, y_m]$, the Euclidean distance (d) is defined as:

$$d(X,Y) = \sqrt{\sum_{i=1}^{n}(x_i - y_i)^2} \tag{13}$$

Calculating the Euclidean distance between a reference healthy coil current signature and a monitored signal allows for a preliminary assessment of the HVCB's condition. Fig. 44-

(a) illustrates the comparison between two healthy operation signals (designated as Normal-A and Normal-B) following noise suppression via the Savitzky-Golay filter. In this ideal scenario, where the measurements are temporally aligned, the calculated distance is minimal. Conversely, Fig. 44-(b) depicts the deviation observed when a healthy signal is compared against a defective case, specifically a stiff latch mechanism. Under the assumption of perfect alignment, the metric effectively highlights the disparity caused by the defect.

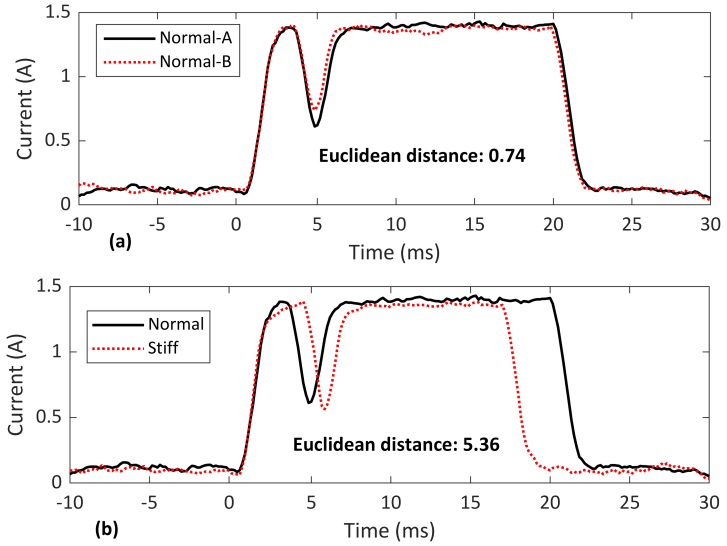


Figure 44: Euclidean distance assessment between filtered coil current signals: (a) comparison of two healthy signals; (b) comparison between a healthy and a defective signal.

To validate the discriminatory power of this metric, an extensive experimental evaluation was conducted using the coil current emulator. Fig. 45 aggregates the Euclidean distance results for a normal reference signal compared against 20 samples of healthy operations and 20 samples for each defect category. The results indicate that a distinct separation boundary exists between healthy and faulty operations. Based on these experimental findings, a threshold value of 1.8 can be established to segregate normal operating conditions from potential defects (threshold line in Fig. 45). Thus, in idealised conditions, Euclidean distance provides a computationally efficient means of fault detection.

However, field measurements of HVCBs may include temporal misalignment. In such cases, the standard Euclidean distance may yield erroneous high values solely due to misalignment. To mitigate this, DTW is utilised, which is an optimisation algorithm capable of measuring the similarity between two temporal sequences that may vary in speed or phase [60, 61]. Simpler alternatives include alignment using the recorded operating command or estimation of a constant time shift through cross-correlation. These methods may be sufficient when the discrepancy is limited to an overall recording offset. DTW provides additional flexibility by allowing local temporal alignment between corresponding waveform segments. However, local timing differences may also indicate mechanical defects, so alignment should preserve their diagnostic significance. The present study demonstrates the benefit of DTW relative to unaligned Euclidean comparison, but does not establish its superiority over simpler alignment methods.

DTW functions by non-linearly warping the time axis of one sequence to achieve

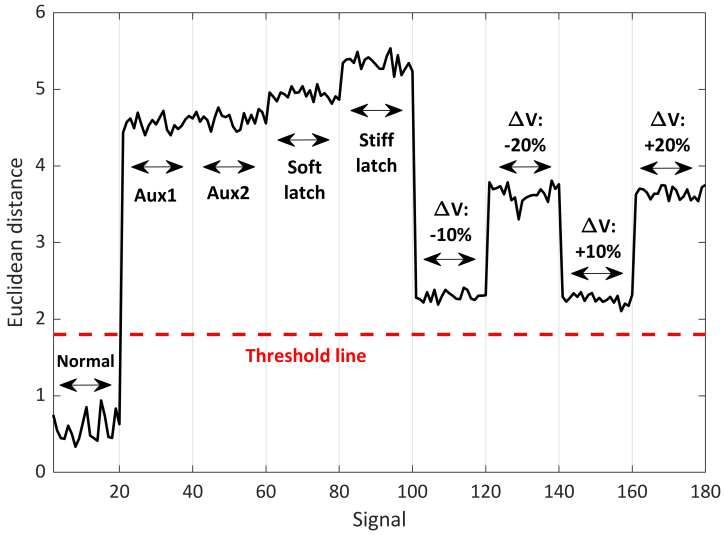


Figure 45: Euclidean distance metrics comparing a reference normal signal against various healthy and defective sample groups.

optimal alignment with the other, thereby minimising the cumulative distance. The DTW cost matrix D between sequences X and Y is constructed recursively as follows:

$$D(i,j) = d(x_i, y_j) + \min\{D(i-1,j), \ldots \\ D(i,j-1), D(i-1,j-1)\} \tag{14}$$

where $d(x_i, y_j) = |x_i - y_j|$ represents the local Euclidean distance between points x_i and y_j. The calculation is constrained by the following boundary conditions:

$$D(0,0) = 0, \quad D(i,0) = \infty, \quad D(0,j) = \infty \tag{15}$$

The optimal alignment path is retrieved by backtracking from the terminal position $D(n,m)$ to the origin.

Given its ability to handle temporal shifts, DTW is particularly advantageous for analysing coil current signatures. Fig. 46 demonstrates the necessity of this technique. In Fig. 46-(a), two healthy signals are compared using the standard Euclidean distance. Due to a temporal offset, the calculated distance is 5.53, which significantly exceeds the previously established threshold of 1.8, leading to a false positive classification of “Normal-B” as defective. However, when the same signals are aligned via DTW as shown in Fig. 46-(b), the distance reduces to 0.36. This value falls well within the healthy range, noting that the acceptance threshold is adjusted (e.g., to 0.6) when utilising the DTW-aligned domain.

In this proposed framework, DTW is implemented as a secondary validation stage. By integrating the Euclidean distance for initial screening with DTW for detailed alignment, the system achieves greater diagnostic performance. Specifically, DTW verifies whether a high distance value indicates a genuine morphological defect or merely a trivial temporal shift.

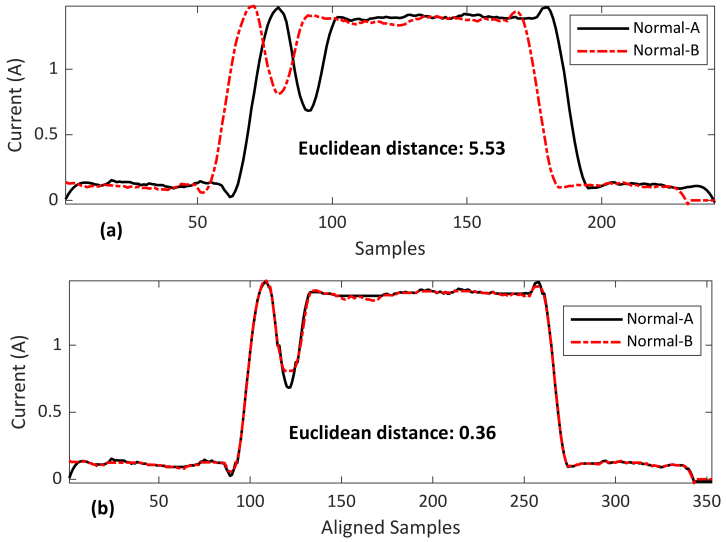


Figure 46: Impact of DTW on signal alignment: (a) misaligned normal signals yielding high Euclidean error; (b) signals aligned via DTW revealing true similarity.

3.8 Proposed Monitoring Framework

The proposed processing sequence is synthesised in the flowchart presented in Fig. 47. This diagram details the sequential logic for real-time condition assessment. The process begins with signal acquisition and noise suppression via the Savitzky-Golay filter. Primary screening is performed using the Euclidean distance in comparison to the reference signal. If the signal deviates beyond the safety threshold, a secondary DTW analysis is triggered to correct for potential time shifts. If the signal remains non-compliant after alignment, it is flagged as defective. The system then proceeds to feature extraction and ML-based classification to identify the specific fault mode. Conversely, signals falling within the thresholds at either stage are classified as healthy.

3.9 Mathematical Modelling of Health Index

The HI is a composite indicator that condenses complex diagnostic data into a single quantitative metric, facilitating decision-making for asset managers. This section demonstrates a mathematical model for HI calculation based on condition monitoring measurements. These measurements may include, i.e., vibration signal, spring charging motor current, coil current, etc. This thesis only focuses on the coil current measurements. Although the measurement type and signal preprocessing techniques might vary for each measurement, the framework is applicable to all of them.

From the preprocessed coil current signal, a vector of critical features $X = [x_1, x_2, ..., x_n]$ is extracted. As mentioned before, these features include first peak current (I_{P1}), the excitation time (T_{P1}), the second peak current (I_{P2}), the auxiliary contact operation time (T_{P2}), the latching time (T_L), and the total energisation time (T_E).

3.9.1 Feature Normalisation

To aggregate features with different physical units, e.g., Amperes, seconds, etc., a normalisation function is applied to map each feature x_i to a dimensionless health score $C_i \in [0, 1]$

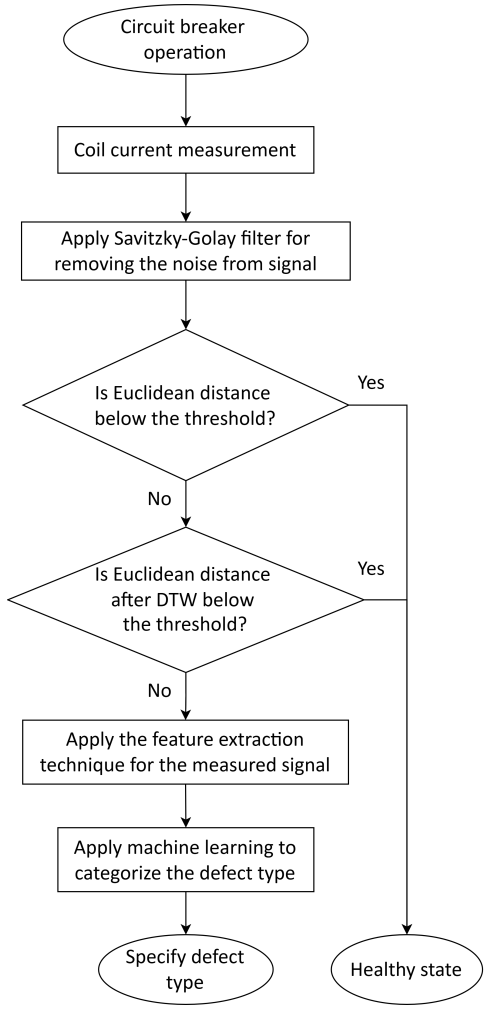


Figure 47: Operational flowchart for the automated detection and classification of HVCB defects.

[47]. A modified Gaussian membership function is utilised for this purpose:

$$C_i = \exp\left(-\frac{(x_i - r_i)^2}{s_i^2}\right) \tag{16}$$

where $r_i = \frac{H_i+L_i}{2}$, $s_i = \frac{H_i-L_i}{2}$, C_i is the normalised value of the ith feature of the condition monitoring measurement, x_i is the ith observed feature, H_i and L_i are upper and lower limits of the ith feature, respectively. The normalised parameter will have a value between 0 and 1. In this model, a C_i value of 1 represents a perfect health state (feature matches the reference), while values approaching 0 indicate a severe deviation. Moreover, both lower and upper limits correspond to the same limit value of the normalised parameter as follows ($x_i = H_i$ or $x_i = L_i$):

$$\tau = C_i(L) = C_i(H) = exp(-1) \tag{17}$$

3.9.2 Overall Health Index Calculation

For each extracted feature, a sub-HI can be calculated based on its deviation from a baseline value or established thresholds. Assuming that the baseline values are known, we can define HI for each feature as follows using (16):

$$HI_i = C_i \tag{18}$$

where the value of τ in (17) serves as a basis for deciding whether the condition falls within the normal or abnormal range. As demonstrated in Fig. 48, considering the fact that HVCBs are composed of multiple components operating in series, the failure of a single critical subcomponent (e.g., a latch) leads to the failure of the entire breaker. Therefore, averaging health scores can mask critical defects.

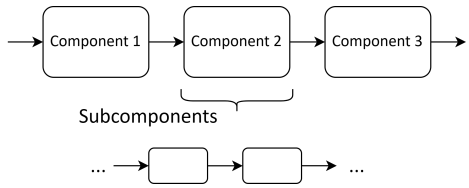


Figure 48: Block diagram of the HVCB components connection

This research proposes adopting a "worst-case" or "weakest link" approach. The overall HI (HI_{HVCB}) is defined as the minimum of all sub-indices:

$$HI_{HVCB} = \min_{\forall j}\{\min_{\forall i}(HI_{i,j})\} \tag{19}$$

where i iterates through features of a single measurement type, and j iterates through different diagnostic methods (e.g., coil current, vibration, etc.). Figure 49 summarises this calculation methodology.

3.9.3 Case Study: Reliability-Based Maintenance Scheduling

The ultimate utility of the HI is related to its application for RCM. By correlating the HI with failure probability, maintenance schedules can be optimised to maximise system reliability while minimising costs. The failure rate of an HVCB is not constant but evolves with condition and age. Drawing upon the methodology established in [47], it is postulated that the HI, derived from normalised condition monitoring parameters, follows an exponential relationship with the effective operating age of the HVCB. This correlation is mathematically expressed as:

$$\begin{aligned} 1 - HI_{HVCB} &= Ae^{Bt_{op}} + E \\ t_{op} &= \frac{1}{B} ln\left(\frac{1 - HI_{HVCB} - E}{A}\right) \end{aligned} \tag{20}$$

where t_{op} represents the effective operating age of the HVCB. The coefficients A, B, and E are determined via nonlinear parameter estimation techniques, utilising a dataset that combines measured condition parameters with the chronological ages of a population of similar HVCBs (categorised by manufacturer, voltage class, etc.).

Once the effective operating age is derived, the failure rate and cumulative probability of failure can be approximated by fitting the data to a lifetime model. Lifetime models are

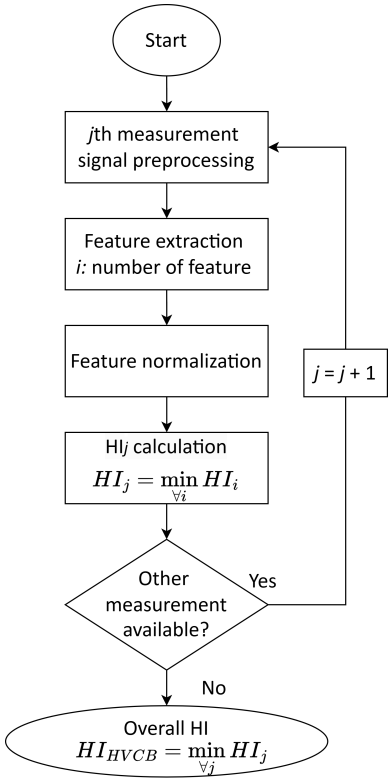


Figure 49: Flowchart of the overall HI calculation for HVCB.

generally classified as either nonparametric or parametric. Nonparametric approaches, such as the Kaplan-Meier estimator, do not presume a specific functional form for the underlying distribution. Conversely, parametric models fit the data to known distributions, such as the exponential or Weibull distributions [62]. In the context of asset management, the Weibull distribution is often favoured due to its versatility. Unlike the exponential model, which implies a constant hazard rate, the Weibull distribution is capable of representing the varying failure kinetics (decreasing, constant, or increasing failure rates) characteristic of different lifecycle stages.

Accordingly, this case study adopts the Weibull distribution to define the failure probability function, $F(t)$, and the failure rate, $\lambda(t)$, for ageing-related failures [47]:

$$F(t_{op}) = 1 - exp\left(-\left(\frac{t_{op}}{\eta}\right)^{\nu}\right)$$
$$\lambda(t_{op}) = \frac{\nu}{\eta}\left(\frac{t_{op}}{\eta}\right)^{\nu-1} \tag{21}$$

where ν denotes the shape parameter and η denotes the scale parameter. These parameters are typically resolved using the least squares method. Utilising this framework, the specific failure metrics of an HVCB can be estimated directly from its calculated HI.

To demonstrate the practical implications of utilising HI-based failure rate estimation in

power system reliability analysis, a simplified case study is presented. The network model, illustrated in Fig. 50, consists of two HVCBs (B_1 and B_2) supplying distinct load points, L_1 and L_2, respectively. The objective is to determine the maintenance priority of these breakers within an RCM framework, utilising the energy not supplied (ENS) index as the decision criterion.

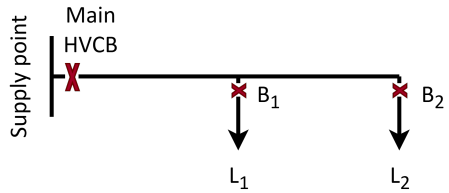


Figure 50: Diagram of the network being analysed

Scenario I: Maintenance Prioritisation using Average Failure Rates

Standard maintenance protocols often rely on population-based statistics. In this scenario, a constant, average failure rate is applied to both HVCBs, regardless of their individual condition. The maintenance priority is determined by the ENS, where a higher ENS signifies a more critical impact on system reliability. The calculation is based on the following system parameters:

$$\begin{aligned} &\lambda = 0.011\ [f/year], && \text{equal for both HVCBs} \\ &r = 90\ [h/repair], && \text{equal for both HVCBs} \\ &U = \lambda \times r && U = 0.99\ [h/year] \\ &L_1 = 8.4\ [MW], && L_2 = 10\ [MW] \end{aligned} \tag{22}$$

Calculating the ENS as $ENS_i = U_i \times L_i$ (assuming an otherwise ideal network), yields $ENS_1 = 8.3\ [MWh/year]$ and $ENS_2 = 9.9\ [MWh/year]$. Under this conventional approach, B_2 is deemed critical and is assigned a higher maintenance priority due to the larger load it serves.

Scenario II: Maintenance Prioritisation using HI-Based Failure Rates

This scenario integrates the specific health condition of each asset into the analysis. The failure rates are derived dynamically using equations (16) through (21), with the HI calculated from coil current. Utilising the condition monitoring parameters detailed in [47], the specific operating age, HI, and resulting failure rates for both breakers are summarised in Table 8. Retaining the repair time and load assumptions from Scenario I, the recalculated indices are $ENS_1 = 12.1\ [MWh/year]$ and $ENS_2 = 10.8\ [MWh/year]$. Contrary to the previous scenario, the condition-aware analysis indicates that B_1 presents a higher risk and should arguably receive maintenance priority.

The comparison between the two scenarios highlights the impact of detailed condition data on asset management. While B_1 and B_2 may share similar chronological ages or population characteristics, their actual degradation levels diverge, as captured by the HI. In this case, the breaker with the lower HI (B_1) exhibits a sufficiently higher failure probability to outweigh the larger load factor of B_2. This demonstrates that integrating HI-based failure rates into the RCM scheme enables the more precise allocation of maintenance resources,

Table 8: HVCBs operating age, HI, and failure rate [47]

HVCB	Operating age (years)	HI	λ (f/year)
$\mathbf{B}_1$	26.01	0.7628	0.016
$\mathbf{B}_2$	23.4	0.8	0.012

therebychanging the maintenance ranking in the illustrative example than relying solely on average statistical data.

3.10 Proposed Enhancements and Practical Implementation

While the core diagnostic framework has been theoretically established and validated in a laboratory setting, there is significant potential to expand its robustness and applicability in real-world scenarios. This section describes two main directions for building upon the current work: the deployment of the measurement solution in a real-time digital substation environment and the refinement of the HI to explicitly account for measurement uncertainty.

3.10.1 Real-Time Validation via Hardware-in-the-Loop Frameworks

To transition the developed condition monitoring strategies from experimental validation to industrial application, a realistic testing framework is required. A HIL simulation provides the necessary environment to evaluate monitoring solutions under dynamic grid conditions without the risks associated with live high-voltage tests.

Fig. 51 demonstrates the proposed implementation which integrates an RTDS with the physical HVCB and the developed measurement system. This setup has been implemented by the available equipment in Taltech's high-voltage laboratory. In this setup, the RTDS models the power grid and generates control signals (trip/close commands), which are transmitted via fibre optic links to a digital output card. This card interfaces with the HVCB control unit to trigger actual mechanical operations. Simultaneously, the coil current is captured by the measurement device (e.g., Raspberry Pi with ACS712 current sensors) and processed in real-time.

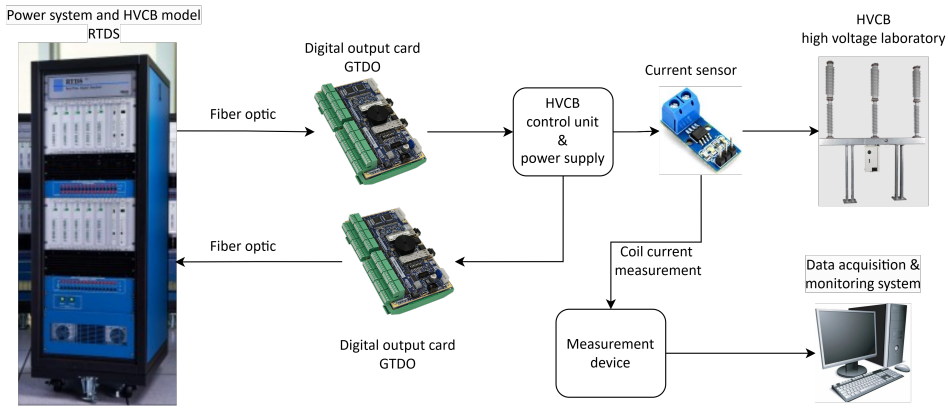


Figure 51: Schematic of the experimental setup

Based on the setup presented in Fig. 51, healthy coil current measurements of a 110 kV HVCB were collected using the same measurement setup proposed in this thesis. The subsequent processing steps, including denoising of the raw signal and extraction of the relevant features, are illustrated in Fig. 52.

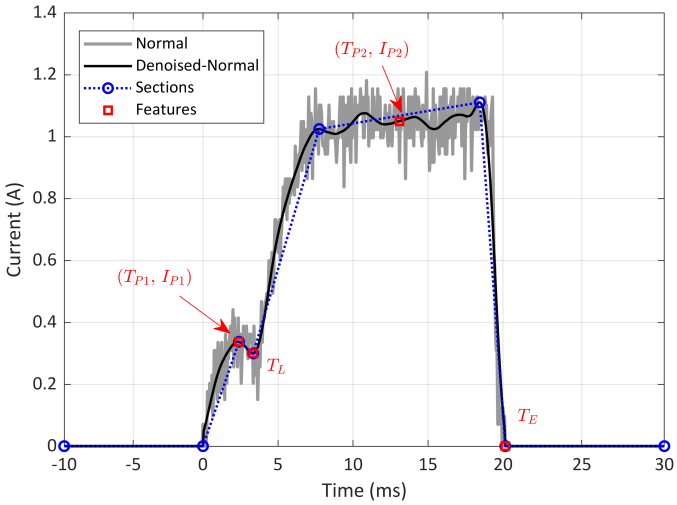


Figure 52: Feature extraction from a real coil current measurement (110 kV circuit breaker).

This HIL approach allows for the safe emulation of various fault scenarios and grid conditions, providing a controlled testbed for evaluating latency, measurement performance, and algorithm behaviour before field trials.

3.10.2 Integration of Measurement Accuracy into the Health Index

Current HI models often treat all measurement data with equal confidence. However, in practice, data sources vary significantly in precision; offline diagnostic tests performed with calibrated laboratory equipment are generally more accurate than continuous online monitoring data, which may be subject to sensor noise and environmental interference.

To address this, future iterations of the HI model should mathematically incorporate measurement uncertainty. A proposed method is to fuse the HI derived from online monitoring (HI_i^{on}) with that obtained from periodic offline monitoring (HI_i^{of}). This dynamic combination can be governed by an update function that weights each source based on its inherent accuracy and the temporal relevance of the offline data:

$$HI_i^{updated}(t) = \frac{HI_i^{on} \cdot \alpha^2 + HI_i^{of} \cdot \beta^2 \cdot f(t)}{\alpha^2 + \beta^2 \cdot f(t)} \tag{23}$$

where α and β ($0 \leq \alpha, \beta \leq 1$) represent the accuracy coefficients for the online and offline measurement systems, respectively. The term $f(t)$ serves as a temporal decay factor, reducing the reliance on offline data as the time t since the last test increases. A proposed model for this decay is an exponential function:

$$f(t) = \exp\left(\frac{-t}{\gamma}\right) \tag{24}$$

where γ controls the rate of decay. This parameter should be calibrated such that as t approaches the next scheduled maintenance interval (ΔT), the weight $f(t)$ becomes

negligible. For example, setting $\gamma = \Delta T/2$ ensures that at the time of the next scheduled test ($t = \Delta T$), the influence of the previous offline measurement drops to approximately 10%, forcing the system to rely primarily on the most recent online data until new high-precision offline data becomes available.

3.10.3 Practical Implementation Framework for Transmission System Operators

The transition of the proposed condition monitoring methodology from a laboratory prototype to an industrial application requires a structured deployment strategy that addresses the operational constraints of TSOs. To ensure scalability and reliability, the practical implementation must focus on non-intrusive hardware integration, decentralised data processing, and seamless interoperability with existing asset management systems.

Hardware Installation

A primary advantage of the proposed coil current monitoring system is its compatibility with legacy infrastructure. Unlike invasive diagnostic techniques that require dismantling the interrupter or gas handling, the sensors utilised in this research can be installed directly within the control cabinet of the HVCB. For field deployment, split core sensors are recommended, as they allow for installation around the trip and close coil circuitry without disconnecting existing wiring. The data acquisition unit, hardened for electromagnetic compatibility in substation environments, can be mounted on standard DIN rails within the cabinet, ensuring a compact footprint.

Edge Computing and Data Architecture

In a transmission network comprising hundreds of HVCBs, transmitting raw waveforms to a central server can impose significant bandwidth constraints and latency issues. Therefore, this framework proposes a decentralised edge computing architecture. The algorithms developed in this thesis, i.e., the Savitzky-Golay filtering, feature extraction, and KNN classification, are computationally efficient enough to be executed locally on the substation level monitoring device. By processing data at the edge, only the extracted diagnostic features, the calculated HI, and critical alarm status flags are transmitted to the control centre. This approach reduces data traffic by orders of magnitude while ensuring that actionable intelligence is available in real-time.

Integration with Asset Management Ecosystems

For the TSO, the value of condition monitoring is realised when diagnostic data informs decision-making. The output of the monitoring system should be integrated into the TSO's wider digital ecosystem through standard communication protocols. The calculated HI can be fed directly into the asset management system, dynamically updating the risk profile of each asset. This integration enables the shift from static TBM intervals to the RCM schedules proposed in Section 3.9.3. Furthermore, critical failure alarms (e.g., "latch defect detected") can be routed to the SCADA system to alert operators of immediate risks to system stability.

Scalability and Economic Viability

The financial feasibility of widespread condition monitoring is a critical factor for TSOs. Commercial analysers, while precise, are often cost-prohibitive for permanent installation on every breaker in the grid. The solution developed in this research, utilising low-cost sensors and open-source algorithmic frameworks, lowers the capital expenditure per monitored unit. This economic efficiency allows TSOs to move beyond monitoring only

critical interconnection points to achieving comprehensive observability across the entire transmission system, thereby minimising the risk of cascading failures originating from peripheral assets.

Practical Deployment

Fig. 53 illustrates a layered architecture for monitoring the condition of the HVCB within a power transmission network, showcasing the interaction between physical outdoor equipment and indoor data processing systems. The process begins with sensors placed on the coil or motor wires of the equipment, like the HVCB and disconnector, to capture operational currents and control commands. This captured information is then funnelled through a terminal to a data aggregator and an IoT device, which facilitates the data flow from the substation environment to an indoor office setting through a server.

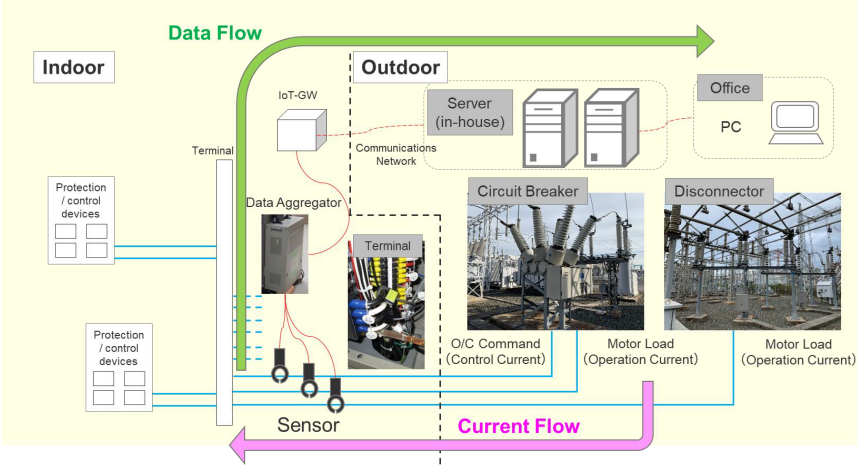


Figure 53: Layered architecture for the practical deployment of HVCB condition monitoring in a transmission network [63].

Conclusions and Further Work

Conclusions

The research presented in this thesis establishes a comprehensive framework for the transition from conventional TBM to a condition-aware asset management strategy for HVCBs. By integrating low-cost sensing technologies with proper signal-processing and ML methods, this work demonstrates that high fidelity diagnostics are achievable within the economic constraints of large-scale substation digitisation.

RQ 1 was addressed by proposing a Gaussian function-based formulation for estimating the RUL. The proposed model provided a closer fit to the available CIGRE MTTF data than the Weibull and exponential models within the observed age range of 2–22 years. The proposed normalisation approach also enabled published service-type failure frequencies to be incorporated as relative adjustments to the baseline ageing trajectory. However, due to the limited number of aggregated data points, the model should be regarded as an exploratory population-level representation rather than a validated predictor of the RUL of an individual HVCB. Extrapolation beyond the observed data range therefore requires further validation using more extensive utility-specific failure data.

To address **RQ2**, the developed emulator was used to acquire coil current signals representing healthy operation and controlled supply voltage, latching, and auxiliary contact defect conditions. The generated signals exhibited sufficiently consistent behaviour and distinguishable variations between the investigated conditions to support feature extraction, distance-based comparison, and supervised classification. This was reflected in the observed separation between the healthy and emulated abnormal signal groups and in the successful implementation of the ML algorithms. The results therefore support the use of the emulator as a laboratory platform for evaluating the proposed diagnostic algorithms. The proposed feature extraction methodology was subsequently applied to measurements obtained from a healthy real HVCB, where the characteristic coil current features were successfully identified. This provides preliminary evidence that the methodology is transferable from the emulator to a real HVCB under healthy operating conditions. However, defective signals from a real HVCB were not available. Therefore, the ability of the proposed methodology to identify defects in operational equipment needs to be experimentally validated.

To address **RQ3**, the coil current generated by the emulator was measured using both the low-cost ACS712 sensor and the TCP0030A reference probe. Following resampling, temporal alignment, and gain correction, several denoising methods were evaluated. Among the investigated methods, the Savitzky–Golay filter provided the lowest waveform error while retaining the characteristic peaks and transitions required for feature extraction. The processed low-cost sensor signals were subsequently used in the feature extraction and classification framework for the emulated operating conditions. These results indicate that appropriate signal preprocessing can improve the suitability of low-cost current measurements for the proposed methodology under the investigated laboratory conditions.

To address **RQ4**, DTW was used alongside Euclidean distance to distinguish temporal misalignment from genuine waveform deviations in the processed coil current signals. The results showed that DTW can reduce erroneous indications caused by time shifts between similar signals, thereby providing a useful validation stage before defect classification. The extracted features were subsequently used with supervised ML classifiers, among which the KNN model achieved the best performance for the investigated emulator dataset. These findings support the combined use of temporal alignment and ML-based classification within the proposed condition-monitoring framework.

Overall, this thesis addresses complementary levels of HVCB assessment, ranging from population-level ageing analysis to condition-aware evaluation based on individual coil current measurements. The proposed service-type adjustment provides a means of accounting for differences in application when interpreting MTTF trends, while the coil current framework demonstrates how low-cost measurements, signal processing, feature extraction, DTW, and ML classification can be applied to laboratory-based condition assessment. The proposed HI formulation further provides a means of incorporating diagnostic results, measurement accuracy, and maintenance information into asset-management decisions. These contributions form elements of a decision-support framework for HVCB maintenance, subject to further validation using utility and field data.

Future Work

As the experimental results were obtained mainly from laboratory and emulated datasets, further work should prioritise validation using measurements from operational substations. A larger field dataset containing both healthy and defective HVCB operations would allow the repeatability, diagnostic performance, and transferability of the proposed methods to be assessed under realistic operating conditions.

The long-term performance of low-cost sensor nodes should also be evaluated under the thermal and electromagnetic conditions encountered in substations. This should include the assessment of sensor drift, calibration requirements, measurement uncertainty, and communication reliability.

Further research may consider combining coil current measurements with complementary diagnostic signals, such as vibration and spring-charging motor current. Such sensor fusion could provide a broader representation of the electrical and mechanical condition of the HVCB and reduce dependence on a single measurement source.

The implementation of feature extraction, DTW, and classification algorithms on edge devices should also be investigated. Local processing could reduce communication requirements and support near-real-time condition assessment, although maintenance decisions should remain subject to appropriate operational verification.

Finally, the ageing model could be extended to include additional environmental variables, such as temperature, humidity, etc. The model should be calibrated and validated using larger utility datasets before it is applied to individual asset RUL estimation or maintenance scheduling.

List of Figures

1 A conceptual framework of the five core stages of the asset lifecycle management 13
2 Mapping the core domains of asset management to the specific research questions and corresponding publications..... 16
3 A typical AC substation schematics [19] 19
4 Air insulated substation [19] 20
5 Gas insulated substation [19] 20
6 Classification of maintenance strategies [29] 21
7 Failure modes of major failures for HVCB (data from [34]) 23
8 Distribution of HVCB failure per component responsible (data from [20])... 24
9 Different types of circuit breakers [19] 25
10 Sample of maximum permissible switching number graph for a 400 kV HVCB (data from [35])..... 26
11 Circuit breaker's spring charging motor current and voltage characteristics . 27
12 Coil current features on a healthy HVCB recorded pattern [20] 28
13 Circuit breaker contacts travel curve for trip/close operation [14]..... 29
14 Generic model of HVCB components [48] 33
15 Component specification of a 110 kV HVCB 34
16 Cross-section comparison of SF_6 gas Interrupters: a) Plain break, (b) Self blast, (c) Double pressure blast, (d) Puffer blast [19] 36
17 Interrupter principle [19]..... 36
18 Schematic configuration of a spring operating mechanism: (a) components (b) close (c) trip [18] 37
19 Schematic of a generalised HVCB control circuit 38
20 Major failure of HVCB according to the service type based on CIGRE survey [34]..... 39
21 Typical time-varying failure rate for the power system equipment throughout the lifetime..... 40
22 Comparison of the proposed model to Weibull and exponential models in analogy to the bathtub curve zones, shown in Fig. 21; Due to a lack of data in Zone I, the proposed model cannot be fully validated in this region, and this unvalidated section is denoted by the solid gray line. 42
23 Example of one sensitivity-analysis iteration showing the original data, perturbed interpolated values, and fitted models. 43
24 Comparison of Gaussian model extrapolation trajectories when fitted on data truncated at 14 years versus 22 years. 44
25 Impact of normalized service-type integration on HVCB life expectancy: (a) normalised failure rates (ζ) per service-type; (b) comparison between $MTTF_{base}$ and $MTTF_{mod}$. 45
26 An output sample from the designed graphical user interface 46
27 The CIBANO 500 HVCB test system [58] 48
28 CIBANO 500 connected to a live tank HVCB (a typical field application) [58] 48
29 HVCB test report by CIBANO 500 [59] 49
30 Schematic representation of the experimental setup for emulating HVCB coil current behaviour and defects. 50
31 Coil current emulator circuit diagram 51

32 Trip/close coil current signal and related diagnostic features. (a) Real HVCB coil current measured with CIBANO 500. (b) Real HVCB coil current measured using Raspberry Pi. (c) Emulator circuit current measured using an inexpensive sensor. 51
33 Time-domain comparison of signals captured by TCP0030A and ACS712 52
34 Demonstration of the reference (TCP0030A) and modified signal (ACS712) . 54
35 Time-domain comparison of denoising techniques..... 55
36 Illustration of the effects of various defects on the coil current waveform: (a) supply voltage, (b) latch operation, (c) auxiliary contact..... 57
37 Trip/close coil current signal feature extraction process. (a) Raw measurement. (b) Filtered signal. (c) Segmentation. (d) Extracting critical points. ... 58
38 Sensitivity analysis of the Savitzky-Golay parameters. (a) Effect of polynomial degree variation by constant window size (W_{len} = 20). (b) Effect of window size variation by constant polynomial degree (p_{deg} = 3)..... 59
39 Confusion matrix, TPR, and FNR of the kNN model: (a) Training validation, (b) Testing..... 61
40 Confusion matrix, TPR, and FNR of the decision tree model: (a) Training validation, (b) Testing 61
41 Confusion matrix, TPR, and FNR of the logestic regression model: (a) Training validation, (b) Testing 62
42 Confusion matrix, TPR, and FNR of the SVM model: (a) Training validation, (b) Testing..... 62
43 Global feature importance plot showing the mean absolute Shapley values for each class 63
44 Euclidean distance assessment between filtered coil current signals: (a) comparison of two healthy signals; (b) comparison between a healthy and a defective signal. 64
45 Euclidean distance metrics comparing a reference normal signal against various healthy and defective sample groups..... 65
46 Impact of DTW on signal alignment: (a) misaligned normal signals yielding high Euclidean error; (b) signals aligned via DTW revealing true similarity... 66
47 Operational flowchart for the automated detection and classification of HVCB defects. 67
48 Block diagram of the HVCB components connection..... 68
49 Flowchart of the overall HI calculation for HVCB..... 69
50 Diagram of the network being analysed 70
51 Schematic of the experimental setup 71
52 Feature extraction from a real coil current measurement (110 kV circuit breaker). 72
53 Layered architecture for the practical deployment of HVCB condition monitoring in a transmission network [63]. 74

List of Tables

1 Comparison of instrument transformer failure frequency based on the applied maintenance scheme (data from [33]) 22
2 MTTF and λ values for HVCB based on third CIGRE survey (data from [34]) . 41
3 R-squared values of the applied models 41
4 Estimated parameters of the applied ageing models for reproducibility. 42
5 Model Sensitivity Evaluation Under Simulated Data Variance 43
6 Comparison of root mean square error across denoising techniques. 56
7 Comparison of ML-based algorithms for classification of coil current defects 63
8 HVCBs operating age, HI, and failure rate [47] 71

References

[1] A. Alquraidi and M. Awad, "Physical asset management for critical utilities—a systematic literature review," *IEEE Access*, vol. 12, pp. 90644–90659, 2024.

[2] X. Han, J. Su, and J. P. Thia, "Impact of infrastructure investment on developed and developing economies," *Economic Change and Restructuring*, vol. 54, no. 4, pp. 995–1024, 2021.

[3] G. Balzer and C. Schorn, *Asset Management for Infrastructure Systems: Energy and Water*. Springer Nature, 2022.

[4] O. Augoye, A. Adewoyin, O. Adediwin, and A. J. Audu, "The role of artificial intelligence in energy financing: A review of sustainable infrastructure investment strategies," *International Journal of Multidisciplinary Research and Growth Evaluation*, vol. 6, no. 2, pp. 277–283, 2025.

[5] M. Ibrahim and A. Rassõlkin, "Hybrid-driven digital twin modelling framework for an EV propulsion drive system," *IET Intelligent Transport Systems*, vol. 19, no. 1, p. e70099, 2025.

[6] S. Asefi, M. Mitrovic, D. Ćetenović, V. Levi, E. Gryazina, and V. Terzija, "Anomaly detection and classification in power system state estimation: Combining model-based and data-driven methods," *Sustainable Energy, Grids and Networks*, vol. 35, p. 101116, 2023.

[7] A. Abiri-Jahromi, M. Parvania, F. Bouffard, and M. Fotuhi-Firuzabad, "A two-stage framework for power transformer asset maintenance management—part I: Models and formulations," *IEEE Transactions on Power Systems*, vol. 28, no. 2, pp. 1395–1403, 2012.

[8] S. Heier, *Grid integration of wind energy: onshore and offshore conversion systems*. John Wiley & Sons, 2014.

[9] M. Kandic, I. Fernando, A. Gole, and L. Wang, "Incorporating multi-year asset replacement time into calculation of asset's expected annual unavailability due to end-of-life failure," *IEEE Transactions on Power Systems*, vol. 36, no. 6, pp. 5164–5174, 2021.

[10] M. Yildirim, X. A. Sun, and N. Z. Gebraeel, "Sensor-driven condition-based generator maintenance scheduling—part I: Maintenance problem," *IEEE Transactions on Power Systems*, vol. 31, no. 6, pp. 4253–4262, 2016.

[11] G. Bretthauer, T. Gamaleja, E. Handschin, U. Neumann, and W. Koffmann, "Integrated maintenance scheduling system for electrical energy systems," *IEEE Transactions on Power Delivery*, vol. 13, no. 2, pp. 655–660, 1998.

[12] N. Zhou, L. Luo, G. Sheng, and X. Jiang, "Scheduling the imperfect maintenance and replacement of power substation equipment: A risk-based optimization model," *IEEE Transactions on Power Delivery*, vol. 40, no. 4, pp. 2154–2166, 2025.

[13] A. Abu-Siada and S. Islam, "A novel online technique to detect power transformer winding faults," *IEEE Transactions on Power Delivery*, vol. 27, no. 2, pp. 849–857, 2012.

[14] A. A. Razi-Kazemi and K. Niayesh, "Condition monitoring of high voltage circuit breakers: past to future," *IEEE Transactions on Power Delivery*, vol. 36, no. 2, pp. 740–750, 2020.

[15] A. L. Brodersson, J. H. Jürgensen, and P. Hilber, "Towards health assessment: Failure analysis and recommendation of condition monitoring techniques for large disconnector populations," in *CIRED Workshop 2016*, pp. 1–4, IET, 2016.

[16] S. Asefi, J. Kilter, N. Akroud, A. Hurtado, I. Gilbert, and I. Orue, "Application of transfer learning for instrument transformer condition monitoring," in *2024 International Conference on Diagnostics in Electrical Engineering (Diagnostika)*, pp. 01–04, IEEE, 2024.

[17] H.-K. Wang, H.-Z. Huang, Y.-F. Li, and Y.-J. Yang, "Condition-based maintenance with scheduling threshold and maintenance threshold," *IEEE Transactions on Reliability*, vol. 65, no. 2, pp. 513–524, 2015.

[18] T. Krieg and J. Finn, *Substations*. CIGRE Green Books, Springer International Publishing, 2018.

[19] H. Ito, *Switching Equipment*. CIGRE Green Books, Springer International Publishing, 2019.

[20] S. Asefi, S. Asefi, H. Afshari, J. Kilter, E. Shayesteh, P. Hilber, and T. Lindquist, "Machine learning based high voltage circuit breaker defect classification utilizing savitzky-golay filter," *IEEE Transactions on Instrumentation and Measurement*, 2025.

[21] G. Balzer, A. Gaul, C. Neumann, and C. Schorn, "The general asset management process of power systems," in *Konferenzbeitrag CIGRE-Symposium, Osaka*, vol. 1, 2007.

[22] N. Zhou, Y. Xu, S. Cho, and C. T. Wee, "A systematic review for switchgear asset management in power grids: condition monitoring, health assessment, and maintenance strategy," *IEEE Transactions on Power Delivery*, vol. 38, no. 5, pp. 3296–3311, 2023.

[23] H. Manninen, J. Kilter, and M. Landsberg, "A holistic risk-based maintenance methodology for transmission overhead lines using tower specific health indices and value of loss load," *International Journal of Electrical Power & Energy Systems*, vol. 137, p. 107767, 2022.

[24] C. Fu, L. Ye, Y. Liu, R. Yu, B. Iung, Y. Cheng, and Y. Zeng, "Predictive maintenance in intelligent-control-maintenance-management system for hydroelectric generating unit," *IEEE Transactions on Energy Conversion*, vol. 19, no. 1, pp. 179–186, 2004.

[25] Y.-C. Huang and H.-C. Sun, "Dissolved gas analysis of mineral oil for power transformer fault diagnosis using fuzzy logic," *IEEE Transactions on Dielectrics and Electrical Insulation*, vol. 20, no. 3, pp. 974–981, 2013.

[26] J. Faiz and M. Soleimani, "Dissolved gas analysis evaluation in electric power transformers using conventional methods a review," *IEEE Transactions on Dielectrics and Electrical Insulation*, vol. 24, no. 2, pp. 1239–1248, 2017.

[27] Q. Su, C. Mi, L. Lai, and P. Austin, "A fuzzy dissolved gas analysis method for the diagnosis of multiple incipient faults in a transformer," *IEEE Transactions on Power Systems*, vol. 15, no. 2, pp. 593–598, 2002.

[28] S. Asefi, G. Andreesen, M. Leinakse, J. Kilter, T. Kalmet, H. Manninen, and M. Landsberg, "Measurement and operation based condition monitoring methodology for high voltage circuit breakers," in *2022 IEEE PES Innovative Smart Grid Technologies Conference Europe (ISGT-Europe)*, pp. 1–5, IEEE, 2022.

[29] G. Balzer and C. Schorn, *Asset Management for Infrastructure Systems*. Springer International Publishing, 2022.

[30] S. Asefi, B. Asad, M. Leinakse, H. Manninen, J. Kilter, T. Vaimann, A. Kallaste, M. Tealane, and M. Landsberg, "Review of high-voltage instrument transformer condition monitoring," *IEEE Transactions on Dielectrics and Electrical Insulation*, vol. 31, no. 6, pp. 3331–3341, 2024.

[31] S. Asefi, J. Kilter, and M. Landsberg, "Non-intrusive defects identification for the high voltage instrument transformers," in *2023 IEEE 17th International Conference on Compatibility, Power Electronics and Power Engineering (CPE-POWERENG)*, pp. 1–5, IEEE, 2023.

[32] S. Asefi, J. Kilter, E. Shayesteh, P. Hilber, and T. Lindquist, "High voltage circuit breaker health index evaluation considering measurement accuracy," in *2024 IEEE PES Innovative Smart Grid Technologies Europe (ISGT EUROPE)*, pp. 1–5, IEEE, 2024.

[33] CIGRÉ Working Group A3.06, "Final report of 2004–2007 international enquiry on reliability of high voltage equipment, part 4—instrument transformers," *CIGRE Techn Broch, vol. 512*, 2012.

[34] CIGRÉ Working Group A3.06, "Final report of 2004–2007 international enquiry on reliability of high voltage equipment, part 2—reliability of high voltage circuit breakers," *CIGRE Techn Broch*, vol. 510, 2012.

[35] Siemens, *Operating Instructions Circuit-Breaker 3AP2 FI*, 2013.

[36] B. Asad, M. U. Sardar, T. Vaimann, A. Kallaste, S. Asefi, and J. Kilter, "High voltage circuit breaker charging motor's condition monitoring–importance, possibilities, and challenges," in *2024 International Conference on Diagnostics in Electrical Engineering (Diagnostika)*, pp. 01–07, IEEE, 2024.

[37] A. A. Razi-Kazemi, M. Vakilian, K. Niayesh, and M. Lehtonen, "Circuit-breaker automated failure tracking based on coil current signature," *IEEE Transactions on Power Delivery*, vol. 29, no. 1, pp. 283–290, 2013.

[38] F. N. Rudsari, A. A. Razi-Kazemi, and M. A. Shoorehdeli, "Fault analysis of high-voltage circuit breakers based on coil current and contact travel waveforms through modified svm classifier," *IEEE Transactions on Power Delivery*, vol. 34, no. 4, pp. 1608–1618, 2019.

[39] A. Bagherpoor, S. Rahimi-Pordanjani, A. A. Razi-Kazemi, and K. Niayesh, "Online condition assessment of interruption chamber of gas circuit breakers using arc voltage measurement," *IEEE Transactions on Power Delivery*, vol. 32, no. 4, pp. 1776–1783, 2016.

[40] Y. Tan, E. Hu, Y. Liu, J. Li, and W. Chen, "Review of digital vibration signal analysis techniques for fault diagnosis of high-voltage circuit breakers," *IEEE Transactions on Dielectrics and Electrical Insulation*, vol. 31, no. 1, pp. 404–418, 2023.

[41] H. Manninen, J. Kilter, and M. Landsberg, "Health index prediction of overhead transmission lines: a machine learning approach," *IEEE Transactions on Power Delivery*, vol. 37, no. 1, pp. 50–58, 2021.

[42] J. A. Grant, I. B. Sperstad, J. Foros, and V. V. Vadlamudi, "Health index calculation using failure modes, effects, and criticality analysis for high-voltage circuit breakers," in *Proceedings of the 33rd European Safety and Reliability Conference (ESREL 2023)*, 2023.

[43] A. Setiawan, W. Adiati, and R. A. Prasojo, "An approach of the analytic hierarchy process to acquire the weighting factor of high voltage circuit breaker health index," in *2020 International Conference on Technology and Policy in Energy and Electric Power (ICT-PEP)*, pp. 317–322, IEEE, 2020.

[44] S. Geng and X. Wang, "Research on data-driven method for circuit breaker condition assessment based on back propagation neural network," *Computers & Electrical Engineering*, vol. 86, p. 106732, 2020.

[45] P. Dehghanian, T. Popovic, and M. Kezunovic, "Circuit breaker operational health assessment via condition monitoring data," in *2014 North American Power Symposium (NAPS)*, pp. 1–6, IEEE, 2014.

[46] J. A. Grant, H. Toftaker, S. Perkin, I. B. Sperstad, and V. V. Vadlamudi, "High-voltage circuit breaker condition-dependent failure rate with covariates," in *2024 Annual Reliability and Maintainability Symposium (RAMS)*, pp. 1–6, IEEE, 2024.

[47] J. Zhong, W. Li, R. Billinton, and J. Yu, "Incorporating a condition monitoring based aging failure model of a circuit breaker in substation reliability assessment," *IEEE Transactions on Power Systems*, vol. 30, no. 6, pp. 3407–3415, 2015.

[48] M. Stanek, *Model-aided diagnosis for high voltage circuit breakers*. PhD thesis, ETH Zurich, 2000.

[49] K. Niayesh and M. Runde, *Power switching components*. Springer, 2017.

[50] E. Parliament and the Council of the European Union, "Regulation (EU) 2024/573 of the european parliament and of the council of 7 february 2024 on fluorinated greenhouse gases, amending directive (EU) 2019/1937 and repealing regulation (EU) no 517/2014 (text with eea relevance)," 2024.

[51] G. Balzer, D. Drescher, F. Heil, P. Kirchesch, R. Meister, and C. Neumann, "Evaluation of failure data of hv circuit-breakers for condition based maintenance," in *CIGRE session*, pp. A3–305, 2004.

[52] S. Asefi, J. Kilter, and M. Landsberg, "Incorporating service type in aging failure model of high voltage circuit breaker," in *2023 27th International Conference Electronics*, pp. 1–5, IEEE, 2023.

[53] C. Chu, J. Moon, H. Lee, and J. Kim, "Extraction of time-varying failure rates on power distribution system equipment considering failure modes and regional effects," *International Journal of Electrical Power & Energy Systems*, vol. 32, no. 6, pp. 721–727, 2010.

[54] R. Ross, "Reliability analysis for asset management of electric power grids," 2018.

[55] W. Li, *Risk assessment of power systems: models, methods, and applications*. John Wiley & Sons, 2014.

[56] R. Billinton and R. N. Allan, *Reliability evaluation of engineering systems*, vol. 198. Springer, 1985.

[57] C. Sweetser, "A systematic approach to high-voltage circuit breaker testing," *Technical Paper, OMICRON electronics Corp*, 2015.

[58] Omicron electronics GmbH, *CIBANO 500 - 3-in-1 test system for medium and high voltage circuit breakers*. Klaus, Austria, 2022. Product brochure.

[59] T. Kalmet, "Development and analysis of condition assessment methodology for SF_6 circuit breakers in estonian transmission network," Master's thesis, Tallinn University of Technology, 2021.

[60] H. Sakoe and S. Chiba, "Dynamic programming algorithm optimization for spoken word recognition," *IEEE Transactions on Acoustics, Speech, and Signal Processing*, vol. 26, no. 1, pp. 43–49, 2003.

[61] K. K. Paliwal, A. Agarwal, and S. S. Sinha, "A modification over sakoe and chiba's dynamic time warping algorithm for isolated word recognition," *Signal Processing*, vol. 4, no. 4, pp. 329–333, 1982.

[62] J. H. Jürgensen, *Individual failure rate modeling and exploratory failure data analysis for power system components*. PhD thesis, KTH Royal Institute of Technology, 2018.

[63] S. Aichi, Y. Yatabe, T. Kanamori, T. Ikeda, and K. Kawakita, "Development and operation of substation condition monitoring system (cms)," in *Proceedings of the CIGRE Condition Monitoring, Diagnosis and Maintenance – CMDM2023 (7th edition)*, (Bucharest, Romania), October 2023.

Acknowledgements

Words cannot fully express the profound gratitude I hold for my family, specifically my parents, whose love, patience, and encouragement have been the absolute foundation of this journey. A very special mention also goes to my wonderful niece and nephew, Sania and Samiar, whose bright spirits brought me immense joy and motivation along the way.

I am highly grateful to my supervisor, Prof. Jako Kilter, for his guidance and support during my studies, and to my co-supervisor, Dr. Mart Landsberg, whose valuable time and insights have been instrumental to my progress. I would also like to acknowledge the opponents for their constructive comments and valuable suggestions, which helped improve the quality of this thesis. I also want to thank my colleagues at TalTech, KTH Royal Institute of Technology, RISE Research Institutes of Sweden, Ormazabal, and Elering for their collaboration, shared expertise, and support throughout my studies.

I would like to extend a special thanks to my good friend, Peyman Koohi, for his invaluable encouragement and support. Finally, I want to kindly acknowledge all of my friends and the dedicated university staff who have so generously helped me throughout these past few years.

Abstract

Advanced Condition Monitoring of High-Voltage Circuit Breaker Utilising Machine Learning

The rapid evolution of modern power systems, driven by the integration of renewable energy sources and the ageing of critical infrastructure, demands a shift in asset management strategies. High-voltage circuit breakers (HVCBs) serve as a primary protection mechanism within the grid. However, their reliability is increasingly challenged by changing operational stresses and the limitations of traditional time-based maintenance regimes. This thesis addresses these challenges by developing a cost-effective measurement solution and a data-driven framework for HVCB condition monitoring and defect classification, with the aim of supporting condition-aware health index (HI) evaluation and asset management decisions. The research begins by analysing HVCB failure modes using international CIGRE survey data, identifying the operating mechanism and control circuitry as major contributors to failures. In addition, a Gaussian function-based ageing model was fitted to aggregated CIGRE data, and published service-type failure frequencies were incorporated as relative adjustments to the baseline trajectory. Owing to the limited data available, this model is presented as an exploratory population-level representation within the observed age range rather than as a validated predictor of the remaining useful life of an individual HVCB. As population-level ageing models cannot determine the current condition of an individual HVCB, direct condition measurements are required to identify changes in its operating mechanism and control circuitry. Coil current measurement was therefore investigated as a non-intrusive means of obtaining condition-related information during breaker operation. To examine an alternative to commercial analysers for continuous monitoring, an experimental measurement arrangement based on a low-cost current sensor and microcontroller-based data acquisition was developed. Measurements from the low-cost sensor were compared with those obtained using a laboratory reference probe. Among the evaluated denoising methods, the Savitzky-Golay filter produced the lowest waveform error while retaining the peaks and transitions required for feature extraction under the investigated laboratory conditions. A coil current emulator was developed to generate repeatable signals representing baseline operation and controlled variations in supply voltage, latch behaviour, and auxiliary contact operation. Features extracted from these signals were used to train machine learning classifiers. For the investigated emulator dataset, the selected classifiers achieved accuracies above 95% in distinguishing the examined operating conditions. Dynamic time warping was also included as a signal comparison stage to reduce erroneous indications caused by temporal misalignment. The feature extraction procedure was subsequently demonstrated using a healthy real HVCB coil current measurement, although validation with defective operational HVCBs remains necessary. Overall, the proposed ageing model, low-cost measurement arrangement and diagnostic methods form a decision support approach for HVCB condition assessment and can be beneficial for TSOs, utility asset managers, and substation maintenance engineers. The results demonstrate their applicability to the investigated laboratory and emulated datasets. Further validation using larger datasets from operational substations, including measurements from defective HVCBs, is required before practical deployment.

Keywords: Asset Management, Condition Monitoring, Coil Current Signature, Dynamic Time Warping, Health Index, High-Voltage Circuit Breaker, Machine Learning, Reliability Centred Maintenance, Savitzky-Golay filter

Kokkuvõte
Kõrgepinge-võimsuslüliti täiustatud seisundiseire masinõppe abil

Tänapäevaste elektrisüsteemide kiire areng, mida veab taastuvate energiaallikate integreerimine ja kriitilise taristu vananemine, nõuab varahaldusstrateegiates põhimõttelist muutust. Kõrgepinge-elektrivõrkude peamiseks kaitse- ja lülitusseadmeks on võimsuslülitid. Nende seadmete töökindluse panevad aga üha enam proovile muutuvad talitlustingimused ja traditsiooniliste ajapõhiste hooldusstrateegiate piirangud. Käesolev doktoritöö lahendab neid väljakutseid, arendades välja töökindla ja kulutõhusa mõõtelahenduse ning rakendades andmepõhist raamistikku kõrgepinge-võimsuslülitite reaalajapõhiseks seisundiseireks ja defektide klassifitseerimiseks, eesmärgiga hõlbustada üleminekut seisunditeadlikule seisundiindeksi määramisele ja varade kulumise kvantifitseerimisele.

Doktoritöö algab kõrgepinge-võimsuslülitite rikkerežiimide analüüsiga, kus lähtudes CIGRE rahvusvahelisest uuringust tuvastatakse vaadeldavate seadmete rikete peamiste põhjustena ajamimehhanism ja juhtimisahelad. Lisaks sobitati CIGRE koondandmetele Gaussi funktsioonil põhinev vananemismudel ja kirjanduses avaldatud käidutüübipõhiseid rikkesagedusi kasutati baastrajektoori suhteliste korrektsioonidena. Andmete piiratud hulga tõttu käsitletakse seda mudelit uurimusliku populatsioonitasandi kirjeldusena vaadeldud vanusevahemikus, mitte valideeritud mudelina üksiku kõrgepinge-võimsuslüliti järelejäänud kasuliku eluea prognoosimiseks. Kuna populatsioonitasandi vananemismudelid ei võimalda määrata üksiku kõrgepinge-võimsuslüliti hetkeolukorda, on selle ajamis ja juhtimisahelates toimuvate muutuste tuvastamiseks vajalikud otsesed seisundimõõtmised. Seetõttu uuriti võimsuslüliti lülitusmähise voolu mõõtmist kui kaudset meetodit seadme talitlemisel tema seisundiga seotud teabe saamiseks. Pidevseireks kasutatavate kommertsanalüsaatorite võimaliku alternatiivi uurimiseks töötati välja katseline mõõtesüsteem, mis põhines odaval vooluanduril ja mikrokontrolleripõhisel andmehõivel. Odava anduriga saadud mõõtetulemusi võrreldi laboratoorse etaloni abil saadud tulemustega. Hinnatud müravähendusmeetoditest andis Savitzky–Golay filter uuritud laboritingimustes väikseima lainekuju vea, säilitades samal ajal mähise voolukõvera kriitilisi geomeetrilisi tunnuseid, nagu amplituudid ja siirdeprotsessi kuju, mida tavapärased lineaarsed keskmistamismeetodid tavaliselt halvendavad. Korratavate signaalide, mis esindaksid normaalset talitlust ja hälbeid toitepinges, lukustusmehhanismi talitlemist, ja abikontaktide tööd, loomiseks arendati lülitusmähise voolu emulaator. Nendest signaalidest eraldatud tunnuseid kasutati masinõppe klassifikaatorite treenimiseks. Uuritud emulaatori andmestiku korral saavutasid valitud klassifikaatorid käsitletud talitlusseisundite eristamisel üle 95% täpsuse. Signaalide võrdlemise ühe etapina kasutati ka dünaamilist ajalist mastaapimist, et vähendada ajalisest nihkest põhjustatud ekslike indikatsioonide arvu. Seejärel demonstreeriti tunnuste eraldamise meetodit töökorras reaalse kõrgepinge-võimsuslüliti lülitusmähise voolu mõõtetulemuse põhjal, kuid meetodi valideerimiseks on endiselt tarvis mõõteandmeid defektidega käidus olevatelt kõrgepinge-võimsuslülititelt.

Kokkuvõttes moodustavad väljapakutud vananemismudel, kulutõhus mõõtesüsteem ja diagnostikameetodid otsustamist toetava lähenemisviisi kõrgepinge-võimsuslülitite seisundi hindamiseks ning võivad olla kasulikud põhivõrguettevõtjatele, võrguettevõtte varahalduritele ja alajaamade hooldusinseneridele. Tulemused näitavad väljatöötatud meetodite rakendatavust uuritud laboratoorsete ja emuleeritud lähteandmestike puhul. Enne praktilist kasutuselevõttu on vajalik täiendav valideerimine suuremate, käidus olevatest alajaamadest kogutud andmestike põhjal, sealhulgas defektidega kõrgepinge-võimsuslülitite mõõteandmetega.

Märksõnad: dünaamiline ajaline mastaapimine, kõrgepinge-võimsuslüliti, masinõpe, mähise voolukõver, seisundiindeks, seisundiseire, töökindlusele suunatud hooldus, Savitzky-Golay filter, varahaldus.

Appendix 1

S. Asefi et al., “Measurement and Operation Based Condition Monitoring Methodology for High-Voltage Circuit Breakers,” in 2022 IEEE PES Innovative Smart Grid Technologies Conference Europe (ISGT-Europe), 2022, pp. 1-5.

Measurement and Operation Based Condition Monitoring Methodology for High Voltage Circuit Breakers

Sajjad Asefi, Guido Andreesen, Madis Leinakse, Jako Kilter
Department of Electrical Power Engineering and Mechatronics
Tallinn University of Technology
Tallinn, Estonia
firstname.lastname@taltech.ee

Tauri Kalmet, Henri Manninen, Mart Landsberg
Grid Maintenance Department
Elering AS
Tallinn, Estonia
firstname.lastname@elering.ee

***Abstract*—High voltage circuit breakers (HVCBs) are essential components for reliability and resiliency of the power system, and it is crucial to optimize principles of condition monitoring for maintenance of this equipment. In this paper a novel methodology based on combination of HVCB's overall health index and expected aging curve is presented to provide an optimal scheduling of HVCB's maintenance. The overall health index of HVCB is acquired by conventional measurements, e.g. contacts dynamic resistance, drive motor current, etc. The methodology has been verified based on experimental tests that are implemented on a 110 kV HVCB. Based on the obtained results, the proposed method would increase the accuracy of HVCB's condition based maintenance scheduling, which will improve system reliability, ensure personnel safety, reduce the unplanned down time, and decrease the overall maintenance cost.**

***Index Terms*—Condition monitoring, High voltage circuit breaker, Health index, Maintenance**

I. Introduction

Because of their importance in operation and protection, high voltage circuit breakers (HVCBs) have been recognised as key components of the power system. Any failure or malfunctioning of the components of HVCBs may lead to undesirable events which results in a significant impact on the reliability of the power systems [1]. Maintenance techniques can be used to detect faults in the initial stages and avoid failures, which will simplify the faulty component's replacement procedure [2].

HVCBs can be divided into three main parts, namely control unit, drive mechanism, and interrupter [3]. It is obvious that a failure can be originated from malfunctioning of the various components available in the HVCB. Therefore, alternative maintenance plans should be implemented to avert malfunctioning and extend the operational life of these assets [4].

The maintenance strategies can be generally divided into two different classes, namely corrective and preventive [5], [6]. In corrective strategy the device is utilized till the failure takes place, and then it would be replaced. Preventive strategy entails a series of actions performed at specific intervals to decrease the wear process of the equipment [6]. This strategy can also be divided into categories, such as time-based maintenance (TBM), condition-based maintenance (CBM), etc. In TBM policy the maintenance is preformed based on a predefined time interval. The main disadvantage of this method would be in case if the failure happens before the next predefined inspection time. In this case CBM policy would be preferable, in which the maintenance schedule of the component would be specified based on the condition of that component. Based on the results indicated in [1], approximately 59%, 6% and 35% of maintenance plans that transmission system operators (TSOs) have implemented are TBM, CBM and a combination of these two, respectively.

The condition of the HVCBs can be assessed based on a variety of measurements, such as trip/close coil current (CC), contact travel curve (TC), dynamic resistance measurement (DRM), etc. From asset management perspective it is highly important to interpret the measured values into indices (so called health index (*HI*)) that indicates the condition of the equipment and simplifies the decision making process for the TSO.

Various efforts have been made in the literature regarding condition monitoring of HVCB. In [7], the trip/close CC waveform features have been specified to detect failures such as supply voltage, coil, etc. The authors have utilized the trip/close CC of normal operations and have processed the measured values in order to determine the statistical characteristics of CC's waveform features. Also in [8] data mining approach has been used to specify the threshold between faulty and normal CC waveform. In [9] CC together with TC have been utilized for failure detection of the HVCB. One of the methods to assess the condition of HVCB's contacts without disassembling the interruption chamber is DRM. Authors in [10], have investigated the effect of main and arcing contacts related failures on the DRM curve. The authors have proposed an algorithm which makes distinguishing failures possible based on deviation in the specified features. Prioritization of the HVCBs' maintenance is discussed in [11], [12], however

This work has been financially supported by the Estonian Transmission System Operator Elering AS through the project "Risk and condition based asset management in future power systems", No. 1.1-4/2021/644/LEEEE21116.

978-1-6654-8032-1/22/$31.00 ©2022 IEEE

measurements such as DRM or pole discrepancy were not considered in those studies.

Recently methods such as vibration signal analysis, arc energy and high frequency, have been investigated as advanced techniques for condition monitoring of HVCBs [13]–[16]. However, these methods are still under development or need additional expensive equipment to be installed for each HVCB which would not be a cost efficient approach from the TSO's perspective. A detailed review of the conventional HVCBs' condition monitoring is presented in [17].

In this paper a novel methodology have been presented based on combination of maximum permissible switching number (MPSN) and other conventional measurement techniques to increase the accuracy of the CBM scheduling for HVCBs. Although some of the presented methods in the literature, have utilized combination of measurements to detect the condition of HVCB, but none of them has considered MPSN to modify the expected aging curve of the HVCBs.

The rest of the paper is organized as follows. Section II describes the methodology and the proposed technique. In section III two possible scenarios, as possible outcomes of the proposed method are presented. Finally, in section IV the paper has been concluded.

II. Methodology

In this section first the mathematical equation related to HI calculation based on the measurements is presented. Later on, maximum switching number method, conventional measurements are briefly described. And finally, the flow chart of the proposed method is presented.

A. Health Index (HI)

In order to assess the overall condition of HVCB, it is necessary to perform various measurements on the HVCB's different components. The measured data can be compared with previous measurement results and limit values, and based on this, it would be possible to provide an estimation of the overall condition of the device in relative units (i.e. *HI*). When performing measurement data analysis, it is important to have the limit for the measured values (from a specific standard or set by the manufacturer). Also, measurement results from the factory test report (provided by the manufacturer) are necessary. It is difficult to evaluate the device's condition without this information.

If the measurement data of the parameters are known for the new HVCB as well as the measurement's limit and the reference values, the condition of the device can be assessed using (1) [12]:

$$HI_i = \frac{V_{i,meas} - V_{i,ref}}{V_{i,max} - V_{i,ref}} \tag{1}$$

where $V_{i,meas}$, $V_{i,ref}$ and $V_{i,max}$ indicate value obtained during measurements, past (or reference) measurements and maximum limit value from the i^{th} measurement, respectively.

The obtained *HI* value from (1) would be in range of 0 and 1, in which 0 indicates that the measured parameter has not changed from the initial (or reference) measurement; and 1 indicates that the measured value is equal to the limit, which means that the device parameter resource is completely worn out. It is to be noted that the HVCB's overall *HI*, would be equal to the highest (i.e. worst) value obtained from measurements, that can be formulated as follows:

$$HI_{oa} = max\{HI_1, HI_2, ..., HI_i\} \tag{2}$$

in which HI_{oa} indicates the overall *HI* of the HVCB.

It is important to interpret the obtained value to facilitate decision-making for the TSO. Similar to the *HI* categorization presented in [11], the obtained HI_{oa} results can be classified as follows:

- $0 \leq HI_{oa} \leq 0.6$: Normal/standard aging
- $0.6 < HI_{oa} \leq 0.8$: Preliminary maintenance required
- $0.8 < HI_{oa} \leq 0.9$: Regular/standard maintenance required
- $HI_{oa} > 0.9$: Urgent maintenance/replacement required

B. Maximum Permissible Switching Number (MPSN)

In Fig. 1 an example of MPSN graph for a HVCB is provided which are commonly given by manufacturer. Based on that graph, it is possible to determine the maximum number of allowed operations. That number depends also on the interrupted current value at the operation moment. If the current value is below the nominal current I_{lim} value, then this counts as one operation. In case of higher current values, the remaining number of operations are scaled according to current value.

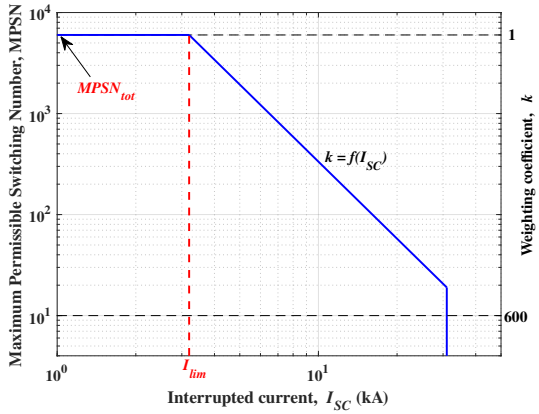


Fig. 1. Sample of MPSN graph for Siemens 3AP1 FG HVCB [18]

It is possible to calculate the breaking current influence to number of operations using (3) [18]:

$$MPSN_x = \frac{MPSN_{tot} - \sum_{i=1}^{m}(SN_i \times k_i)}{k_x} \tag{3}$$

where k_i and k_x are weighting coefficient for interrupted current I_{SC} and $I_{SC,x}$, respectively; SN_i is the number of

performed switching at current I_{SC}; $MPSN_x$ is the MPSN at current $I_{SC,x}$; $MPSN_{tot}$ is the total number of MPSN for this specific HVCB which is equal to 6000; and m is total number of carried out interruptions.

C. Implemented measurements

As mentioned before, variety of measurements can be implemented to identify the condition of HVCB. Here the experimented measurements that are implemented on the 110 kV HVCB are briefly explained. Acquired measurements' values are presented in section III. They are compared with allowed upper limits and re-calculated into *HI* scale (using (1)).

1) Trip Time: This measurement is applied to evaluate the time that it takes for HVCB to trip (open contacts). High value of this measurement may be caused by the mechanical part. The longer opening time may lead to disconnection of other HVCBs and disconnect a larger substation area.

2) Close Time: This measurement is made to determine the time, which is needed to close the contacts of the HVCB. The measurement higher value could be caused from mechanical part. In case of defect, the HVCB is not able to reconnect the connection within nominal time.

3) Pole Discrepancy: This parameter is measured to acquire the contacts opening time difference between each phase. If one of the phase measurement value is higher than other phases, then there could be defects in the arcing chamber or mechanical component.

4) Drive Motor Current: The motor current analysis is used to evaluate the inrush and steady-state currents. That measurement gives also the spring charging time. The results could indicate, that there is not enough momentum for the operation of mechanical part of HVCB.

5) Spring Charging Time: This parameter value indicates the time, which takes to recharge the spring after the HVCB operation. The higher recharge time could mean that motor voltage is lower than required nominal voltage. This can be used to assess the condition of DC supply.

6) Contacts Dynamic Resistance: The dynamic contact resistance is measured to gain contact resistance value during HVCB operation. Acquired results can indicate the main and arcing contacts potential degradation.

D. Proposed Method

As mentioned above, MPSN graph for a HVCB will be provided by the manufacturer. Additionally there are techniques which can measure the condition of HVCB components. Combining these techniques with switching curve would result in a better understanding of the HVCB's condition. The flowchart in Fig. 2 presents the proposed process for updating and modification of HVCB's CBM plan.

The principle structure of the method starts with gathering the necessary information for HVCB's condition monitoring such as factory test data, reference values of the parameters, and previous measurements. Then, the limits would be specified based on the proposed classification of *HI*. In another word, HI_{lim} which is the limit to perform preliminary

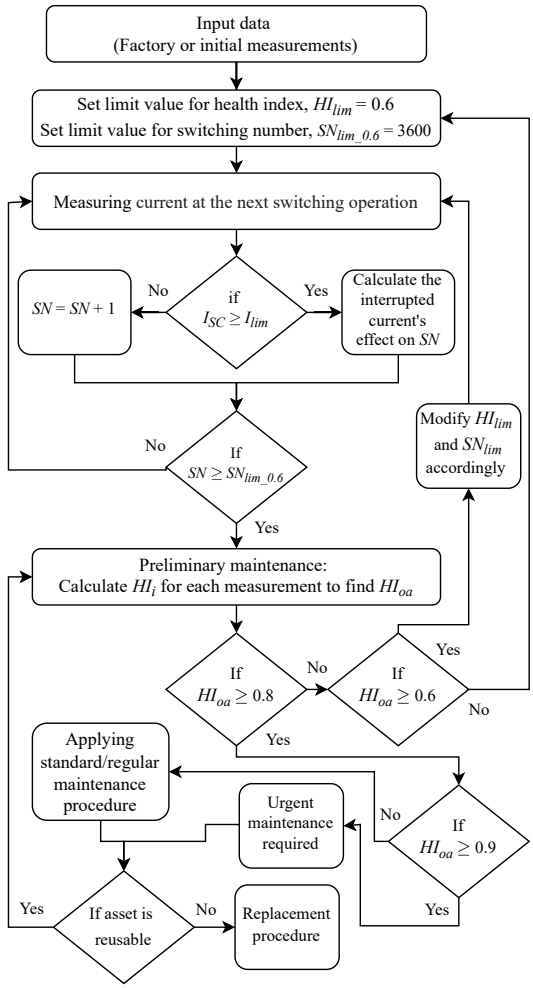


Fig. 2. Implementation process of the proposed method for HVCB's CBM

maintenance (PM) will be set to 0.6. Accordingly, the limit for switching number ($SN_{lim\_0.6}$) would be set to 3600, based on the assumption that all interrupted currents (I_{SC}) would be less than or equal to nominal current (I_{lim}). It is to be noted that, SN_{lim} is specified based on the type of the HVCB. After each switching, if the I_{SC} is less than I_{lim}, then switching numbers (*SN*) would increase one. Else, *SN* would be recalculated from (3). The process continues, until *SN* reaches to $SN_{lim\_0.6}$. This is the time when PM will be performed by implementing measurements and finding HI_{oa} utilizing (1) and (2). At this stage, based on MPSN curve, the expected HI_{oa} is to be 0.6. However, if the HI_{oa} is less than 0.6 the HI_{oa} should be updated and the process goes back to initial setting of the limit values. If HI_{oa} is between 0.6 and 0.8, then apart from

HI_{oa}, the SN_{lim} and HI_{lim} should be updated (for regular maintenance (RM)). And finally, if HI_{oa} is between 0.8 and 0.9, the RM planning should be done; else if HI_{oa} is more than 0.9, then equipment should be in the list of urgent maintenance (UM). If after maintenance the equipment is still usable, then the HI_{oa} would be recalculated. Otherwise, the equipment would be replaced.

III. Results and Discussion

In this section, the results of the implemented experimental tests on a Siemens 3AP1-FG 110 kV HVCB are presented. Additionally two possible scenarios based on the proposed procedure are simulated and discussed here.

Fig. 3 presents the *HI* obtained from conventional testing methods (which are explained in section II-C) together with the HVCB's expected aging curve (which is based on manufacturer's data). This test have been done when the switching count of the HVCB is at 286. Although we have proposed that the PM to be implemented when the *SN* is at 3600, due to the fact that a HVCB with that *SN* was not accessible, this HVCB is selected for implementation of the experimental measurements. It is shown in Fig. 3 that the obtained *HI* from measurements can have different values, but within this set of tests, the HI_{oa} would be equal to the highest *HI* value that is obtained by "Trip time" measurement. So, the aging curve of HVCB must updated at that stage.

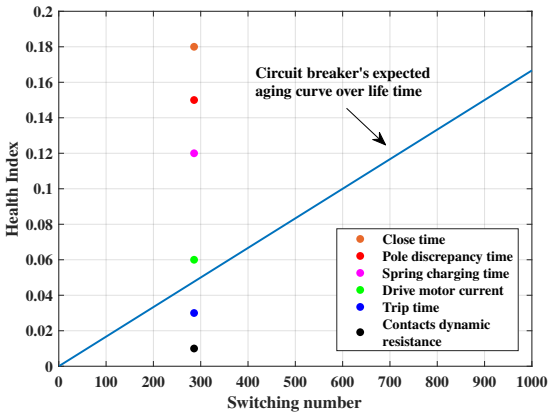


Fig. 3. Experimental measurement tests on Siemens 3AP1-FG model 110 kV HVCB

Fig. 4 and Fig. 5 are presenting two conceivable scenarios that might be possible to happen for the HVCB's expected aging curve, based on the proposed procedure. The horizontal dash lines specify the classification which is made in section II-A.

In Fig. 4, A indicates the HVCB's expected aging curve. Point B is were PM is planned. After PM, if the HI_{oa} is lower than limit, it will be updated to point C. The expected aging curve, will be set to the orange one. When the switching number reaches to the point D, again PM is implemented. If

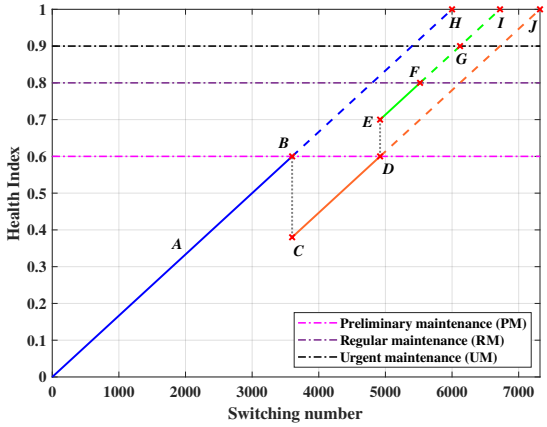


Fig. 4. Modification of expected aging curve of the HVCB using the proposed method (scenario 1)

the HI_{oa} is higher than it was expected, it will be updated to point E. Then the SN_{lim} and HI_{lim} will be updated. Point F is the limit for RM and point G is the limit for UM. Points H, I and J indicate the place where the equipment is entirely worn out, based on the expected aging curve.

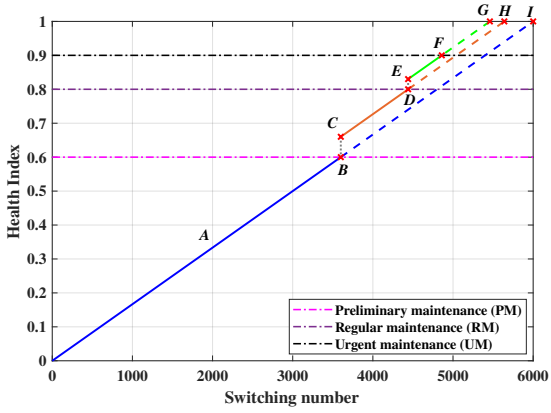


Fig. 5. Modification of expected aging curve of the HVCB using the proposed method (scenario 2)

Similarly as in Fig. 4, the A in Fig. 5 indicates expected aging curve of the HVCB; however in this scenario, when PM is implemented at point B, it is assumed that HI_{oa} would be worst and the transition would happen from B to C; then the SN_{lim} and HI_{lim} will be updated. When the number of switching reaches to the point D, RM is activated. Again, it is assumed that the HI_{oa} is higher than it was expected, so the curve will be updated to point E. Consequently, the final aging curve would be the green one, in which at point F the UM must be activated. Finally, points G, H and I indicate

entire worn out stage, based on the expected aging curve. should also be mentioned that, Fig. 5 realizes a case when the HVCB is degrading faster than expected, based on the occurred circumstances.

The situations presented in Fig. 4 and Fig. 5 show two possible cases that might take place in actual network. Note that, the transient happening for updating HI_{oa} (e.g. between points B to C) shall not only move vertically, but also can move horizontally due to the effect of interrupted current on the MPSN that is presented in (3).

IV. Conclusion

This paper presents a novel methodology to determine the actual condition of the HVCB. The proposed approach allows combination of the evaluated HVCB's HI (which is obtained utilizing different measurements) and the expected aging curve of HVCB, to assist TSO for proper scheduling of HVCB's maintenance. Two possible cases for application of the proposed method were illustrated. In the first case, where the life time of HVCB is more than expected, the TSO will avoid early stage maintenance. In the second case that the HVCB is deteriorating earlier than expected, the TSO will schedule maintenance in a way that it will prevent HVCB failure. Either way the proposed method would refine condition based monitoring of HVCB that will lead to improve system reliability, ensure personnel safety, reduce the unplanned down time, and decrease the overall maintenance cost.

References

[1] CIGRÉ Working Group A3.06, "Final report of 2004–2007 international enquiry on reliability of high voltage equipment, part 2—reliability of high voltage circuit breakers," *CIGRE Techn Broch*, vol. 510, 2012.

[2] T. Krieg and J. Finn, *Substations*, ser. CIGRE Green Books. Springer International Publishing, 2018.

[3] M. Stanek, "Model-aided diagnosis for high voltage circuit breakers," Ph.D. dissertation, ETH Zurich, 2000.

[4] K. Niayesh and M. Runde, *Power switching components*. Springer, 2017.

[5] S. R. Khuntia, J. L. Rueda, S. Bouwman, and M. A. van der Meijden, "A literature survey on asset management in electrical power [transmission and distribution] system," *International Transactions on Electrical Energy Systems*, vol. 26, no. 10, pp. 2123–2133, 2016.

[6] G. Balzer and C. Schorn, *Asset Management for Infrastructure Systems*. Springer International Publishing, 2022.

[7] A. A. Razi-Kazemi, M. Vakilian, K. Niayesh, and M. Lehtonen, "Circuit-breaker automated failure tracking based on coil current signature," *IEEE Transactions on Power Delivery*, vol. 1, no. 29, pp. 283–290, 2014.

[8] S. M. Strachan, S. D. McArthur, B. Stephen, J. R. McDonald, and A. Campbell, "Providing decision support for the condition-based maintenance of circuit breakers through data mining of trip coil current signatures," *IEEE Transactions on Power Delivery*, vol. 22, no. 1, pp. 178–186, 2006.

[9] F. N. Rudsari, A. A. Razi-Kazemi, and M. A. Shoorehdeli, "Fault analysis of high-voltage circuit breakers based on coil current and contact travel waveforms through modified svm classifier," *IEEE Transactions on Power Delivery*, vol. 34, no. 4, pp. 1608–1618, 2019.

[10] M. Abdollah and A. A. Razi-Kazemi, "Intelligent failure diagnosis for gas circuit breakers based on dynamic resistance measurements," *IEEE Transactions on Instrumentation and Measurement*, vol. 68, no. 9, pp. 3066–3077, 2018.

[11] E. A. Vianna, A. R. Abaide, L. N. Canha, and P. L. Vianna, "SF6 gas circuit breakers reliability estimation, considering likely wear points," in *2016 51st International Universities Power Engineering Conference (UPEC)*. IEEE, 2016, pp. 1–6.

[12] E. A. Vianna, A. R. Abaide, L. N. Canha, and V. Miranda, "Substations SF6 circuit breakers: Reliability evaluation based on equipment condition," *Electric Power Systems Research*, vol. 142, pp. 36–46, 2017.

[13] Q. Yang, J. Ruan, Z. Zhuang, D. Huang, and Z. Qiu, "A new vibration analysis approach for detecting mechanical anomalies on power circuit breakers," *IEEE Access*, vol. 7, pp. 14 070–14 080, 2019.

[14] B. Feizifar and O. Usta, "A novel arcing power-based algorithm for condition monitoring of electrical wear of circuit breaker contacts," *IEEE Transactions on Power Delivery*, vol. 34, no. 3, pp. 1060–1068, 2018.

[15] W. Gao, R.-J. Wai, S.-P. Qiao, and M.-F. Guo, "Mechanical faults diagnosis of high-voltage circuit breaker via hybrid features and integrated extreme learning machine," *IEEE Access*, vol. 7, pp. 60 091–60 103, 2019.

[16] J. Lopez-Roldan *et al.*, "Development of non-intrusive monitoring for reactive switching of high voltage circuit breaker," *International Journal of Electrical Power & Energy Systems*, vol. 61, pp. 219–228, 2014.

[17] A. A. Razi-Kazemi and K. Niayesh, "Condition monitoring of high voltage circuit breakers: past to future," *IEEE Transactions on Power Delivery*, vol. 36, no. 2, pp. 740–750, 2020.

[18] *Operating Instructions Circuit-Breaker 3AP2 Fl*, Siemens, 2013.

Appendix 2

S. Asefi, J. Kilter, and M. Landsberg, "Incorporating Service Type in Ageing Failure Model of High-Voltage Circuit Breaker," in 2023 27th International Conference Electronics, 2023, pp. 1-5.

Incorporating Service Type in Aging Failure Model of High Voltage Circuit Breaker

Sajjad Asefi, Jako Kilter
Department of Electrical Power Engineering and Mechatronics
Tallinn University of Technology
Tallinn, Estonia
sajjad.asefi@taltech.ee, jako.kilter@taltech.ee

Mart Landsberg
Grid Maintenance Department
Elering AS
Tallinn, Estonia
mart.landsberg@elering.ee

Abstract—Reliability and security of the power system are dependent on the proper operation of the high voltage circuit breakers (HVCBs). This paper presents a novel Gaussian function-based model to forecast the remaining useful lifetime (RUL) of the HVCBs based on the historical failure data. The model deals with the mean time to failure reliability index instead of failure rate. Furthermore, the service type of the HVCBs is also incorporated into the proposed model. Forecasting RUL of the HVCBs is of significant value for electric utilities, especially to optimize maintenance schedules and prevent catastrophic failures. CIGRE's third survey data is utilized to compare the proposed model with the conventional models. The obtained results demonstrate that the proposed model can accurately forecast the RUL for the HVCB.

Index Terms—Predictive maintenance, Circuit breaker, remaining useful lifetime, Gaussian model.

I. Introduction

High voltage circuit breakers (HVCBs) are essential equipment in power systems that are utilized to reconfigure network topologies and isolate faulty sections of the power system [1]. Any HVCB malfunction could result in a system outage, which would be extremely costly from the economical perspective and bring out an undesirable social impact as well [2]. Performing the HVCB maintenance at the proper time is vital to ensure the reliability of its operation [3]. One of the main applications of the aging failure model is to assist with the maintenance strategy of the equipment. Historical failure data analysis can be applied to forecast the remaining useful lifetime (RUL) of the HVCBs, and to assist the system operator as a decision support mechanism [3].

The RUL of the equipment can be forecasted via two methods: 1) degradation modeling using the physical properties of the equipment, or 2) data-driven model based on historical data [4], [5]. Based on the total number of operations and the average failure rate, the HVCB's availability degradation model was built in [6]. On the basis of data from online monitoring, a model of the HVCB's exponential degradation was developed in [7]. However, the service type of the HVCB has not been taken into account in [6], [7]. In [8], a method to combine the HVCB's overall health index and operation based expected aging curve is presented to provide optimal scheduling of the HVCB's maintenance. In [9] and [10], an assessment of the reliability status of the HVCBs using a is proposed. However, the studies in [8]–[10] only assess the instantaneous status of the HVCB degradation and they are unable to provide any information regarding RUL of the equipment.

To provide a data-driven model that forecasts the condition of the equipment, the availability of historical failure data is essential. Three global assessments on the reliability of the HVCBs have been conducted by CIGRE so far. A distinction between a failure of a HVCB that results in the termination of one or more of its core functions, major failure (MaF), trivial failures or minor failure (MiF), and defects can be made from the perspective of reliability. The scope of the most recent CIGRE survey which involves 83 utilities from 26 countries, covers voltage ranges above 60 kV [11]. Shunt capacitor banks and shunt reactors totally cover less than 5% of the entire HVCB population, yet they account for more than 20% of the MaF [12]. This is not only due to improper specification of the HVCB characteristics, but also because of the frequent operation of these HVCB service types.

The focus of this research work is on applying MaF data. When a MaF occurs, the operating parameters of the power system will change immediately (for example, the backup protective equipment must be utilized to clear the fault), or the system must be taken out of service for unscheduled maintenance within 30 minutes [12]. The maloperation of the HVCB which is counted as a MaF can have three modes, namely mechanical, electrical, and insulation. For instance, if the HVCB does not open or close on command it will be a MaF of mechanical mode. If the HVCB fails to carry the current, it would be MaF of electric mode. Break down across open poles is an example of MaF of the HVCB's electrical mode.

In this paper, a novel model to forecast RUL of the HVCB is presented. The model is based on Gaussian function. The historical MaF data of the most recent CIGRE survey has been utilized to provide a data-driven model of RUL of the HVCB. Apart from the Weibull or exponential models which are commonly used in the literature, a novel Gaussian function-based model is introduced in this paper to demonstrate the aging behavior of the HVCB during its lifetime in a more accurate manner. Moreover, the service type that has a considerable effect on the MaF of the HVCB is incorporated in the model

This work has been financially supported by the Estonian Transmission System Operator Elering AS through the project "Risk and condition based asset management in future power systems", No. 1.1-4/2021/644/LEEEE21116.

using a normalization technique, which has not been done in the literature.

The rest of the paper is organized as follows. Section II discusses the concept behind the various stages of equipment failure and the mathematical modeling of conventional techniques. Section III describes the proposed methodology, and the obtained results based on the comparison with conventional methods are provided in section IV. Section V concludes this paper.

II. Equipment Failure Modeling

This section provides an insight into the general scheme of equipment failure modeling. Additionally, the Weibull distribution and z-score normalization technique are briefly explained.

A. Bathtub curve

In reliability engineering, failure frequency or failure rate is commonly presented by the λ symbol and indicates the number of failures of the equipment per unit of time [11]. The overall failure rate of the equipment that are installed in the power system varies throughout their lifetime and would follow a curve, which is roughly shaped like a bathtub curve, as demonstrated in Fig. 1. The overall failure curve is composed of the aggregation of three curves, namely early-stage failure, random failure, and aging failure [13].

Due to manufacturing defects and improper installment, the initial stage (i.e., early-stage failure) has a significant failure rate. During the time, the initial stage's failure rate decreases, and it reaches a constant failure rate which is the beginning of the second stage. It is assumed that random failure is the main factor within the second stage. In the final stage (i.e., aging failure), the aging of the equipment is causing an increase in the failure rate, until the device fails.

It is to be noted that due to operational circumstances, the period for each of the mentioned three stages can be different for each piece of equipment.

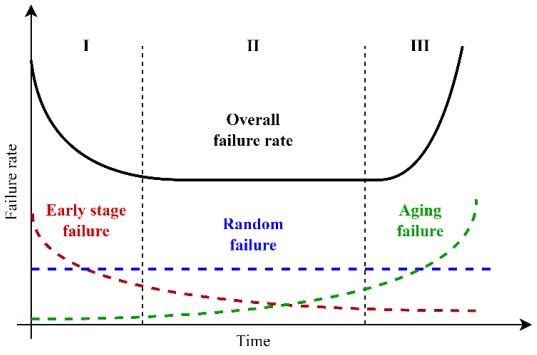


Fig. 1. Typical time-varying failure rate for the power system equipment throughout the lifetime [13]

Another parameter that can be used instead of the failure rate and makes it more understandable is the mean time to failure (MTTF). MTTF can be calculated as follows:

$$MTTF = \frac{1}{\lambda} \tag{1}$$

For example, if a device has λ = 0.02 failures/year, using (1), $MTTF$ = 50 which means that ideally, the average time during which the device is expected to work reliably is 50 years. In this paper, the failure rate values from historical data have been converted to the MTTF and then the rest of the analysis has been done.

B. Weibull distribution

Weibull distribution is frequently used in reliability engineering and other fields because of its flexibility and relative simplicity [14].

The failure process of the HVCB can be modeled using a Weibull distribution [15], [16]. The failure rate and MTTF of the HVCB during the time, λ_W and $MTTF_W$, can be determined using the Weibull distribution's definition as follows:

$$\lambda_W(t) = \frac{a}{b}\left(\frac{t}{b}\right)^{a-1} \tag{2}$$

$$MTTF_W(t) = \frac{b}{a}\left(\frac{t}{b}\right)^{1-a} \tag{3}$$

where t, a, and b indicate time (or age), shape parameter, and scale parameter, respectively. The Weibull distribution's behavior can be significantly affected by the shape parameter's value and may be transformed into other distributions for specific values of the shape parameter. For instance, the Weibull distribution simplifies to the exponential distribution when b = 1. Considering the bathtub curve in Fig. 1, Weibull distribution with different parameters can be attributed to each stage. If b < 1, Weibull distribution will have a high early-stage failure rate that diminishes over time. The failure rate of Weibull distributions with $b \approx 1$ is rather stable, indicating the random failure stage. Weibull distributions with b > 1 demonstrate the aging failure stage, which are Weibull distributions with an increasing failure rate over time.

III. Proposed Methodology

Curve fitting is the method of developing a curve or mathematical function that has the best fit to a set of data points. This fitted function on the data might be subjected to constraints. Curve fitting can involve either interpolation or smoothing. Interpolation requires an exact fit to the data. However, smoothing involves building a smooth function that roughly fits the data. In this paper, instead of using Weibull model a Gaussian function-based model is presented to fit the MTTF data of the HVCB.

A. Gaussian model

Gaussian distribution (also called normal distribution) is a kind of continuous probability distribution for a random variable. Its probability density function's generic form for a random variable x is represented by:

$$P(x) = \frac{1}{\sigma\sqrt{2\pi}} e^{-(x-\mu)^2/2\sigma^2} \quad (4)$$

where the distribution's mean or expected value is shown by the parameter μ, and the standard deviation is indicated by the parameter σ.

In this research work, MTTF data of the HVCB are fitted by adding two different Gaussian functions having six parameters to be identified. This function can be presented as follows:

$$MTTF'_G(t) = \frac{1}{a_1} e^{-(t-b_1)^2/c_1^2} + \frac{1}{a_2} e^{-(t-b_2)^2/c_2^2} \quad (5)$$

where $MTTF'_G(t)$ indicates the average duration for which the HVCB is expected to continue working reliably at time t, and a_1, a_2, b_1, b_2, c_1, and c_2 are the parameters of the model. In order to validate the accuracy of the proposed model in (5) to fit the MTTF data in comparison to the conventional models, the R-squared method has been applied. R-squared or coefficient of determination is the percentage of the variation in the dependent variable that can be predicted from the independent variable [17]. It is used in the context of statistical models whose main objective is to either predict future outcomes or test hypotheses using data from other relevant sources. The R-squared value normally ranges from 0 to 1. A higher R-squared value indicates better fitting. If the R-squared is one, it shows that the model perfectly fits the data.

B. Normalization

Normalization refers to adjusting the measured values on different scales to a standard scale. The aim is to normalize the failure rate values of the service type of the HVCBs, to incorporate them for MTTF calculations. The z-score method has been applied for the normalization of the HVCB service type in this paper. Although there are various methods for the normalization of the data, analyzing them is out of the scope of this paper. Using the z-score method, the sample data, x, with the mean value, $\bar{X}$, and the standard deviation, S, can be transformed to the normalized data as follows [18]:

$$\zeta = \frac{x - \bar{X}}{S} \quad (6)$$

where ζ is the normalized data set with mean zero and standard deviation one. It is worth noting that the normalization maintains the original data set's shape characteristics.

C. Incorporating service type

Service type refers to the place where the HVCB is installed. Based on the recent CIGRE survey the service type for HVCB can be shunt reactor, capacitor banks, bus-coupler, overhead line, transformer, and cable. The service type of the HVCB in the power system affects its frequency of failure. As it is shown in Fig. 2, if the HVCB is used for the shunt reactor, the MaF is higher than the case where the HVCB is used for the cables. The

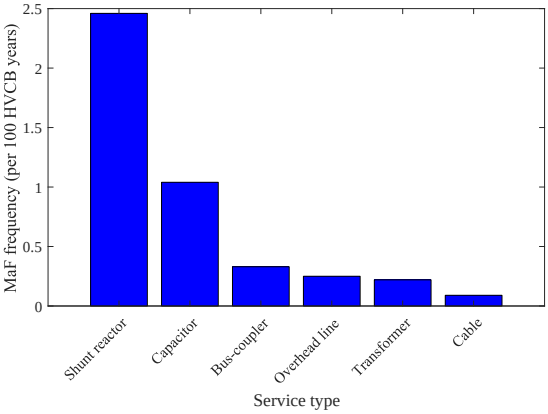


Fig. 2. MaF of HVCB according to the service type based on CIGRE survey [11]

normalization technique can be used to normalize the data presented in Fig. 2. In order to incorporate the service type in the aging failure model of the HVCB the following equation is proposed:

$$MTTF_G(t) = MTTF'_G(t) \times \left(1 - \frac{\zeta}{10}\right) \quad (7)$$

where $MTTF_G(t)$ stands for MTTF of HVCB incorporating normalized service type MaF using (6) into the proposed Gaussian function-based model in (5).

IV. Results and Discussion

In this section the results obtained via the proposed model and its comparison with the conventional models is presented. As mentioned before, HVCB MaF data from CIGRE survey is utilized which is provided in Table I.

TABLE I. MTTF and λ values for HVCB based on third CIGRE survey [11]

Age (years)	λ (failure/100 HVCB years)	MTTF (years)
2	0.14	714.3
6	0.25	400
10	0.25	400
14	0.26	384.6
18	0.36	277.7
22	0.49	204.1

The data presented in Table I are utilized and MTTF of the HVCB based on the proposed model in comparison with the conventional ones, are demonstrated in Fig. 3. It is obvious that the proposed model fits the data better than the exponential and Weibull models. Moreover, the behavior of the proposed model complies with the equipment failure rate throughout the lifetime which is shown in Fig. 1. Initially, the MTTF decreases which can be due to manufacturing or installment errors. Then it approaches an approximately constant MTTF value which

aligns with the second stage of the bathtub curve. Finally, the degradation expedites until the device fails.

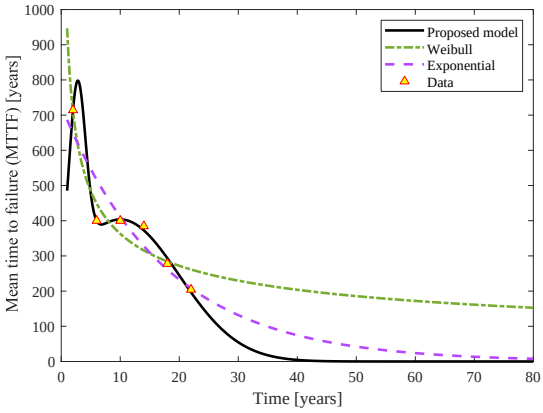


Fig. 3. Comparison of the proposed model to Weibull and exponential models

To compare the performance of the presented models, the R-squared value for each of them is provided in Table II. Based on the R-squared values, it is clear that the proposed method has a better performance.

TABLE II. R-SQUARED VALUES OF THE APPLIED MODELS

Method	Weibull	Exponential	Proposed
Value	0.9024	0.8583	0.9977

Using (6) and the MaF of various service types that are presented in Fig. 2, the effect of service type on the proposed method is demonstrated in Fig. 4.

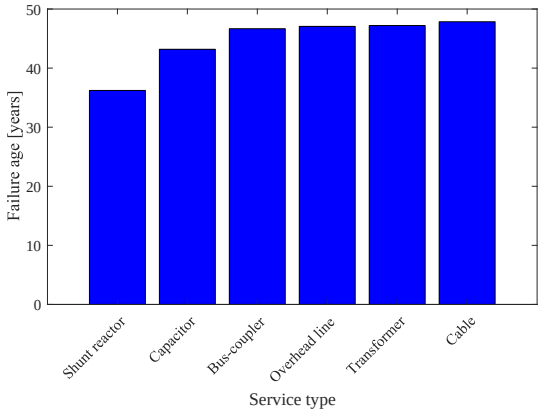


Fig. 4. Incorporating service type for failure age of HVCB based on the proposed model

Assuming that the lower limit is *MTTF* = 1, i.e., the HVCB fails at the time it reaches *MTTF* = 1, based on the proposed method the time (or the age of the HVCB) will be approximately 45 years. The normalized MaF values for service type are applied and the modified ages are demonstrated for each service type in Fig. 4. Note that, the specification of the failure limit highly depends on the risk endurance of the system. Because close to the final years of HVCB's RUL, the risk of failure would increase. It is worth mentioning that (7) is proposed according to available MaF values of service types. However, these values may vary based on the operating conditions of different system operators and it would require slight modification based on the available data.

It can be seen that incorporating service type gives out a more realistic forecast of the failure age of the HVCB. This evades underestimating the failure time of HVCB and prevents unexpected failures.

V. CONCLUSION

This paper presents a novel model to forecast the remaining useful lifetime of HVCBs. The proposed model is based on Gaussian distribution. The failure rate data of HVCB has been taken from the third CIGRE survey and they are converted to mean time to failure. The fitted model on the data demonstrates a better accuracy in comparison with the conventional Weibull and exponential models. The proposed model aligns with the bathtub failure curve, which is a typical time-varying failure rate for power system equipment. Moreover, service types of the HVCB are incorporated into the aging failure modeling which will lead to avoiding underestimating the failure characteristics of the HVCB and to provide more realistic measures of the remaining useful lifetime of the HVCB.

Analysis of different voltage levels of the HVCB and the physical characteristics of the equipment can be proposed for further research.

REFERENCES

[1] T. Krieg and J. Finn, *Substations*, ser. CIGRE Green Books. Springer International Publishing, 2018.

[2] D. Zhang, W. Li, X. Xiong, and R. Liao, "Evaluating condition index and its probability distribution using monitored data of circuit breaker," *Electric Power Components and Systems*, vol. 39, no. 10, pp. 965–978, 2011.

[3] X. Wei, K. Li, H. Wang, F. Chang, Y. Lu, and L. Sun, "Real-time remaining useful life prediction for high-voltage circuit breakers based on the degradation model and data-driven," in *2021 IEEE Sustainable Power and Energy Conference (iSPEC)*. IEEE, 2021, pp. 3781–3786.

[4] S. Lipirodjanapong, C. Suwanasri, and T. Suwanasri, "The reliability evaluation of configuration of bus arrangement in substations by the variable failure rate of power circuit breaker under time-based maintenance," in *2016 International Conference on Condition Monitoring and Diagnosis (CMD)*. IEEE, 2016, pp. 705–708.

[5] C. Suwanasri, S. Lipirodjanapong, T. Suwanasri, and W. Wangdee, "Failure rate analysis of circuit breaker and its preventive maintenance application," in *2014 International Conference on Probabilistic Methods Applied to Power Systems (PMAPS)*. IEEE, 2014, pp. 1–6.

[6] X. Liu, M. Shahidehpour, Y. Cao, Z. Li, and W. Tian, "Risk assessment in extreme events considering the reliability of protection systems," *IEEE Transactions on Smart Grid*, vol. 6, no. 2, pp. 1073–1081, 2015.

[7] J. Zhong, W. Li, R. Billinton, and J. Yu, "Incorporating a condition monitoring based aging failure model of a circuit breaker in substation

reliability assessment," *IEEE transactions on power systems*, vol. 30, no. 6, pp. 3407–3415, 2015.

[8] S. Asefi, G. Andreesen, M. Leinakse, J. Kilter, T. Kalmet, H. Manninen, and M. Landsberg, "Measurement and operation based condition monitoring methodology for high voltage circuit breakers," in *2022 IEEE PES Innovative Smart Grid Technologies Conference Europe (ISGT-Europe)*. IEEE, 2022, pp. 1–5.

[9] P. Dehghanian, Y. Guan, and M. Kezunovic, "Real-time life-cycle assessment of high-voltage circuit breakers for maintenance using online condition monitoring data," *IEEE Transactions on Industry Applications*, vol. 55, no. 2, pp. 1135–1146, 2018.

[10] J. Zhong, W. Li, C. Wang, and J. Yu, "A rankboost-based data-driven method to determine maintenance priority of circuit breakers," *IEEE Transactions on Power Delivery*, vol. 33, no. 3, pp. 1044–1053, 2017.

[11] CIGRE Working Group A3.06, "Final report of 2004–2007 international´ enquiry on reliability of high voltage equipment, part 2—reliability of high voltage circuit breakers," *CIGRE Techn Broch*, vol. 510, 2012.

[12] A. Janssen, D. Makareinis, and C.-E. Solver, "International surveys on¨ circuit-breaker reliability data for substation and system studies," *IEEE Transactions on Power Delivery*, vol. 29, no. 2, pp. 808–814, 2013.

[13] C. Chu, J. Moon, H. Lee, and J. Kim, "Extraction of time-varying failure rates on power distribution system equipment considering failure modes and regional effects," *International Journal of Electrical Power & Energy Systems*, vol. 32, no. 6, pp. 721–727, 2010.

[14] H. Rinne, *The Weibull distribution: a handbook*. Chapman and Hall/CRC, 2008.

[15] R. Billinton and R. N. Allan, *Reliability evaluation of engineering systems*. Springer, 1992, vol. 792.

[16] W. Li, *Risk assessment of power systems: models, methods, and applications*. John Wiley & Sons, 2014.

[17] J. Miles, "R-squared, adjusted r-squared," *Encyclopedia of statistics in behavioral science*, 2005.

[18] M. Spiegel and L. Stephens, *Schaum's outline of statistics*. McGraw Hill Professional, 2007

Appendix 3

B. Asad, M. U. Sardar, T. Vaimann, A. Kallaste, S. Asefi, and J. Kilter, "High-Voltage Circuit Breaker Charging Motor's Condition Monitoring-Importance, Possibilities, and Challenges," in 2024 International Conference on Diagnostics in Electrical Engineering (Diagnostika), 2024, pp. 1-7.

High Voltage Circuit Breaker Charging Motor's Condition Monitoring – Importance, Possibilities, and Challenges

Bilal Asad
Department of Electrical Power Engineering and MechatronicsTallinn University of Technology Tallinn, Estonia
bilal.asad@taltech.ee

Muhammad Usman Sardar
Department of Electrical Power Engineering and MechatronicsTallinn University of Technology Tallinn, Estonia
muhammad.sardar@taltech.ee

Toomas Vaimann
Department of Electrical Power Engineering and MechatronicsTallinn University of Technology Tallinn, Estonia
toomas.vaimann@taltech.ee

Ants Kallaste
Department of Electrical Power Engineering and MechatronicsTallinn University of Technology Tallinn, Estonia
ants.kallaste@taltech.ee

Sajjad Asefi
Department of Electrical Power Engineering and MechatronicsTallinn University of Technology Tallinn, Estonia
sajjad.asefi@taltech.ee

Jako Kilter
Department of Electrical Power Engineering and MechatronicsTallinn University of Technology Tallinn, Estonia
jako.kilter@taltech.ee

***Abstract*— The reliable operation of high voltage circuit breakers (HVCB), their unfailing control and monitoring from remote locations is becoming increasingly significant day by day as the world is moving towards Internet of Things (IoT) and other industry 4.0 standards. Among other parts of HVCB, the spring charging motor (SCM) plays a very crucial role by keeping the HVCB ready for operation without manual interference. The failing of SCM may start the cascading faults in the power network by ending the possibility of its control from remote locations. Hence the continuous health monitoring of SCM for control and predictive maintenance is of paramount importance. This paper provides a comprehensive overview on the possible faults of SCM, the importance of their detection at incipient stage, an insight into the future of the advanced fault detection techniques and their implementation challenges.**

Keywords— ***Artificial intelligence, Circuit breakers, Condition monitoring, Mathematical models, Power System Reliability, Signal Processing, Wearable Health Monitoring***

I. Introduction

HVCBs play a very significant role in facilitating the reliable operation of power systems. These are responsible for managing high voltage and current based electric stresses and are used to extinguish the electric arc which occurs between contacts while interrupting the flow of current under normal or healthy operating conditions. Under faulty conditions they should be able to isolate the fault for maintaining the safe operation of other parts of the power network.The growing trend of renewable energy resources with variable generation patterns, utilization of non-linear loads such as electronic devices, power converters, variable speed drives has had a significant impact on the power quality of the network which may increase the frequency of HVCB's operation, increasing the importance of its continuous condition monitoring.

Generally, the faults in HVCBs can be broadly classified into two categories: the major faults and the minor faults [1]. Major faults represent the clear maloperation of HVCBs and these may include failure to execute open or close commands, opening or closing without command, extensive arcing while opening or closing, failure to carry current, dielectric breakdown to earth or poles, or locking in any open or close position. The minor faults represent a worsening of the performance of the HVCB and may include leakage of insulating and cooling systems, increase in the vibrations, corrosion, and smaller changes in the operating characteristics. Obviously, minor faults can easily lead towards major faults if not addressed properly at the appropriate time. The main power system components utilizing HVCB based protection are overhead lines, transformers, bus couplers, cables, shunt reactors, capacitor banks etc. The percentage utilization of HVCBs with different components of the power system, and also the rate of major and minor faults is summarized in the first [2], second [3] and third worldwide surveys [4].

Many kinds of CB failures, including explosions, are reported in the literature. Among these failures 43% to 44% are related to the main components of the CB such as compressors, energy storage devices, actuators (spring charging motors), and control elements, 20% to 29% are related to auxiliary devices such as trip circuits, heaters, gas density monitors, and 21% to 31% are related to current path interruption components [5][6].

Consequently, the continuous health monitoring, testing and inspection of the HVCBs for improved performance and reliability of the overall power network is of paramount importance. Among the various maintenance approaches such as, reactive maintenance (RM), preventive maintenance (PM) and predictive maintenance (PRM), the PRM is becoming more popular [7]–[9]. This is due its ability to detect the fault at an incipient stage, which results in a more favorable economic outcome.

Among many other parts, electrical charging motors (ECM) are arguably one of the most important components of a high voltage CB. The fault in ECM can lead towards a major fault by keeping the CB in open or closed position permanently and physical on-site intervention by the operator is required for charging the spring(s). The main purposes of ECM in CBs are charging the energy storage subsystem of the CB which facilitates the opening and closing of CB contacts with precision and reliability. Their response to interrupt the fault current should be very swift and stable.

This work has been financially supported by the Estonian Transmission System Operator Elering AS through the project "Risk and condition-based asset management in future power systems", No. 1.1-4/2021/644/LEEEE21116.

979-8-3503-6149-0/24/$31.00 ©2024 IEEE

A variety of state variables and their coupling effect makes electrical machines complex engineering equipment. Therefore, if the vulnerability of all subsystems of a HVCB is individually evaluated then the probability of a fault occurring in its charging motor is quite significant. This is due to its complicated structure and the interactions between its electric, magnetic, and mechanical parts. The frequent electrical, thermal, mechanical, and magnetic stresses continuously deteriorate parts of the charging motor. This may lead to its abnormal operation with resultant CB failure. Mostly these motors are DC series motor because of their high starting torque and load-based self-regulating capabilities.

The main purposes of the health monitoring of HVCB charging motors may be summarized as follows:

- Obtaining real time assurance of the CB's normal operation and its remote control and monitoring capabilities under the power network's healthy and faulty conditions. If the charging motor fails, the CB can no longer be controlled without the physical presence of the operator.
- Assessment of the remaining useful life (RUL) of CB and its charging motor by checking the signs of degradation, wear, or other electromechanical issues.
- Increase the reliability of the power network by avoiding cascading effects of the faults.
- Progressing towards the implementation of advanced AI based diagnostic algorithms by collecting and analyzing the simulations and real time data for the development of fault defining rules.
- The collection and analysis of data for advancing towards predictive maintenance and the implementation of industry 4.0 standards on the CBs.

II. Types of Faults in Charging Motors

A universal motor is a special type of machine designed to operate on either a direct or single-phase alternating current. It is a DC motor in which the armature and field windings are connected in series. It can produce high starting current [10] with load-dependent speed and torque profiles. A universal motor used in the charging mechanism of a HVCB is shown in Fig. 1.

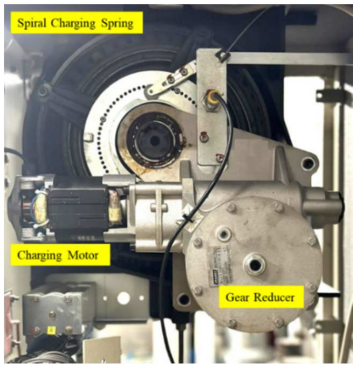


Fig. 1. Universal motor employed for circuit breaker spring charging.

At no load, the universal motors operate at high speed and produce low torque, but when load increases as in the case of charging spring, upon compressing the spring, the load of the motor increases, and it automatically decreases speed to increase the torque. This self-regulation phenomenon reduces the need for a sophisticated drive and control setup for the motor with resultant economic benefits. This is the main advantage which makes this motor the best candidate for application in the spring charging mechanism of HVCBs.

To reduce the effect of armature reaction and resultant sparking on the commutator, the compensation windings are used. The inclusion of a compensation winding in any motor depends on its duty cycle. If the motor is less frequently used as in case of CBs, the compensation winding can be omitted to reduce the cost and complexity. But if the motor's on and off intervals are more frequent, then the motor with a compensation winding may be preferred. In CBs, both types of motors are being used. The basic schematic diagram of a universal motor is shown in Fig. 2.

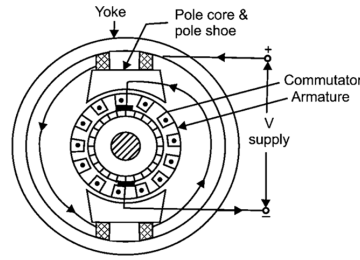


Fig. 2. Schematic of a universal motor [3]

Spring charging in CBs can be performed using other kinds of motors as well, i.e., induction motors, synchronous motors, brushless DC (BLDC) motors, or stepper motors, but the requirement of sophisticated control and power supply (drive) mechanisms would make them unnecessarily complicated and expensive. Since the required duty cycle is not extensive and cost and complexity needs to be reduced, the universal motors are usually best suited for use in CBs. The field winding of the universal motor, which is a series motor, is connected to the armature winding. The distinction of the universal motor among others is as follows [10]-[12]:

- The field winding has a small number of coils compared to other motor types.
- The same current flows in the stator and rotor of the motor through the brushes of the machine; hence the torque is proportional to the square of the stator current. Therefore, a larger current flow in the field winding compared to the shunt field winding.
- The current in the stator of the shunt motor is constant regardless of the armature (rotor). However, universal motors have field current, which depends on the loading current. The higher current drawn by the load creates a high torque, especially at the starting point.

The specifications of a HVCB's charging motor used as a case study are presented in Table I.

TABLE I. CHARGING MOTOR SPECIFICATIONS

Motor type	**Universal traction motor**
Serial number	535673
Rated voltage (DC/AC)	220/250 V
Rated current	4.09 A
Power	900 W
Turns	9000 rpm
Power factor (AC)	0.87
Class of enclosure	B

In the case of a fault in the motor, the overall process which depends on it undergoes unexpected failure or downtime, which results in production impact with unavoidable loss, high cost of operation, and profit loss [13]. The different types of faults that occur in the motors are classified in Table II [14][15]:

TABLE II. TYPES OF FAULTS IN CHARGING MOTORS

Fault Domain	Associated Component	Possible fault	Contribution
Electrical	Abnormality in supply (DC or AC)	• Increased or decreased voltage in comparison with the rated voltage • High voltage ripples with resultant increased vibrations, sparks on commutator and overheating • Complete supply failure	Frequent
	Field winding faults	• Field winding open circuit • Field winding short circuit • Overheating	
	Commutator	• Arcing on the commutator • Eroded commutator segments • Commutator overheating • Shift in magnetic neutral axis • Bad carbon brushed	
	Armature	• Armature winding partial or complete open circuit both in steady and temporal state. • Armature winding short circuit. • Field distortion due to armature reaction	
Mechanical	Eccentricity	• Static eccentricity • Dynamic eccentricity • Mixed eccentricity	Moderate
	Bearings	The bearings with bad lubricant, overheated, defected inner or outer race, corroded or shift in axis with resultant increase in eccentricity	
Load Side	Gears	• Misaligned • Broken teeth with resultant change in gear ratio • Increased vibration and speed and torque ripples	Rare
	Spring tension	Change in spring dynamics due to internal or external (weather) factors	

The basic research directions for the condition monitoring of electrical machines in general and universal motors specifically available in literature can be summarized as follows [16]-[21]:

- Current and voltage monitoring and analysis
- Temperature analysis (infrared monitoring, thermal emission)
- Radio-frequency emission
- Vibration analysis
- Acoustics or noise analysis
- Chemical analysis
- Stray flux analysis
- Motor current signature analysis

These methods can be used to gather the data which can be analyzed using conventional signal processing techniques, model dependent estimation techniques or advanced statistical or intelligent methods.

III. ADVANCED DIAGNOSTIC PROCEDURES

The fundamental physics underlying electric machine operation is the foundation for the traditional modelling techniques. Analytical models were used to analyze the effects of faults on different parameters while considering the model's outputs. The approximations used for developing these models were their limitation. Analytical models are difficult to execute precisely in real-world situations. However, the increasing computational capabilities of modern-day computers, the analytical models with less approximations, the finite element method (FEM) based, and hybrid FEM-analytical models are being developed. For predictive maintenance of electrical machines these more accurate models are instrumental in progressing towards the successful implementation of parameters estimation [22], inverse problem theory [23], hardware-in-the-loop and digital twin [24] technologies as shown in Fig. 3.

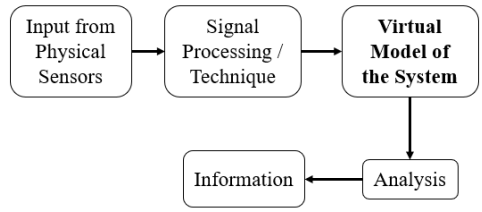


Fig. 3. Digital twin framework of an electrical system

Moreover, the adoption of data-driven models is becoming feasible, in which the system is accurately described using data gathered from sensors, data gathering systems and mathematical models. Over the past decade, researchers have become increasingly more interested in artificial intelligence (AI) which precisely predicts the relationship involving input and output, or the behavior of a system. The emergence of data-driven strategies and the advancement of computing technology have facilitated the AI techniques to model unsteady and imprecise information. The field of condition monitoring and fault detection has evolved in the twenty-first century due to advances in digital signal processing, improved computer power, and artificial intelligence approaches.

In the literature which has been published over the last ten years, these data-driven strategies are described as being popular among academics. Artificial Neural Networks (ANN) [25], Convolutional Neural Networks (CNN) [26], Recurrent Neural Networks (RNN) [27], Long Short-Term Memory (LSTM) [28], Support Vector Machines (SVM) [29], Random Forests (RF) [30], Hidden Markov Models (HMM) [31], Particle Swarm Optimization (PSO) [32], K-Nearest Neighbors (KNN) [33], Reinforcement Learning (RL) [34], Gaussian Mixture Models (GMM) [35], Self-Organizing Maps (SOM) [36], Genetic Algorithms (GA) [37], fuzzy logic [38], Adaptive Neuron-fuzzy Inference Systems (ANFIS) [39], and hybrids of these techniques are among the AI

approaches which are frequently used in the fault diagnosis of electric machines.

The most significant advantage of these methods is the self-assessment, detection, preventive and control strategies. It reduces human involvement, and the probability of human analysis-based errors are minimized. Moreover, the accuracy of these models continuously increases as they continuously train themselves when exposed to different single and composite fault data while working in different environments. A flowchart diagram representing the connections between the conventional and advanced diagnostic methods is shown in Fig. 4.

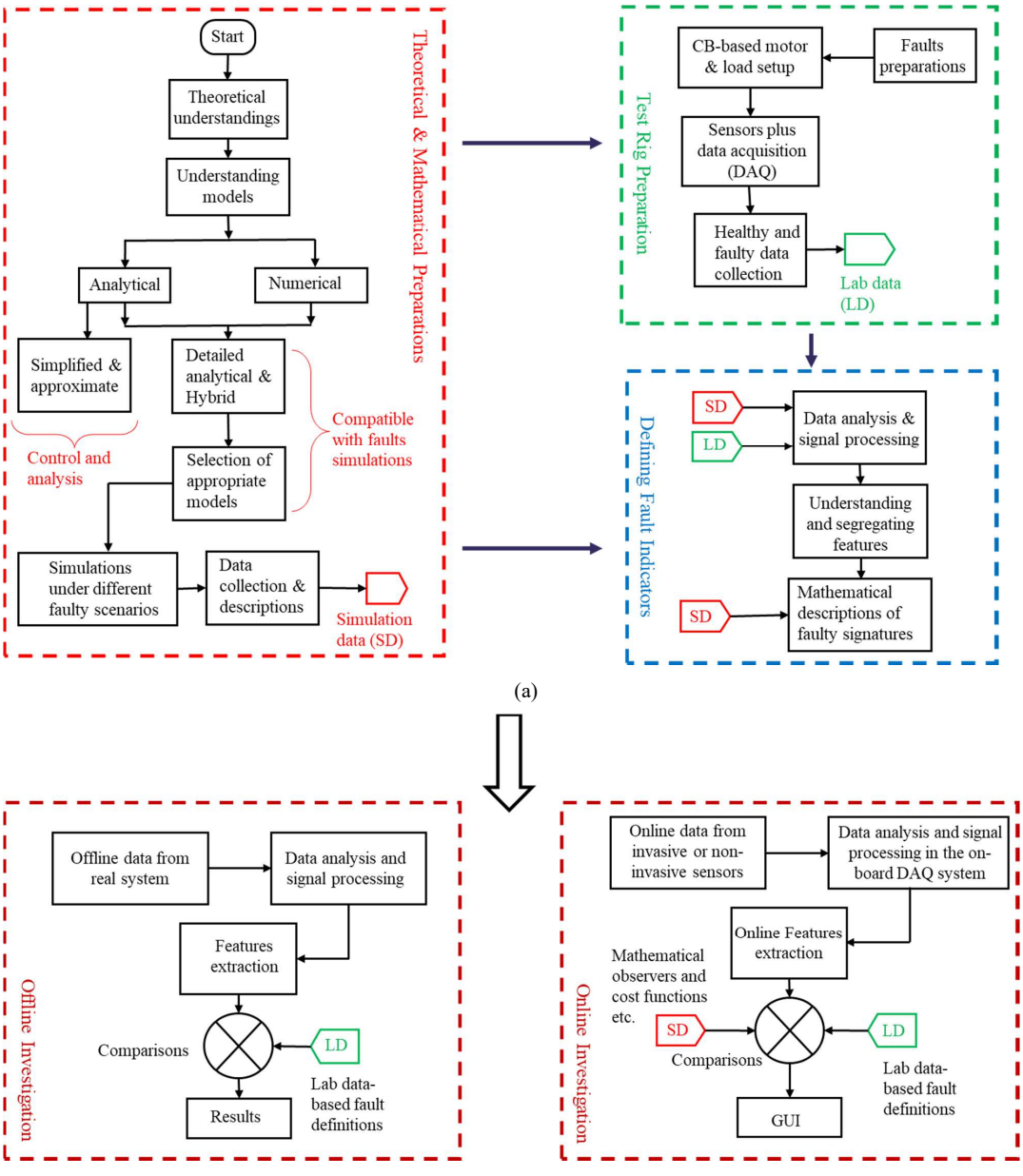


Fig. 4. (a) The simulations, test rig preparations and defining benchmark fault indicators, (b) implementation of rules in online and offline predictive maintenance environments

IV. REAL-TIME IMPLEMENTATION

Real-time implementation of the condition monitoring and diagnostics for the HVCB involves many critical challenges and potential considerations. Since the motor used for charging is a supercritical component of the system responsible for breaking the power circuit, it has become crucial for protecting the power substation and overall power grid. Hence, detecting and diagnosing the motor for potential to precipitate future faults and preventing it from failure can reduce power outages and facilitate rapid replacement of the equipment to maintain the power system's high reliability [40]-[42].

The challenges which can be encountered are described individually with detailed descriptions below. Up to five potential obstacles are described based on the available literature [43]-[47].

The primary challenge in implementing the fault diagnosis (FD) algorithm for charging motors is the complexity of its motor system. The universal motor system consists of several components including mechanical and electrical parts. These are, for example, field winding, armature winding, commutator segments, carbon brushes, bearing system, and the cooling system with a certain allowed duty cycle for each motor. The winding design is also a factor which must be considered, as well as general mechanical wear related to normal operation and the thermal limitations. Consequently, each of the sub-systems will undergo unavoidable wear. The mechanical faults are degenerative and can cause failure if these are not mitigated and monitored in a timely fashion. Therefore, the developed algorithm must consider the effective analysis of the motor and interpretation of motor performance to identify and diagnose these faults with a thorough recognition of the operation and particular design.

The second challenge is acquiring real-time operating data from the working system for fault diagnostics. For example, obtaining the sample of current signals, voltage, vibration, temperature, speed or another relevant variable with sensors must have high sensitivity and accuracy. It must be capable of measurement with a sufficiently high sampling rate. This is essential for the fault diagnosis algorithm's accuracy and reliability, which is required for real-time and historical data sets from the applicable sensor and installed monitoring devices. Integrating and synthesizing a high volume of data is complex and resource-intensive, but also a primary requirement to ensure the algorithm's quality and reliability.

The third challenge for intelligent condition monitoring and fault diagnostics management is obtaining a voluminous dataset for training and validation purposes. The dataset must contain several fault scenarios and motor performance parameters which are captured. Gathering real-time data can be time-consuming, and costly, especially if some new operational power system or specialized equipment is used.

The next possible challenging problem is the selection of appropriate diagnostic techniques. Numerous approaches are available regarding diagnostics, including model-based techniques, signal processing approaches, statical analysis, artificial intelligence, and expert systems, whereas each method has its pros and cons. The overall selection of techniques depends on factors like available data, the complexity of the charging motor system, computational time, power of computer processing, accuracy desired regarding its attainment, and robust output at the deliverable.

The most important challenge is the validation and testing procedure in implementing the algorithm. Robustness defines the range of variable input regions in which the output or response remains effective and insensitive. Because the change in output which accompanies a marginal change in input can lead to spurious results and vice versa, the final algorithm validation may also include comparing diagnostic data with known fault scenarios, performance evaluations, collaboration with the experts of this domain and other utilities to utilize their expertise and feedback.

V. CONCLUSIONS

This review article provides a comprehensive overview of the condition monitoring of high voltage circuit breaker charging motors. It emphasizes the significance of condition monitoring in ensuring reliable and efficient operation of high voltage circuit breakers. By monitoring the charging motor, detection of faults at an incipient stage becomes possible, reducing downtime and possibly preventing catastrophic failures.

The article summarizes a range of signal processing techniques, both conventional and advanced, for analyzing the local and global signals generated by the charging motor. These techniques enable the extraction of meaningful features and patterns, facilitating fault detection and diagnosis. Integration of AI-based methods further enhances accuracy and efficiency in fault detection and classification.

Additionally, mathematical modeling and simulation techniques are discussed to play a crucial role in comprehending the behavior of charging motors under different fault conditions. These provide understanding into the primary physics and foster the development of more precise models for fault analysis and data generation.

While significant improvements have been made in the field of health monitoring of charging motors, several challenges remain. These include the establishment of standardized monitoring techniques, integration of multiple monitoring parameters, and interpretation of extensive monitoring data. Addressing these challenges should be the focus of future research, aimed at advancing the field. The benefits and limitations of major techniques are also discussed in each section which helps the researchers and practitioners to go in the right direction.

To conclude, this review serves as a comprehensive resource for researchers, engineers, and practitioners interested in the condition monitoring of the charging motor of high voltage circuit breakers. By implementing effective monitoring strategies and leveraging advanced techniques, the reliable and safe operation of high voltage circuit breakers can be ensured, minimizing the risk of failures, and enhancing overall system performance.

REFERENCES

[1] A. Janssen, D. Makareinis, and C. E. Solver, "International surveys on circuit-breaker reliability data for substation and system studies," *IEEE Transactions on Power Delivery*, vol. 29, no. 2, pp. 808–814, 2014, doi: 10.1109/TPWRD.2013.2274750.

[2] G. Mazza and R. Michaca, "The first international enquiry on circuit breaker failures and defects in service," *Electra*, vol. 79, pp. 21–91, Dec. 1981.

[3] P. L. Fletcher and W. Degen, "Summary of the final results and conclusions of the second international enquiry on the reliability of

high voltage circuit-breakers," *IEE Conference Publication*, no. 406, pp. 24–30, 1995, doi: 10.1049/CP:19950213.

[4] M. Runde, "Failure frequencies for high-voltage circuit breakers, disconnectors, earthing switches, instrument transformers, and gas-insulated switchgear," *IEEE Transactions on Power Delivery*, vol. 28, no. 1, pp. 529–530, 2013, doi: 10.1109/TPWRD.2012.2220638.

[5] X. Zhang, J. Zhang, E. Gockenbach, and H. Borsi, "Life mangement of SF6 circuit breakers based on monitoring and diagnosis," *IEEE Electrical Insulation Magazine*, vol. 25, no. 3, pp. 21–29, 2009, doi: 10.1109/MEI.2009.4976899.

[6] A. A. Razi-Kazemi, M. Vakilian, K. Niayesh, and M. Lehtonen, "Circuit-breaker automated failure tracking based on coil current signature," *IEEE Transactions on Power Delivery*, vol. 29, no. 1, pp. 283–290, 2014, doi: 10.1109/TPWRD.2013.2276630.

[7] J. Schlabbach and T. Berka, "Reliability-centred maintenance of MV circuit-breakers," *2001 IEEE Porto Power Tech Proceedings*, vol. 4, pp. 301–305, 2001, doi: 10.1109/PTC.2001.964850.

[8] A. A. Razi-Kazemi, M. Vakilian, K. Niayesh, and M. Lehtonen, "Priority Assessment of Online Monitoring Investment for Power System Circuit Breakers - Part I: Qualitative-Quantitative Approach," *IEEE Transactions on Power Delivery*, vol. 28, no. 2, pp. 928–938, 2013, doi: 10.1109/TPWRD.2013.2243921.

[9] A. A. Razi-Kazemi and K. Niayesh, "Condition monitoring of high voltage circuit breakers: Past to future," *IEEE Transactions on Power Delivery*, vol. 36, no. 2, pp. 740–750, Apr. 2021, doi: 10.1109/TPWRD.2020.2991234.

[10] S. K. Sharma and M. S. Manna, "Performance Analysis of Universal Motor Based on Matlab Simulation," 2022 International Conference for Advancement in Technology, ICONAT 2022, 2022, doi: 10.1109/ICONAT53423.2022.9726017.

[11] P. Girovský and J. Kaňuch, "Analysis of the Power Supply Influence on the Universal Motor," Power Electronics and Drives, vol. 7, no. 1, pp. 103–111, Jan. 2022, doi: 10.2478/PEAD-2022-0008.

[12] R. Garg, "Behavioral analysis of a universal motor when operated on DC and AC supply," 2019 International Conference on Intelligent Computing and Control Systems, ICCS 2019, pp. 705–710, May 2019, doi: 10.1109/ICCS45141.2019.9065475.

[13] H. A. Toliyat, Electric machines : modeling, condition monitoring, and fault diagnosis. CRC Press, 2013.

[14] S. Nandi, H. A. Toliyat, and X. Li, "Condition Monitoring and Fault Diagnosis of Electrical Motors—A Review," IEEE Transactions on Energy Conversion, vol. 20, no. 4, pp. 719–729, Dec. 2005, doi: 10.1109/TEC.2005.847955.

[15] M. Burth and D. Filbert, "Fault Diagnosis of Universal Motors During Run-Down by Nonlinear Signal Processing," IFAC Proceedings Volumes, vol. 30, no. 18, pp. 411–416, Aug. 1997, doi: 10.1016/S1474-6670(17)42436-0.

[16] M. Sun, H. Wang, P. Liu, S. Huang, and P. Fan, "A sparse stacked denoising autoencoder with optimized transfer learning applied to the fault diagnosis of rolling bearings," Measurement, vol. 146, pp. 305–314, Nov. 2019, doi: 10.1016/J.MEASUREMENT.2019.06.029.

[17] K. You, G. Qiu, and Y. Gu, "Rolling Bearing Fault Diagnosis Using Hybrid Neural Network with Principal Component Analysis," Sensors 2022, Vol. 22, Page 8906, vol. 22, no. 22, p. 8906, Nov. 2022, doi: 10.3390/S22228906.

[18] C. Guo, L. Li, Y. Hu, and J. Yan, "A Deep Learning Based Fault Diagnosis Method with Hyperparameter Optimization by Using Parallel Computing," IEEE Access, vol. 8, pp. 131248–131256, 2020, doi: 10.1109/ACCESS.2020.3009644.

[19] M. Hakim, A. A. B. Omran, A. N. Ahmed, M. Al-Waily, and A. Abdellatif, "A systematic review of rolling bearing fault diagnoses based on deep learning and transfer learning: Taxonomy, overview, application, open challenges, weaknesses and recommendations," Ain Shams Engineering Journal, vol. 14, no. 4, p. 101945, Apr. 2023, doi: 10.1016/J.ASEJ.2022.101945.

[20] L. Frosini, "Monitoring and diagnostics of electrical machines and drives: A state of the art," Proceedings - 2019 IEEE Workshop on Electrical Machines Design, Control and Diagnosis, WEMDCD 2019, pp. 169–176, Apr. 2019, doi: 10.1109/WEMDCD.2019.8887815.

[21] L. Frosini, "Novel Diagnostic Techniques for Rotating Electrical Machines—A Review," Energies 2020, Vol. 13, Page 5066, vol. 13, no. 19, p. 5066, Sep. 2020, doi: 10.3390/EN13195066.

[22] S. Bachir, S. Tnani, J.-C. Trigeassou, and G. Champenois, "Diagnosis by parameter estimation of stator and rotor faults occurring in induction machines," IEEE Transactions on Industrial Electronics, vol. 53, no. 3, pp. 963–973, Jun. 2006, doi: 10.1109/TIE.2006.874258.

[23] T. Vaimann, A. Belahcen, and A. Kallaste, "Necessity for implementation of inverse problem theory in electric machine fault diagnosis," in 2015 IEEE 10th International Symposium on Diagnostics for Electrical Machines, Power Electronics and Drives (SDEMPED), IEEE, Sep. 2015, pp. 380–385. doi: 10.1109/DEMPED.2015.7303718.

[24] A. Rassolkin et al., "Interface Development for Digital Twin of an Electric Motor Based on Empirical Performance Model," IEEE Access, vol. 10, pp. 15635–15643, 2022, doi: 10.1109/ACCESS.2022.3148708.

[25] T. A. Shifat and J. W. Hur, "ANN Assisted Multi Sensor Information Fusion for BLDC Motor Fault Diagnosis," IEEE Access, vol. 9, pp. 9429–9441, 2021, doi: 10.1109/ACCESS.2021.3050243.

[26] I. Mukherjee and S. Tallur, "Light-Weight CNN Enabled Edge-Based Framework for Machine Health Diagnosis," IEEE Access, vol. 9, pp. 84375–84386, 2021, doi: 10.1109/ACCESS.2021.3088237.

[27] X. Li, A. Palazzolo, and Z. Wang, "Rotating machinery monitoring and fault diagnosis with neural network enhanced fuzzy logic expert system," Turbomachinery Technical Conference and Exposition, 2016, doi: 10.1115/GT2016-58102.

[28] P. Konar and P. Chattopadhyay, "Bearing fault detection of induction motor using wavelet and Support Vector Machines (SVMs)," Applied Soft Computing Journal, vol. 11, no. 6, pp. 4203–4211, Sep. 2011, doi: 10.1016/j.asoc.2011.03.014.

[29] X. Peng et al., "Random Forest Based Optimal Feature Selection for Partial Discharge Pattern Recognition in HV Cables," IEEE Transactions on Power Delivery, vol. 34, no. 4, pp. 1715–1724, Aug. 2019, doi: 10.1109/TPWRD.2019.2918316.

[30] F. Sloukia, M. El Aroussi, H. Medromi, and M. Wahbi, "Bearings prognostic using Mixture of Gaussians Hidden Markov Model and Support Vector Machine," Proceedings of IEEE/ACS International Conference on Computer Systems and Applications, AICCSA, 2013, doi: 10.1109/AICCSA.2013.6616438.

[31] L. Lu, Y. He, Y. Ruan, and W. Yuan, "Wind Turbine Planetary Gearbox Condition Monitoring Method Based on Wireless Sensor and Deep Learning Approach," IEEE Trans Instrum Meas, vol. 70, 2021, doi: 10.1109/TIM.2020.3028402.

[32] J. Xiong, Q. Zhang, G. Sun, X. Zhu, M. Liu, and Z. Li, "An Information Fusion Fault Diagnosis Method Based on Dimensionless Indicators with Static Discounting Factor and KNN," IEEE Sens J, vol. 16, no. 7, pp. 2060–2069, Apr. 2016, doi: 10.1109/JSEN.2015.2497545.

[33] K. S. H. Ong, W. Wang, N. Q. Hieu, D. Niyato, and T. Friedrichs, "Predictive Maintenance Model for IIoT-Based Manufacturing: A Transferable Deep Reinforcement Learning Approach," IEEE Internet Things J, vol. 9, no. 17, pp. 15725–15741, Sep. 2022, doi: 10.1109/JIOT.2022.3151862.

[34] M. He and W. Guo, "An Integrated Approach for Bearing Health Indicator and Stage Division Using Improved Gaussian Mixture Model and Confidence Value," IEEE Trans Industr Inform, vol. 18, no. 8, pp. 5219–5230, Aug. 2022, doi: 10.1109/TII.2021.3123060.

[35] S. Haroun, A. Nait Seghir, and S. Touati, "Self-Organizing Map and feature selection for of im broken rotor bars faults detection and diagnosis," Proceedings of 2018 3rd International Conference on Electrical Sciences and Technologies in Maghreb, CISTEM 2018, Jan. 2019, doi: 10.1109/CISTEM.2018.8613361.

[36] Z. Ke, C. Di, and X. Bao, "Adaptive Suppression of Mode Mixing in CEEMD Based on Genetic Algorithm for Motor Bearing Fault Diagnosis," IEEE Trans Magn, vol. 58, no. 2, Feb. 2022, doi: 10.1109/TMAG.2021.3082138.

[37] L. Song, H. Wang, and P. Chen, "Step-by-Step Fuzzy Diagnosis Method for Equipment Based on Symptom Extraction and Trivalent Logic Fuzzy Diagnosis Theory," IEEE Transactions on Fuzzy Systems, vol. 26, no. 6, pp. 3467–3478, Dec. 2018, doi: 10.1109/TFUZZ.2018.2833820.

[38] C. Chen, B. Zhang, G. Vachtsevanos, and M. Orchard, "Machine condition prediction based on adaptive neuro-fuzzy and high-order particle filtering," IEEE Transactions on Industrial Electronics, vol. 58, no. 9, pp. 4353–4364, Sep. 2011, doi: 10.1109/TIE.2010.2098369.

[39] G. Papa, B. Koroušić-Seljak, B. Benedičič, and T. Kmecl, "Universal motor efficiency improvement using evolutionary optimization," IEEE Transactions on Industrial Electronics, vol. 50, no. 3, pp. 602–611, Jun. 2003, doi: 10.1109/TIE.2003.812455.

[40] T. Sun, Y. Wang, and M. Ding, “A novel method for actuator fault detection considering complex operating processes,” J Process Control, vol. 110, pp. 1–10, Feb. 2022, doi: 10.1016/J.JPROCONT.2021.12.003.

[41] Isermann Rolf, “Fault-diagnosis applications: model-based condition monitoring: actuators, drives, machinery, plants, sensors, and fault-tolerant systems,” vol. 1, 2011.

[42] C. Nunes, E. J. S. Pires, A. Reis, C. Nunes, E. J. S. Pires, and A. Reis, “Machine Learning and Deep Learning applied to End-of-Line Systems: A review,” WSEAS Transactions on Systems, vol. 21, pp. 147–156, 2022, doi: 10.37394/23202.2022.21.16.

[43] D. Pal, R. Meyur, S. Menon, M. J. B. Reddy, and D. K. Mohanta, “Real-time condition monitoring of substation equipment using thermal cameras,” IET Generation, Transmission & Distribution, vol. 12, no. 4, pp. 895–902, Feb. 2018, doi: 10.1049/IET-GTD.2017.0096.

[44] W. Wang, “An intelligent system for machinery condition monitoring,” IEEE Transactions on Fuzzy Systems, vol. 16, no. 1, pp. 110–122, Feb. 2008, doi: 10.1109/TFUZZ.2007.896237.

[45] B. D. Russell and C. L. Benner, “Intelligent systems for improved reliability and failure diagnosis in distribution systems,” IEEE Trans Smart Grid, vol. 1, no. 1, pp. 48–56, 2010, doi: 10.1109/TSG.2010.2044898.

[46] U. Benko, J. Petrovčič, and D. Juričić, “IN-DEPTH FAULT DIAGNOSIS OF SMALL UNIVERSAL MOTORS BASED ON ACOUSTIC ANALYSIS,” IFAC Proceedings Volumes, vol. 38, no. 1, pp. 323–328, Jan. 2005, doi: 10.3182/20050703-6-CZ-1902.01856.

[47] B. Benedik, J. Rihtaršič, J. Povh, and J. Tavčar, “Failure modes and life prediction model for high-speed bearings in a through-flow universal motor,” Eng Fail Anal, vol. 128, p. 105535, Oct. 2021, doi: 10.1016/J.ENGFAILANAL.2021.105535..

Appendix 4

S. Asefi, J. Kilter, E. Shayesteh, P. Hilber, and T. Lindquist, "High-Voltage Circuit Breaker Health Index Evaluation Considering Measurement Accuracy," in 2024 IEEE PES Innovative Smart Grid Technologies Europe (ISGT EUROPE), 2024, pp. 1-5.

High Voltage Circuit Breaker Health Index Evaluation Considering Measurement Accuracy

Sajjad Asefi, Jako Kilter
Department of Electrical Power Engineering and Mechatronics, Tallinn University of Technology
Tallinn, Estonia

Ebrahim Shayesteh, Patrik Hilber
Department of Electromagnetic Engineering KTH Royal Institute of Technology
Stockholm, Sweden

Tommie Lindquist
Department of Electric Power Systems RISE – Research Institutes of Sweden
Stockholm, Sweden

***Abstract*—The reliable operation of high voltage circuit breakers (HVCBs) is crucial for ensuring the security of the power system. Therefore, the accurate calculation of the health index (HI) for proper maintenance of HVCBs is essential. However, existing methods often neglect two key challenges: proper signal preprocessing for feature extraction and incorporating measurement accuracy into the HI model. This paper addresses these shortcomings by proposing a methodology for improving HI representation for HVCBs. We account for measurement accuracy by considering the varying precision of different monitoring schemes. Furthermore, the impact of signal preprocessing on the condition monitoring data is analyzed. Finally, a case study exhibits how the HI based failure rate can affect the reliability centered maintenance scheduling in the power system.**

***Index Terms*—Circuit breaker, Condition monitoring, Health index, Measurement accuracy, Reliability**

I. Introduction

High voltage circuit breakers (HVCBs) are critical substation components, ensuring reliable and resilient operation of the power system. In addition to HVCB's functionality effect on routine operations, it directly impacts the ability of the power system to withstand disturbances [1]. To prevent widespread power outages with significant economic and social consequences, ensuring the reliability of HVCBs through proper maintenance strategy is crucial [2].

Maintenance strategies can be categorized into two main approaches: corrective and preventive. Corrective maintenance addresses equipment failures after they occur, aiming to restore functionality in a timely manner. Preventive maintenance, on the other hand, takes a proactive approach to prevent degradation and associated failures from happening in the first place. Preventive maintenance has various subcategories, including time-based maintenance (TBM) which follows predetermined schedules, condition-based maintenance (CBM) triggered by real-time monitoring data, reliability-centered maintenance (RCM) focused on critical equipment based on the reliability indices, and risk-based maintenance (RBM) prioritizing assets with potentially severe failure consequences [3].

This work was funded by the European Union and co-funded by the Estonian Ministry of Education and Science (project No TemTa-134).

The main disadvantage of traditional TBM is that the failure may occur before the next predefined inspection time. CBM mitigates this issue, while it may lead to unnecessary maintenance on low-risk assets while neglecting critical components. However, a transition towards RCM or RBM strategies prioritizes maintenance based on the potential consequences of failure, improving resource utilization and reducing overall maintenance costs [3]. Both RCM and RBM prioritize the maintenance activities considering the condition of the equipment whether as failure rate or failure probability, respectively. To increase the accuracy of the RCM and RBM, it is important to utilize a condition-aware failure rate rather than a constant or average failure rate for HVCBs without considering their condition [4].

In order to obtain a condition-aware failure rate, it is required to define an index based on the condition monitoring measurements. In the literature, this index is called the health index (HI), and several methods are investigated to translate the HVCB's HI into a qualitative or quantitative failure rate [5]. In [6], HVCB's coil current (CC) measurement is utilized to present a HI model. The proposed HI model is a weighted factor of CC measurement together with operation and maintenance records, and the weights are specified based on expert judgment. In [4], a condition-dependent failure rate has been introduced. To obtain the failure rate, the covariates and regression parameters in the Cox proportional hazard model are replaced with the HI value that is obtained based on the model in [6]. In [7], a weighted model is presented for HI calculation. The proposed model combines condition assessment measurements, such as contact resistance measurement, with operational factors, such as HVCB age, using the analytical hierarchy process based on experts' interviews and surveys. In [8], a neural network base model is proposed to express a HI for HVCB. Various types of measurements such as CC features, SF_6 gas pressure, operation time, etc., are applied as feature indicators. Knowing the upper and lower bound of these features, they are normalized using the min-max normalization method, and finally the overall HI is categorized based on expert opinion. In [9], a method has been presented to modify the maintenance scheduling based on the HI and HVCB operation combination. In [10], a HI calculation method is presented

979-8-3503-9042-1/24/$31.00 © 2024 IEEE

based on various parameters such as temperature, operation time, SF_6 gas pressure, etc. The HI is formulated using the concept of a hyper-ellipse. In [11], a failure model is presented based on condition monitoring measurements, such as CC and SF_6 gas pressure.

One of the obstacles in the calculation of HI, which is not considered in the literature, is the proper preprocessing of the condition measurement signals to extract relevant features. Moreover, these measurements can be implemented via devices with various accuracies and in different time schemes. Therefore, another concern is considering the accuracy of the measurements within the HI model.

Motivated by the aforementioned research gaps, this paper proposes a methodology for improving the representation of HI for HVCB, taking into account measurement accuracy. Furthermore, the effect of signal preprocessing on the condition monitoring data is demonstrated. Finally, the importance of HI for reliability calculations is demonstrated via a simple case study. The paper is organized as follows. Section II discusses the various types of condition monitoring measurements. Section III presents the proposed methodology for HI calculation. Section IV provides the correlation between HI and the failure rate and probability of failure. Section V presents a case study to demonstrate the effect of the HI based failure rate calculation on reliability analysis. Finally, the paper is concluded in Section VI.

II. Condition Monitoring Measurements

Generally, HVCBs can be divided into three main subcomponents which are stated below together with their contribution to major failures, based on the latest CIGRE statistics [12]:

- Operating mechanism, 43.5 %
- Insulation and arc extinguishing medium, 26 %
- Control and auxiliary, 24.5 %
- Other, 6 %

HVCBs are susceptible to various defects that can compromise their performance and reliability. Condition monitoring techniques are employed to assess the health and integrity of HVCBs, enabling advanced maintenance techniques and preventing potential failure. Condition monitoring encompasses a range of measurements, such as CC, SF_6 gas pressure, travel curve, dynamic/static resistance, vibration, etc., employed to assess the health and performance of HVCBs [13]. These techniques can be broadly classified into two main categories, offline and online monitoring. Offline condition monitoring refers to analyzing HVCB parameters while the HVCB is disconnected and non-operational. However, online condition monitoring for HVCB refers to the process of continuously or periodically collecting and analyzing measurement data while the HVCB is in operation.

The key distinction in condition monitoring approaches lies in the timing and accuracy of data acquisition. Online monitoring involves continuous or periodic measurement of various parameters during the operation of the HVCB. However, the accuracy of online measurements can be affected by factors like electrical noise and sensor limitations. Offline monitoring provides a more accurate and comprehensive assessment of the HVCB's condition but requires taking the equipment out of service. Additionally, offline testing might not capture transient issues that could occur during operation. By combining online and offline monitoring data, a broader view of the HVCB's health can be obtained, enabling effective maintenance strategies and ultimately enhancing the overall reliability and safety of the power grid. It is to be noted that, this combination brings in a trade-off between accuracy and time that necessitates careful consideration when developing the HI formula. More details are provided in the following section.

III. Health Index Calculation

This section outlines a comprehensive approach for calculating a HI for HVCBs based on condition monitoring measurements. The HI serves as a quantitative indicator of the overall health of the HVCB, enabling informed maintenance decisions. Fig. 1 visualizes the various stages involved in HI calculation.

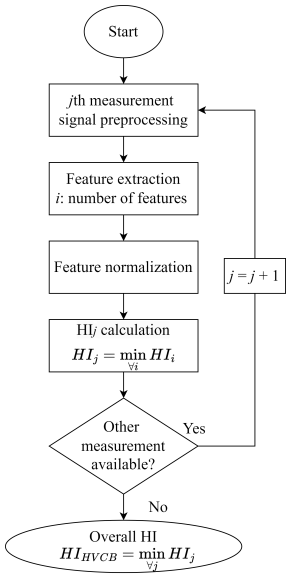


Fig. 1. Flowchart of the overall HI calculation for HVCB

The method is illustrated with CC measurements as an example, but the framework can be adapted to incorporate data from various monitoring techniques. The flowchart would typically consist of the following stages:

1) Measurement Signal Preprocessing: This stage addresses potential noise or inconsistencies in the raw CC data. Techniques like filtering or smoothing algorithms can

be employed to enhance signal quality. Fig. 2 demonstrates a comparison between smoothed and raw data of CC measurement, together with the extracted features. The data is based on the laboratory measurements of a 110 kV HVCB, and the data is smoothed using the moving average method with a scale factor of 0.03. As emphasized in Fig. 2, it's important to acknowledge that curve smoothing or other preprocessing techniques might introduce slight alterations to the extracted features. To mitigate this potential impact, the chosen preprocessing method should be carefully selected to minimize distortion of the underlying signal. Additionally, validating the chosen method's performance by comparing preprocessed and raw data can be beneficial.

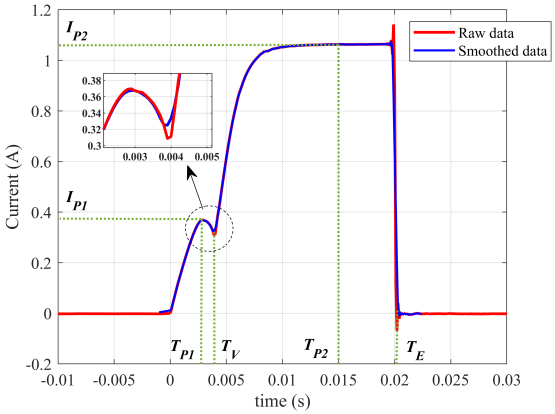


Fig. 2. Smoothing and feature extraction from CC measurement

2) Feature Extraction and Normalization: From the preprocessed CC signal, relevant features indicative of HVCB HI are extracted as shown in Fig. 2. These features include first peak current (I_{P1}), excitation time (T_{P1}), second peak current (I_{P2}), auxiliary contact operation time (T_{P2}), latching time (T_V), and total energizing time of the coil (T_E). The extracted features are normalized to a common scale, ensuring each feature contributes equally to the HI calculation regardless of its inherent unit of measurement. Common normalization techniques include min-max, z-score, etc. Based on [2], a modified Gaussian can be utilized for normalizing the features:

$$C_i = exp\left(-\frac{(x_i - r_i)^2}{s_i^2}\right) \qquad r_i = \frac{H_i + L_i}{2}, \quad s_i = \frac{H_i - L_i}{2} \tag{1}$$

where C_i is the normalized value of the ith feature of the condition monitoring measurement, x_i is the ith observed feature, H_i and L_i are upper and lower limits of the ith feature, respectively. The normalized parameter will have a value between 0 and 1, where values closer to 1 indicate a healthier state and vice versa. Moreover, both lower and upper limits correspond to the same limit value of the normalized parameter as follows ($x_i = H_i$ or $x_i = L_i$):

$$\tau = C_i(L) = C_i(H) = exp(-1) \tag{2}$$

3) HI Calculation: For each extracted feature, a sub-HI can be calculated based on its deviation from a baseline value or established thresholds. Assuming that the baseline values are known, we can define HI for each feature as follows using (1):

$$HI_i = C_i \tag{3}$$

where the value of τ in (2) serves as a basis for deciding whether the condition falls within the normal or abnormal range.

4) Offline and Online Measurement Combination: This stage combines the HI of a feature derived from online measurements (HI_i^{on}) with HI obtained from periodic offline testing (HI_i^{of}) for the same feature (if applicable). Considering the accuracy of each measurement and the time elapsed since the last offline test, the following equation is proposed to be used for this combination:

$$HI_i^{updated}(t) = \frac{HI_i^{on} \times \alpha^2 + HI_i^{of} \times \beta^2 \times f(t)}{\alpha^2 + \beta^2 \times f(t)} \tag{4}$$

where α and β belong to the range of 0 to 1, and specify the accuracy of the online and offline measurement, respectively; $f(t)$ is a factor that reduces the weight of the offline measurement as time t increases. A proposal for the $f(t)$ can be as follows:

$$f(t) = exp\left(\frac{-t}{\gamma}\right) \tag{5}$$

where γ determines the rate of exponential decay and should be chosen such that when t approaches the next periodic offline measurement (ΔT), the coefficient $f(t)$ approaches zero, reflecting the diminishing relevance of the outdated offline measurement. For instance, $\gamma = \frac{\Delta T}{2}$, will ensure that at $t = \Delta T$ the effect of offline measurement will reach approximately 10 %. This value can be selected based on the number of operations of the HVCB.

5) Overall HI Calculation: Traditionally, for the overall HI calculation, methods in the literature often assign weights to different features based on their perceived importance to overall HVCB health. However, for HVCBs, a compelling argument can be made against using weights. As demonstrated in Fig. 3, components within HVCB operate in series. Therefore, the failure of a single critical sub-component (and as a result the main component) can lead to a complete equipment outage. This suggests that the overall health of the CB should be determined by its weakest link, not an average weighted value.

Therefore, the proposed approach recommends a worst-case scenario logic for calculating the overall HI. This can be achieved by taking the minimum value among all the sub-health indices. The following approach ensures that a failing

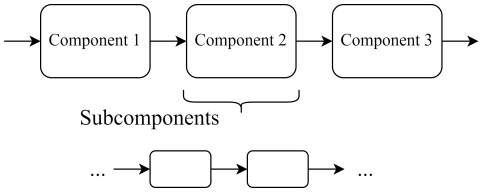


Fig. 3. Block diagram of the HVCB components connection

component, regardless of its perceived importance in the weighting scheme, is not masked by the healthy performance of other components:

$$\begin{aligned} HI_{HVCB} &= \min_{\forall j}\{\min_{\forall i}(HI_i)\} \\ i = 1, ..., m \quad &\& \quad j = 1, ..., n \end{aligned} \tag{6}$$

where m and n indicate the number of features and number of measurements, respectively. By following this comprehensive framework and considering the worst-case scenario for the final HI calculation, a more robust and reliable assessment of the health of HVCBs can be achieved.

IV. Failure Rate and Probability of Failure Estimation

The calculated HI can be correlated with historical failure data of similar HVCBs to estimate the failure rate and probability of failure. Based on [11], it is assumed that the HI, calculated from normalized condition monitoring parameters, exhibits an approximately exponential correlation with the operating age of the HVCB as follows:

$$\begin{aligned} 1 - HI_{HVCB} &= Ae^{Bt_{op}} + D \\ t_{op} &= \frac{1}{B} ln\left(\frac{1 - HI_{HVCB} - D}{A}\right) \end{aligned} \tag{7}$$

where t_{op} is the operating age of the HVCB; A, B, and D, are three coefficients, which can be estimated using a nonlinear parameter estimation method. This method combines measured condition monitoring data and the ages of HVCBs of the same category, such as manufacturer, voltage level, etc.

After finding the operating age of HVCB, it's possible to approximate its failure rate and probability of failure by modeling its lifetime using historical data. Generally, liftime model can be non-parametric or parametric. In non-parametric models, such as Kaplan-Meier estimator, no assumption about the form of the failure distribution function is made. In contrast, parametric models assume a particular distribution for the failure data, such as exponential and Weibull [14]. The Weibull distribution is preferred for lifetime modeling because it offers greater flexibility. Unlike the exponential model, which assumes a constant failure rate, the Weibull distribution allows for modeling situations where the failure rate can be increasing, decreasing, or constant throughout the lifetime of an asset.

In this paper, the failure probability function, $F(t)$, and failure rate, $\lambda(t)$, for aging failure are calculated according to the Weibull distribution as follows [11]:

$$\begin{aligned} F(t_{op}) &= 1 - exp\left(-\left(\frac{t_{op}}{\eta}\right)^{\nu}\right) \\ \lambda(t_{op}) &= \frac{\nu}{\eta}\left(\frac{t_{op}}{\eta}\right)^{\nu-1} \end{aligned} \tag{8}$$

where ν is the shape parameter; and η is the scale parameter. A least squares method can be used to estimate the parameters. Based on the established relationship, the probability of failure and failure rate of HVCB within a specific timeframe can be estimated based on the HI.

V. Reliability Centered Maintenance

This section presents a simplified case study where the effect of estimating failure rate using HI for reliability calculations for power systems is demonstrated. Two HVCBs (B_1 and B_2) are analyzed, each connected to a different load point, L_1 and L_2, respectively, as shown in Fig. 4. The goal is to prioritize the maintenance of two HVCBs based on the reliability index of energy not supplied (ENS) within the RCM scheme.

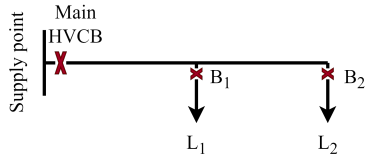


Fig. 4. The scheme of the network under study

A. Scenario I: Average Failure Rate

In this scenario, an average failure rate is assumed for both HVCBs. The ENS reliability index is calculated for each breaker. The HVCB with the higher ENS, indicating a potentially greater impact on overall system reliability in case of failure, would be prioritized for maintenance actions under RCM scheme. The following assumptions are made:

$$\begin{aligned} &\lambda = 0.011\ [f/year], && \text{equal for both HVCBs} \\ &r = 90\ [h/repair], && \text{equal for both HVCBs} \\ &U = \lambda \times r && U = 0.99\ [h/year] \\ &L_1 = 8.4\ [MW], && L_2 = 10\ [MW] \end{aligned} \tag{9}$$

The ENS, $ENS_i = U_i \times L_i$, for these load points (considering the rest of the network is ideal) is $ENS_1 = 8.3\ [MWh/year]$ and $ENS_2 = 9\ [MWh/year]$. This indicates that B_2 has higher priority compared to B_1 in RCM scheme.

B. Scenario II: HI Based Failure Rate

In this scenario, the actual condition of each HVCB is considered. Failure rates are estimated based on (1) to (8). The HI is calculated based on the CC measurements. Among the various online monitoring techniques, CC measurement stands out as one of the easiest to implement due to the nonintrusive measurement process and requiring minimal sensor installation. Moreover, CC waveforms offer a considerable amount of information about the operating mechanism, such as supply voltage, latching, coil resistance, and auxiliary contacts, making it a valuable and convenient tool for the condition monitoring of HVCBs [15]. Based on the condition monitoring parameters in [11], the operating age, HI, and failure rate of the HVCBs are presented in Table I. Taking the same assumptions from scenario I for repair time and load values, the ENS is $ENS_1 = 12.1\ [MWh/year]$ and $ENS_2 = 10.8\ [MWh/year]$. This indicates that B_1 has higher priority compared to B_2 in RCM scheme based on its current condition.

TABLE I
HVCBs OPERATING AGE, HI, AND FAILURE RATE [11]

HVCB	**Operating age** $[years]$	**HI**	λ $[f/year]$
$\mathbf{B}_1$	26.01	0.7628	0.016
$\mathbf{B}_2$	23.4	0.8	0.012

As it was expected, the HI-based approach (scenario II) leads to a different maintenance prioritization compared to the average failure rate approach (scenario I). Even if B_1 and B_2 have the same age and are from the same population and hence have the same expected age based on these exterior data, their actual health conditions, reflected by the HI, could differ. The HVCB with a lower HI (indicating potentially deteriorating health) might have a higher estimated failure rate and consequently a higher ENS value. This would prioritize maintenance for that specific HVCB under RCM scheme. This simplified case study demonstrates that utilizing the HI provides a more comprehensive approach to reliability calculations and maintenance prioritization for HVCBs. By incorporating the actual health condition of the breakers, maintenance resources can be allocated more effectively, potentially leading to improved power grid reliability and reduced risks.

VI. CONCLUSION

This paper proposed a methodology to enhance the precision of HI calculations for HVCBs. Two key areas that are often neglected in the literature were identified. Firstly, the signal preprocessing for feature extraction and secondly incorporating measurement accuracy into the HI evaluation model. To address these shortcomings, a methodology was proposed. This methodology accounts for the varying precision of different monitoring devices and techniques (i.e., online or offline), ensuring a more accurate reflection of the HVCB's condition.

Additionally, the impact of signal preprocessing techniques on the extracted features was analyzed. Finally, a case study showcased the significant impact that HI-based failure rate estimation can have on reliability analysis and maintenance scheduling within the power system. The proposed approach can lead to improved decision-making for maintenance and ultimately to enhance the overall security and reliability of the power system.

Future research directions could explore considering HI-based failure probability of HVCB in risk assessment of substations and considering more complex substation configurations.

REFERENCES

[1] T. Krieg and J. Finn, *Substations*, ser. CIGRE Green Books. Springer International Publishing, 2018.

[2] D. Zhang, W. Li, X. Xiong, and R. Liao, "Evaluating condition index and its probability distribution using monitored data of circuit breaker," *Electric Power Components and Systems*, vol. 39, no. 10, pp. 965–978, 2011.

[3] G. Balzer and C. Schorn, *Asset Management for Infrastructure Systems*. Springer International Publishing, 2022.

[4] J. A. Grant, H. Toftaker, S. Perkin, I. B. Sperstad, and V. V. Vadlamudi, "High-voltage circuit breaker condition-dependent failure rate with covariates," in *2024 Annual Reliability and Maintainability Symposium (RAMS)*. IEEE, 2024, pp. 1–6.

[5] N. Zhou, Y. Xu, S. Cho, and C. T. Wee, "A systematic review for switchgear asset management in power grids: condition monitoring, health assessment, and maintenance strategy," *IEEE Transactions on Power Delivery*, vol. 38, no. 5, pp. 3296–3311, 2023.

[6] J. A. Grant, I. B. Sperstad, J. Foros, and V. V. Vadlamudi, "Health index calculation using failure modes, effects, and criticality analysis for high-voltage circuit breakers," in *Proceedings of the 33rd European Safety and Reliability Conference (ESREL 2023)*, 2023.

[7] A. Setiawan, W. Adiati, and R. A. Prasojo, "An approach of the analytic hierarchy process to acquire the weighting factor of high voltage circuit breaker health index," in *2020 International Conference on Technology and Policy in Energy and Electric Power (ICT-PEP)*. IEEE, 2020, pp. 317–322.

[8] S. Geng and X. Wang, "Research on data-driven method for circuit breaker condition assessment based on back propagation neural network," *Computers & Electrical Engineering*, vol. 86, p. 106732, 2020.

[9] S. Asefi *et al.*, "Measurement and operation based condition monitoring methodology for high voltage circuit breakers," in *2022 IEEE PES Innovative Smart Grid Technologies Conference Europe (ISGT-Europe)*. IEEE, 2022, pp. 1–5.

[10] P. Dehghanian, T. Popovic, and M. Kezunovic, "Circuit breaker operational health assessment via condition monitoring data," in *2014 North American Power Symposium (NAPS)*. IEEE, 2014, pp. 1–6.

[11] J. Zhong, W. Li, R. Billinton, and J. Yu, "Incorporating a condition monitoring based aging failure model of a circuit breaker in substation reliability assessment," *IEEE Transactions on Power Systems*, vol. 30, no. 6, pp. 3407–3415, 2015.

[12] A. Carvalho *et al.*, "Final report of the 2004–2007 international enquiry on reliability of high voltage equipment," *Electra (Paris)*, vol. 264, pp. 49–53, 2012.

[13] A. A. Razi-Kazemi and K. Niayesh, "Condition monitoring of high voltage circuit breakers: past to future," *IEEE Transactions on Power Delivery*, vol. 36, no. 2, pp. 740–750, 2020.

[14] J. H. Jürgensen, "Individual failure rate modeling and exploratory failure data analysis for power system components," Ph.D. dissertation, KTH Royal Institute of Technology, 2018.

[15] A. A. Razi-Kazemi, M. Vakilian, K. Niayesh, and M. Lehtonen, "Circuit-breaker automated failure tracking based on coil current signature," *IEEE Transactions on Power Delivery*, vol. 29, no. 1, pp. 283–290, 2013.

Appendix 5

S. Asefi et al., "Machine Learning-Based High-Voltage Circuit Breaker Defect Classification Utilising Savitzky-Golay Filter," in IEEE Transactions on Instrumentation and Measurement, vol. 74, pp. 1-9, 2025.

Machine Learning-Based High-Voltage Circuit Breaker Defect Classification Utilizing Savitzky–Golay Filter

Sajjad Asefi, Soheil Asefi, Hossein Afshari, *Member, IEEE*, Jako Kilter, *Senior Member, IEEE*, Ebrahim Shayesteh, *Senior Member, IEEE*, Patrik Hilber, *Senior Member, IEEE*, and Tommie Lindquist

***Abstract*—High-voltage circuit breakers (HVCBs) are critical components in power systems to maintain reliable operation. Accurate condition monitoring of HVCBs is vital to reduce maintenance costs and consequently to enhance the grid reliability. However, achieving this with low-cost measurement devices, which often provide noisy signals, poses a significant challenge. In this article, a novel defect classification framework for HVCBs is proposed that uses the Savitzky–Golay filter to preprocess the most common condition monitoring signal, which is the trip/close coil current. This filter is well-known for denoising while preserving critical signal features. Following signal preprocessing, a robust defect detection and classification methodology is introduced, combining time-series similarity assessment techniques, such as Euclidean distance and dynamic time warping (DTW), with machine learning (ML) algorithms. Moreover, an experimental setup is designed to emulate the behavior of an HVCB's coil mechanism. To further enhance the model transparency, Shapley additive explanations (SHAP) analysis is applied, providing interpretability into feature contributions toward model decisions. The obtained results validate the effectiveness of the proposed hybrid approach, demonstrating its potential to provide a cost-effective, accurate, and reliable solution for HVCB condition monitoring.**

***Index Terms*—Circuit breaker, condition monitoring, dynamic time warping (DTW), machine learning (ML), Savitzky–Golay.**

I. Introduction

HIGH-VOLTAGE circuit breakers (HVCBs) play a significant role in facilitating the reliable operation of power systems [1]. In addition to HVCB's functionality effect on power system routine operations, HVCBs should be able to isolate the fault rapidly and reliably to maintain the safe operation of the rest of the power network. Maloperation of HVCB may lead to cascading failures. Therefore, the timely detection and maintenance of defects in HVCBs is crucial to avoid a large-scale blackout and the significant economic losses associated with it [2], [3].

Among various maintenance approaches, reliability-centered maintenance (RCM) and risk-based maintenance (RBM) are becoming more popular and compatible with the future smart grid concept compared with conventional time-based maintenance [4], [5]. Transition toward RCM or RBM strategies prioritizes maintenance based on the potential consequences of failure, which leads to improve resource utilization and reducing overall maintenance costs [6], [7]. RCM and RBM prioritize the maintenance activities based on failure rate or failure probability, respectively. To increase the accuracy of the RCM and RBM, it is important to utilize a condition-aware failure rate rather than a constant or average failure rate for HVCBs without considering their condition [8]. Therefore, the implementation of a proper condition monitoring method is essential.

Condition monitoring of the HVCB enables predictive techniques to identify the defects at an incipient stage in many cases through measuring and recording signals such as coil current, operation timing, vibration, and SF_6 gas pressure. The choice of a measurement signal is highly dependent upon the specific component of the HVCB under investigation. HVCBs include three fundamental components, namely, the operating mechanism, the arching chamber, and the control unit, and each component is the cause of 43.5%, 26%, and 24.5% of the major failures, respectively [9].

One of the most common measurement signals for condition monitoring is the coil current, which is applicable in both online and offline condition monitoring schemes [10]. The coil current measurement signal offers valuable insights into the control unit and, to a certain extent, the operating mechanism. In addition, the required measurement equipment, such as a simple current sensor, is both cost-effective and straightforward to implement [11]. The coil current measurement signal reflects the energization processes of the HVCB's trip/close coil, and deviations from expected patterns can indicate emerging defects such as trip/close coil supply voltage, latch operation, auxiliary contacts, and coil resistance. Based on the aforementioned reasons, our research will focus on analyzing the coil current measurement signal.

Received 26 March 2025; revised 15 July 2025; accepted 8 August 2025. Date of publication 2 September 2025; date of current version 10 September 2025. This work was supported in part by Estonian Transmission System Operator Elering AS through the Project "Risk and Condition Based Asset Management in Future Power Systems" under Grant 1.1-4/2021/644/LEEEE21116 and in part by European Union and co-funded by Estonian Ministry of Education and Science under Project TemTa-134. The Associate Editor coordinating the review process was Dr. Ming Zhang. *(Corresponding author: Sajjad Asefi.)*

Sajjad Asefi, Soheil Asefi, Hossein Afshari, and Jako Kilter are with the Department of Electrical Power Engineering and Mechatronics, Tallinn University of Technology, 19086 Tallinn, Estonia (e-mail: sajjad.asefi@taltech.ee).

Ebrahim Shayesteh and Patrik Hilber are with the Department of Electromagnetic Engineering, KTH Royal Institute of Technology, 114 28 Stockholm, Sweden.

Tommie Lindquist is with the Department of Electric Power Systems, Research Institutes of Sweden (RISE), 164 40 Gothenburg, Sweden.

Digital Object Identifier 10.1109/TIM.2025.3604980

1557-9662 © 2025 IEEE. All rights reserved, including rights for text and data mining, and training of artificial intelligence and similar technologies. Personal use is permitted, but republication/redistribution requires IEEE permission.
See https://www.ieee.org/publications/rights/index.html for more information.

Authorized licensed use limited to: Tallinn University of Technology. Downloaded on September 19,2025 at 06:05:13 UTC from IEEE Xplore. Restrictions apply.

In [2], a quantitative approach is presented to assess the reliability status and to identify the deterioration states of HVCB by using condition monitoring measurements, such as coil current. In [13], the coil current measurement is utilized to present a health index model for HVCB. The health index model is a weighted factor of features extracted from coil current measurements together with operation and maintenance records, and the weights are specified based on expert judgment. In [8], a condition-dependent failure rate has been introduced. To obtain the failure rate, the covariates and regression parameters in the Cox proportional hazard model are replaced with the health index value that is obtained using coil current features [13]. In [14], a weighted model is presented for health index calculation. The proposed model combines condition monitoring measurements, such as coil current, with operational factors, such as HVCB age, using the analytical hierarchy process based on experts' interviews and surveys. In [15], a neural network-based model is proposed to express a health index for HVCB. Various types of measurements, such as coil current, and their extracted features, are applied as feature indicators for the model. In [16], a failure model is presented based on condition monitoring measurements, such as coil current and SF_6 gas pressure. In [12], an insight into the impacts of the various defects on the coil current waveform is provided categorizing defects and their causes.

Despite the advantages of coil current monitoring, noise in the measurements often complicates the accurate assessment of HVCB condition [17]. Particularly for online condition monitoring purposes, measurement devices should be installed in the substations [18]. Consequently, noisy measurements are unavoidable. Noise may originate from external electromagnetic interference, sensor inaccuracies, or environmental factors. Consequently, the raw coil current signal needs to be processed and cleaned before it can be used for meaningful analysis. To the best of the authors' knowledge, the previous studies have not addressed the challenges associated with feature extraction from noisy coil current measurements. To denoise the measurement data, the Savitzky–Golay filter is applied in this article. The main reason for applying this filter is the peak shape preservation property. In other words, it reduces noise while maintaining the shape and height of waveform peaks [19]. Furthermore, a more robust approach for defect detection and classification is proposed, integrating time series similarity assessment techniques, such as Euclidean distance and dynamic time warping (DTW), with machine learning (ML) algorithms. In addition, to enhance model transparency and interpretability, Shapley additive explanations (SHAP) analysis is utilized to evaluate the contribution of each input feature to the final classification outcome [20].

This article is organized as follows. Section II provides information about various types of defects and discusses the features available in coil current measurement that can be useful in classifying them. Moreover, the experimental setup and the measured current related to each defect are demonstrated. Section III presents the proposed methodology for the detection and classification of defects, including the Savitzky–Golay filter, DTW, and ML. Section IV demonstrates and compares the results of defect classification based on different ML algorithms. Finally, this article is concluded in Section V.

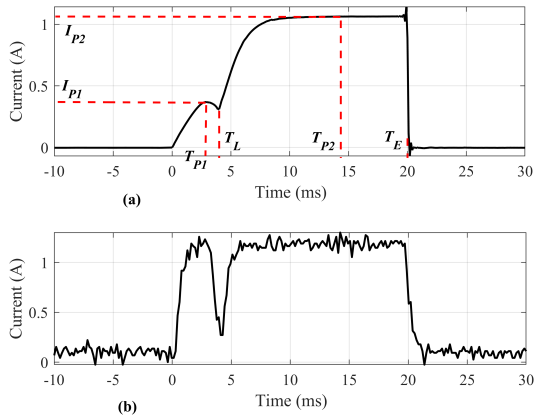


Fig. 1. Trip/close coil current signal and related diagnostic features. (a) Real HVCB coil current measured with a commercial device. (b) Emulator circuit current measured using an inexpensive sensor (normal coil current).

II. Coil Current Monitoring

This section presents a typical coil current measurement signal and points out the features that must be extracted for defect classification purposes. Also, the proposed feature extraction process in this study has been discussed. Moreover, the various types of defects and their effect on the coil current measurement signal are discussed and demonstrated via an experimental setup.

A. Coil Current Measurement Signal and Defects

The features reflecting the HVCB abnormalities (referring to the voltage level above 60 kV) are illustrated on a typical measured coil current waveform in Fig. 1(a), which is measured from a real HVCB coil by a high accuracy and expensive commercial device. These parameters can assist with the detection of defects associated with trip/close coil supply voltage, latch operation, auxiliary contacts, and coil resistance. More detail about the defects implementation and their effect on coil current is summarized in Table I. The coil current features that are specified in Fig. 1(a) are explained as follows.

1) I_{P1}: First peak current.
2) T_{P1}: Excitation time.
3) I_{P2}: Second peak current.
4) T_{P2}: Auxiliary contact operation time.
5) T_L: Initiation of HVCB operation (latching time).
6) T_E: Total energizing time of the coil.

Due to the scarcity and restricted accessibility of fault-specific coil current measurement recordings, this study leverages a coil current emulator to validate the proposed methodology. This experimental setup is developed as a cost-effective and flexible alternative, allowing for controlled testing and evaluation of various defect scenarios. Despite

Authorized licensed use limited to: Tallinn University of Technology. Downloaded on September 19,2025 at 06:05:13 UTC from IEEE Xplore. Restrictions apply.

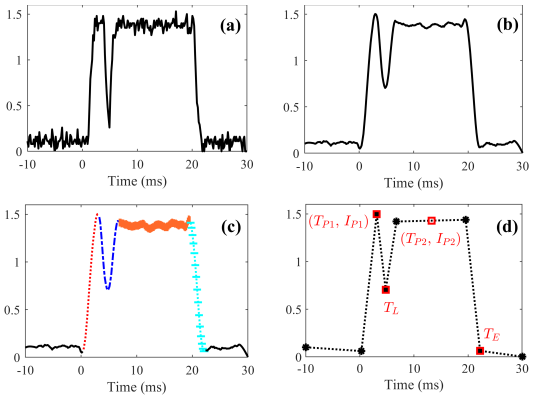


Fig. 2. Trip/close coil current signal feature extraction process. (a) Raw measurement. (b) Filtered signal. (c) Segmentation. (d) Extracting required features.

being an approximation, the experimental setup effectively emulates the key characteristics of HVCB coil current signals and facilitates the validation of the designed feature extraction strategy. Fig. 1(b) presents the current, which is measured from the coil current emulator circuit using an inexpensive sensor. Fig. 1(b) shows the benchmark for the healthy (hereinafter, normal) coil current in this study.

An algorithm has been developed to extract the aforementioned features from the measured coil current signals. Given that the acquired signals are inherently noisy, an initial denoising step is necessary to ensure accurate parameter extraction. In this study, the Savitzky–Golay filter is employed for this purpose, and its methodology and advantages are explained thoroughly in Section III.

B. Feature Extraction

Fig. 2 demonstrates different stages of the feature extraction process. Feature extraction is a challenging task, and automating the extraction of the required points from coil current measurement cannot be accomplished through anticipation.

The proposed process of feature extraction in this study was dividing the signal into multiple segments. Initially, the raw coil current measurement, as shown in Fig. 2(a), needs to be filtered, Fig. 2(b). Then, the filtered coil current signal has been divided into different segments, as shown in Fig. 2(c). The logic behind the segmentation is utilizing the calculation of the cumulative maximum and minimum. Finally, identifying different segments would make feature extraction straightforward, and the required points for condition monitoring purposes can be specified as shown in Fig. 2(d).

C. Experimental Setup

The experimental setup developed in this study is designed to emulate the behavior of an HVCB's coil mechanism. A schematic of the setup is shown in Fig. 3. The setup incorporates various components, including an ACS712 current sensor, which is employed to measure the coil current signal.

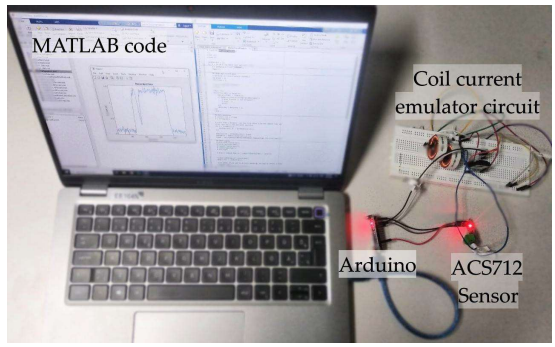


Fig. 3. Schematic of the experimental setup for emulating HVCB coil current behavior.

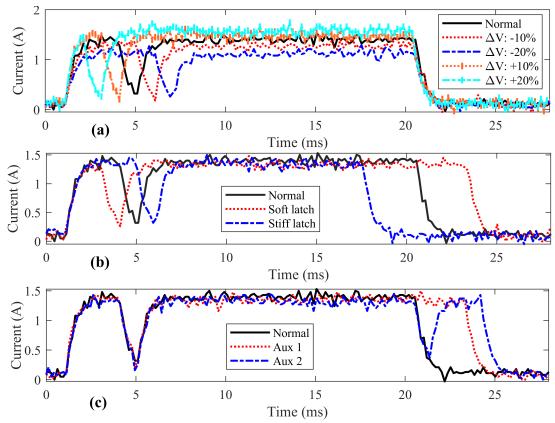


Fig. 4. Illustration of the effects of various defects on the coil current waveform. (a) Supply voltage. (b) Latch operation. (c) Auxiliary contact.

The ACS712 current sensor is a widely used Hall-effect-based sensor, known for its simplicity and affordability. However, its measurements may exhibit noise due to limited precision. This characteristic should be considered when analyzing the captured data and interpreting the results. Efforts to mitigate noise through filtering techniques, which the Savitzky–Golay filter is utilized in this study, as mentioned before.

D. Defect Demonstration

Fig. 4 illustrates the impact of various defects on the coil current waveform, i.e., the potential alterations in the waveform caused by common defects. Defects such as supply voltage, latch operation, and auxiliary contact are demonstrated in Fig. 4. These variations in the waveform provide diagnostic signatures that can be utilized for condition monitoring and defect detection.

Fig. 4(a) is related to the supply voltage defects. For better visualization, the supply voltage of the coil in the emulator circuit has been increased from −20% to +20% and compared with the normal coil current. As it has been demonstrated,

Authorized licensed use limited to: Tallinn University of Technology. Downloaded on September 19,2025 at 06:05:13 UTC from IEEE Xplore. Restrictions apply.

TABLE I
HVCB DEFECTS, PRACTICAL IMPLEMENTATION, AND THEIR EFFECT ON COIL CURRENT WAVEFORM [12]

Defect Category	Description	Implementation	Expected Effects
Supply Voltage	Deviations in the voltage supplied to the HVCB control unit, impacting the coil electromagnetic force and plunger movement.	A specific percentage of coil supply voltage can be increased/decreased.	Both under-voltage and over-voltage affect coil current features and HVCB operation time. Voltage variations shift coil current curves and impact features like peak currents, excitation time, and latching time.
Latch Operation	Defects in the latch mechanism, causing sluggish operation, affecting the coil current waveform and HVCB opening/closing time.	Stiff and soft latch adjustments.	Latch sluggishness causes discrepancies in HVCB opening time. Increased sluggishness may result in longer or shorter operation times based on latch mechanisms. This defect mainly impacts energizing, latching, operation, and excitation time.
Auxiliary Contact	Defects in the auxiliary contacts, often from mechanical issues like friction or lubricant problems.	Malfunction in the closing spring.	These defects affect operation time and total energizing time of the coil current.
Trip/Close Coils	Problems within the coils themselves, potentially impacting resistance and coil current.	Adding external resistance to the coil.	Changes in coil resistance alter HVCB operation time and impact features like peak currents, excitation time, and latching time.

the variation in the supply voltage will impact peak currents, excitation time, and latching time. Fig. 4(b) is related to the latch operation defect, which is caused by the latch sluggishness. It demonstrates the cases of soft and stiff latching, which impact energizing, latching, operation, and excitation time, in comparison to the normal coil current. Fig. 4(c) is related to the auxiliary contact defect, which is caused by the malfunctioning in the closing (or tripping) spring, and that is mainly due to friction or lubrication problems. Also, it can be related to the auxiliary contact itself when the contact bounces during the operation. The demonstrated cases in Fig. 4(c) are related to both defects by spring and auxiliary contact bouncing that are noted as "Aux1" and "Aux2," respectively. This defect mainly impacts the operation time and total energizing time.

A summary of various defect categories and their expected effects on the coil current measurements is presented in Table I. It is to be noted that, since the expected effects of the supply voltage and trip/close coil resistance are similar, it has been excluded from the experimental demonstration, but further details are provided in Table I.

III. PROPOSED CONDITION MONITORING METHODOLOGY

This section discusses the denoising technique applied in this article, i.e., the Savitzky–Golay filter and its parameters. Then, the time warping technique is discussed, which is useful for comparing the defective and normal coil current signals. Furthermore, the applied ML techniques are discussed. Finally, the flowchart of the proposed methodology is presented, which illustrates a multistage approach to HVCB condition monitoring, combining signal processing techniques, distance metrics, and ML to detect and classify defects accurately.

A. Savitzky–Golay Filter

The Savitzky–Golay (also known as polynomial or least-squares smoothing) filter is a widely used signal processing technique for reducing noise while preserving important signal characteristics, such as peaks and slopes [19]. In [21], the advantages of the Savitzky–Golay filter over conventional filtering techniques have been demonstrated in the context of condition monitoring signals for power transformers. Therefore, it has been proposed to apply this filter for denoising the coil current measurement in this study. Unlike basic smoothing methods like moving averages, the Savitzky–Golay filter fits a low-degree polynomial to a sliding window of data points using the least-squares method and evaluates the polynomial at the central point of the window [22].

Consider a discrete signal $z[n]$ consisting of noisy data samples. For each point in the signal, e.g., z_i, the Savitzky–Golay filter approximates the underlying signal within a symmetric window of size N, centered around z_i, by fitting a polynomial of degree p

$$\hat{z}_i = a_0 + a_1 i + a_2 i^2 + \cdots + a_p i^p \tag{1}$$

where $a_0, a_1, \ldots, a_p$ are the polynomial coefficients.

To determine the coefficients, the method minimizes the sum of squared residuals between the observed data z_i and the fit polynomial $\hat{z}_i$ at each data point in the window

$$J = \text{Min} \sum_{k=-m}^{m} \left(z_k - \sum_{j=0}^{p} a_j k^j \right)^2 \tag{2}$$

where $m = (N-1)/2$ is the half-width of the window. This optimization problem can be expressed in matrix form.

1) $\mathbf{y} = [z_{-m}, z_{-m+1}, \ldots, z_m]^T$ represent the vector of observed data within the window.
2) $\mathbf{S}$ denote the *design matrix*, where each row contains the powers of the window indices up to degree p

$$\mathbf{S} = \begin{bmatrix} 1 & -m & (-m)^2 & \cdots & (-m)^p \\ 1 & (-m+1) & (-m+1)^2 & \cdots & (-m+1)^p \\ \vdots & \vdots & \vdots & \ddots & \vdots \\ 1 & m & m^2 & \cdots & m^p \end{bmatrix}. \tag{3}$$

The solution for the polynomial coefficients $\mathbf{a} = [a_0, a_1, \ldots, a_p]^T$ is given by

$$\mathbf{a} = \left(\mathbf{S}^T \mathbf{S}\right)^{-1} \mathbf{S}^T \mathbf{y}. \tag{4}$$

Authorized licensed use limited to: Tallinn University of Technology. Downloaded on September 19,2025 at 06:05:13 UTC from IEEE Xplore. Restrictions apply.

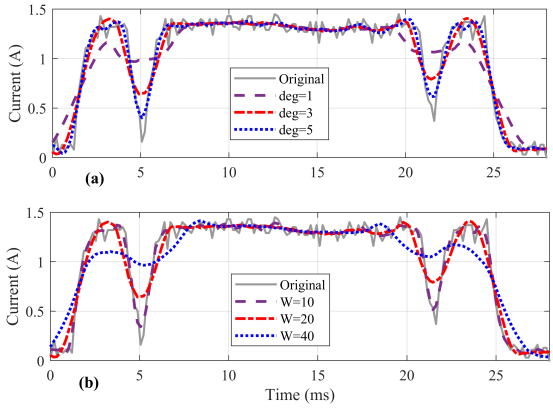


Fig. 5. Sensitivity analysis of the Savitzky–Golay parameters. (a) Effect of polynomial degree variation by constant window size ($W = 20$). (b) Effect of window size variation by constant polynomial degree (deg = 3).

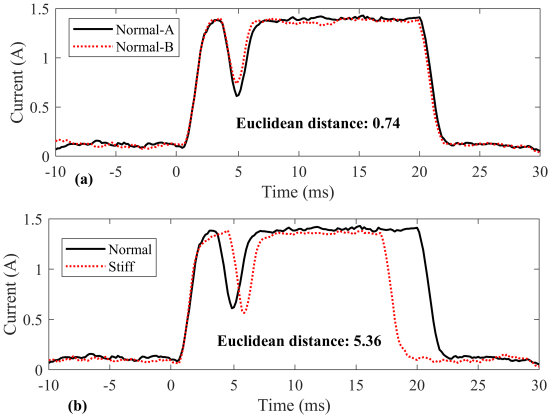


Fig. 6. Euclidean distance between two filtered coil current signals. (a) Both signals are normal and (b) normal versus defected signal.

For noise reduction, we are primarily interested in the central value of the fit polynomial, a_0, which corresponds to the smoothed value at z_0. This value can be efficiently computed using a precomputed convolution kernel c, applied to the windowed data

$$\hat{z}_0 = \sum_{i=-m}^{m} c_i z_i \tag{5}$$

where c depends only on the window size N and the polynomial degree p.

B. Savitzky–Golay Filter Parameter Selection

As mentioned before, the Savitzky–Golay filter is well-known for preserving signal features such as peaks and transitions. However, its performance can degrade if the signal is highly noisy or if the window size N and the polynomial degree p are not appropriately chosen [23]. To justify the choice of Savitzky–Golay filter parameters, a comparative analysis was conducted using a coil current signal with an auxiliary contact defect, as shown in Fig. 5. As demonstrated in Fig. 5(a), a first-degree polynomial excessively simplifies the signal, while higher degree polynomials better preserve transient features. However, overly high degrees may compromise the stability of the smoothing process. The third degree offers the best balance between detail retention and noise suppression. Similarly, Fig. 5(b) illustrates that window size also influences filter performance, i.e., the smaller windows retain more detail but less effectively suppress noise, while overly large windows (e.g., 40 samples) overly smooth the signal and obscure key transitions.

A moderate window size of 20 samples combined with a third-degree polynomial was found to provide an optimal tradeoff for the coil current signal analyzed. It is to be noted that these empirically determined parameters may require adaptation when applied to different time-series data, particularly if the sampling rate, signal characteristics, or noise profile differ significantly.

C. DTW for Signal Comparison

The Euclidean distance is a widely used technique that provides a straightforward measurement of similar time-series data. It assumes that both time series are of equal length and perfectly aligned in time. The Euclidean distance (d) between two time series, $X = [x_1, x_2, \ldots, x_n]$ and $Y = [y_1, y_2, \ldots, y_m]$, is calculated in the following equation:

$$d(X, Y) = \sqrt{\sum_{i=1}^{n} (x_i - y_i)^2}. \tag{6}$$

Comparing the Euclidean distance of the normal coil current signal with the defected signals can lead to a preliminary detection of defects. Fig. 6(a) demonstrates the Euclidean distance between two normal signals (noted as Normal-A and Normal-B) after being smoothed using the Savitzky–Golay filter. This is the case when two measurements are perfectly aligned. On the other hand, Fig. 6(b) demonstrates the Euclidean distance between a normal and a defected signal (the defect is latch stiffness) after being smoothed using the Savitzky–Golay filter. Here, the measurements are assumed to have perfect alignment as well.

Fig. 7 demonstrates the Euclidean distance between a normal signal and various scenarios of defected and normal signals, while each scenario is composed of 20 signal samples. In other words, 20 samples of normal and each defect type are reproduced using the coil current emulator circuit. It is assumed that comparing the Euclidean distance of the normal coil current signal with the defected signals can lead to a preliminary detection of defects. As expected, Fig. 7 shows the possibility to specify a threshold line (e.g., 1.8 based on the experimental results) that distinguishes the normal and defected signals from each other using their Euclidean distance. Consequently using the Euclidean distance technique can easily provide the possibility to distinguish the normal and defected signals.

However, in practical cases, the measured signals might have temporal distortions. To address this issue, DTW can be beneficial that is an alignment algorithm designed to compare

Authorized licensed use limited to: Tallinn University of Technology. Downloaded on September 19,2025 at 06:05:13 UTC from IEEE Xplore. Restrictions apply.

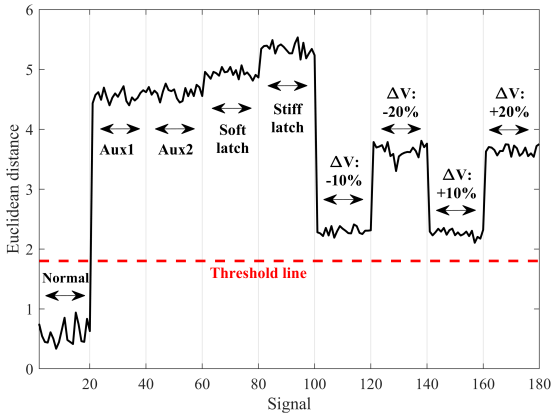


Fig. 7. Euclidean distance between normal and defected signals.

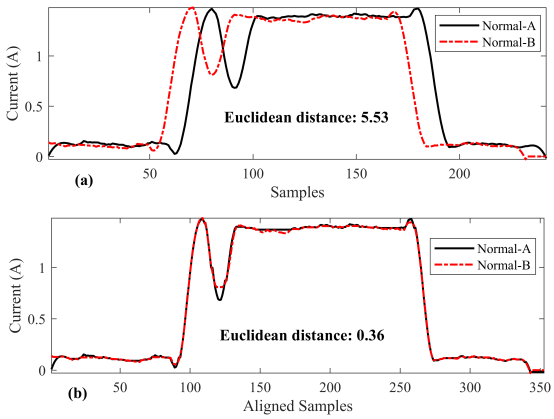


Fig. 8. Application of DTW for signal alignment. (a) Two misaligned normal signals and (b) aligned signals after applying DTW.

time series, even when they are misaligned or have variable lengths [24]. DTW achieves this by dynamically stretching or compressing the sequences along the time axis to minimize the cumulative distance. Mathematically, given two sequences X and Y, the DTW distance is computed as follows:

$$D(i,j) = d\left(x_i, y_j\right) + \text{Min}\left\{D(i-1,j), \ldots, D(i,j-1),\ D(i-1,j-1)\right\} \tag{7}$$

where $d(x_i, y_j) = |x_i - y_j|$ is the local distance between elements x_i and y_j. The boundary conditions are

$$D(0,0) = 0, \quad D(i,0) = \infty, \quad D(0,j) = \infty. \tag{8}$$

The warping path is determined by tracing back from $D(n,m)$, which represents the optimal alignment cost. Considering the ability of DTW to handle temporal misalignments and time series of different lengths, it becomes a suitable choice when analyzing coil current measurements that might be misaligned. Fig. 8 presents the application of DTW for two normal coil current measurement signals. Fig. 8(a) shows two misaligned normal coil current measurements, and due to the temporal misalignment, the Euclidean distance between them is 5.53. Considering the threshold specified in Fig. 7, and assuming "Normal-A" as the reference coil current, the system will produce a false alarm and state the coil current "Normal-B" as a defected coil current. Therefore, solely using Euclidean distance can lead to misinterpretation and detect a normal signal as defected. Alternatively, the same two measurements as shown in Fig. 8(a) are initially aligned using DTW technique, and then their Euclidean distance is calculated which is 0.36, as shown in Fig. 8(b). It is to be noted that the Euclidean distance threshold will also decrease after applying DTW (0.6 is an appropriate choice based on our experimental results). Therefore, based on the updated threshold, the "Normal-B" will be considered as normal.

In this article, DTW has been employed as a secondary index. Combining Euclidean distance with DTW leads to a more robust and reliable condition assessment system. In other words, DTW can help to ensure that a significant increase in the Euclidean distance is not solely due to a time shift, but rather indicates an actual change in the signal pattern.

D. Machine Learning

By extracting relevant features from coil current signals, ML models can be trained to classify defect types, offering a data-driven solution to HVCB condition monitoring. In this study, the following features were utilized as input to the classification models: the first peak current (I_{P1}), excitation time (T_{P1}), second peak current (I_{P2}), auxiliary contact operation time (T_{P2}), latching time indicating the initiation of HVCB operation (T_L), and total coil energizing time (T_E). Among the broad categories of ML, this study focuses specifically on supervised classification techniques. These methods are well-suited for applications where labeled datasets are available, enabling the model to learn mappings between input features and predefined classes. More details about the implementation of ML are provided in Section IV.

E. Remarks

The proposed methodology can be summarized in a flowchart as demonstrated in Fig. 9. The flowchart outlines the steps involved in real-time monitoring and assessment of the HVCB condition. Initially, the coil current signal is measured and preprocessed using a Savitzky–Golay filter to remove noise. Subsequently, the Euclidean distance is calculated between the filtered signal and a reference healthy signal. If the distance exceeds a predefined threshold, DTW is employed to account for potential time shifts. Suppose that the DTW distance also exceeds its threshold. In that case, after applying the feature extraction method, ML algorithms are utilized to classify the extracted features and identify the specific type of defect, if any. If the Euclidean distance or DTW distance is within their respective threshold, the HVCB is considered healthy.

IV. Results and Discussion

The results of well-known supervised classification models, decision trees, logistic regression, k-nearest neighbors (KNNs),

Authorized licensed use limited to: Tallinn University of Technology. Downloaded on September 19,2025 at 06:05:13 UTC from IEEE Xplore. Restrictions apply.

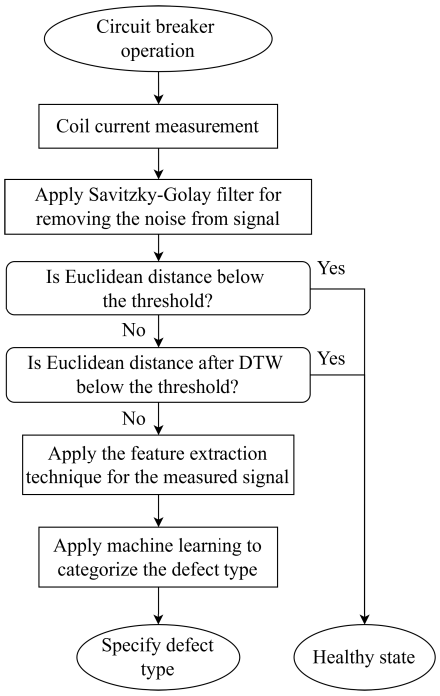


Fig. 9. Flowchart of detection and classification of defect in HVCB.

TABLE II
COMPARISON OF ML-BASED ALGORITHMS FOR CLASSIFICATION OF COIL CURRENT DEFECTS

Model	Training accuracy (%)	Test accuracy (%)	Training time (s)
Decision tree	97.39	92.59	5.79
KNN	98.8	100	8.013
Logistic regression	75.82	74.08	7.72
SVM	71.9	74.07	7.36

and support vector machines (SVMs), are presented [25]. The models were evaluated based on their ability to classify coil current signals into normal and defective states, as well as to distinguish among different defect categories. Table II summarizes the training and testing accuracy of the four algorithms. The input dataset consisted of extracted features from 200 measurement signals obtained from the coil current emulator. Taking into account that six features are extracted from each signal, the input dataset is a 200 × 6 matrix, i.e., each column represents a feature. Since each of these 200 signals is labeled, the label is a 200 × 1 matrix. Elements of the label matrix, output classes, are the specified defects ("auxiliary," "latch," and "voltage") or normal operation ("normal"). The input dataset was split into 80% for training (160 signals) and 20% for testing (40 signals). A fivefold cross-validation scheme was employed during training to ensure model robustness and generalization.

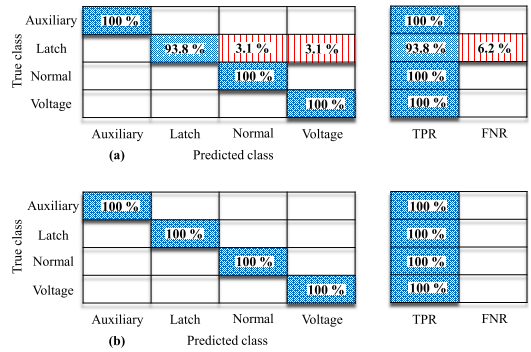


Fig. 10. Confusion matrix, TPR, and FNR of the KNN model. (a) Training validation. (b) Testing.

TABLE III
CLASSIFICATION REPORT ON TESTING SET FOR KNN MODEL

Class	Precision	Recall	F1-score
Auxiliary	1.00	1.00	1.00
Latch	1.00	1.00	1.00
Normal	1.00	1.00	1.00
Voltage	1.00	1.00	1.00

The comparative analysis of the models highlights the strengths and weaknesses of each approach considering their accuracy and training time. Logistic regression and SVM provided were not able to perform classification at an acceptable level considering their high training time. KNN outperformed the other models in terms of accuracy, making it the most suitable choice for defect classification in HVCBs. However, as expected, its training time is slightly higher than the rest of the models. It is assumed that the training process occurs offline in this study. Therefore, accuracy has a higher priority than the training time.

A. K-Nearest Neighbors

The KNN algorithm classifies a data point based on the majority class of its KNNs. It does not make assumptions about the underlying data distribution, and it simply uses the training data to make predictions. However, it can be computationally intensive for large datasets. The value of the parameter k in the KNN algorithm was set to 10 based on cross validation to ensure a balance between classification accuracy and model robustness. To provide a more detailed insight into the model's behavior, the confusion matrix of the KNN classifier is presented in Fig. 10. This matrix illustrates the distribution of true versus predicted class labels and enables a deeper understanding of the model's strengths and potential areas of misclassification. The accuracy points out the percentage of observations that are correctly classified. In addition, the true positive ratio (TPR) and false negative ratio (FNR) for each class of defects are presented next to the confusion matrices.

Table III presents the classification report for the test set, detailing the performance metrics for each class. All classes

Authorized licensed use limited to: Tallinn University of Technology. Downloaded on September 19,2025 at 06:05:13 UTC from IEEE Xplore. Restrictions apply.

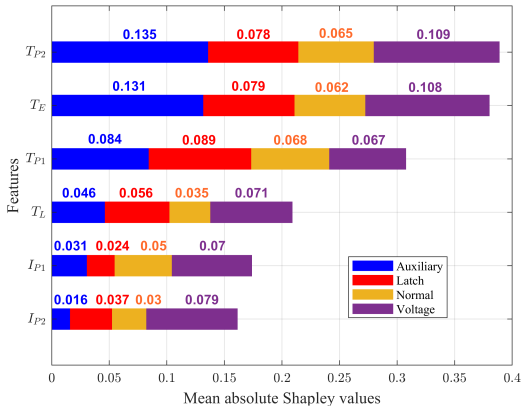


Fig. 11. Global feature importance plot showing the mean absolute Shapley values for each class.

achieved perfect scores of 1.00 for precision, recall, and $F1$-score, indicating an accurate classification by the model on the unseen testing data.

B. Model Interpretability and Feature Importance

To enhance the transparency and interpretability of our trained multiclass classification model, SHAP has been employed [20]. SHAP is a game-theoretic approach that assigns an importance value to each feature for a particular prediction. It ensures "fair" attribution by considering all possible coalitions of features and calculating the marginal contribution of each feature to the prediction. For global interpretability, SHAP values can be aggregated. The mean absolute SHAP value for each feature provides a measure of its overall impact on the model's output, indicating how much that feature, on average, pushes the prediction away from the base value across all possible outputs.

Fig. 11 presents the global feature importance of the model, calculated as the mean of the absolute Shapley values for each feature, aggregated across the entire training dataset. This stacked bar chart dissects each feature's overall importance by indicating its specific contribution to the prediction of each of the four classes: "auxiliary," "latch," "normal," and "voltage" (as indicated in the legend), and is sorted by total importance in descending order.

As observed from Fig. 11, features T_{P2} and T_E emerge as the most globally influential features, exhibiting the largest mean absolute Shapley values. They are closely followed by T_{P1}. This strong influence of the time-related parameters suggests their critical role in the model's overall decision-making process for HVCB coil defect classification.

Delving into the class-specific contributions, it is evident that a substantial portion of the importance for T_{P2}, T_E, T_{P1}, and T_L is attributed to their role in classifying the "auxiliary" defect. This indicates that these time-related parameters are particularly critical for identifying issues specifically related to auxiliary contact abnormalities.

The "voltage" and "latch" defect types also show significant reliance on these top features, particularly T_{P2}, T_E, and T_{P1}. This implies that these features are versatile in discriminating across multiple defect types. Features I_{P1} and I_{P2} (current related) exhibit lower overall global importance compared to the time-related parameters, but still contribute to distinguishing between classes, with notable contributions to the "voltage."

C. Remarks

As shown in Fig. 10, the normal category has also been included to demonstrate the classification performance of ML algorithms considering defected and normal classes together. Based on the results, the main misclassification for the ML algorithms has occurred for the normal category. This highlights the effectiveness of the proposed methodology, which utilizes Euclidean distance as an initial index. As shown in Fig. 9, finding the similarity of the measured signal with the normal one using Euclidean distance (before or after applying DTW) will identify the normal category before utilizing ML, which will increase the accuracy of the ML algorithms.

The SHAP analysis provides clear insights into the factors driving our model's classifications. The dominance of time-related parameters in defect identification aligns with the expected dynamic behavior of the HVCB coil. These findings not only validate the model's learning but also offer actionable insights for engineers, allowing them to prioritize diagnostic efforts on these critical temporal parameters when troubleshooting circuit breaker coils.

To summarize, the results demonstrate that supervised ML techniques can effectively classify HVCB defects, even utilizing a low-cost sensor, subject to the proper feature extraction from coil current measurements. In other words, the preprocessing phase, particularly the denoising technique, played a significant role in improving the signal quality and, subsequently, the model performance. The proposed methodology can be applied to measurements with similar characteristics and is not limited to only one device.

V. Conclusion

This article presents a comprehensive framework for the condition monitoring and defect classification of HVCBs using inexpensive measurement devices. The proposed approach effectively addresses the challenges of noisy signal data by employing the Savitzky–Golay filter. The filter's ability to preserve essential signal features while removing noise ensures accurate feature extraction for further analysis. To classify HVCB defects, the study proposes integrating time series similarity assessment techniques, such as DTW, with ML algorithms. Moreover, the developed experimental setup enabled to emulate coil current under various defects, and to measure it using a simple and inexpensive current sensor. The features extracted from these measurements were utilized to train ML-based algorithms, among which the KNN algorithm had the highest accuracy. Furthermore, the interpretability of the trained KNN model was enhanced using SHAP analysis, which revealed the relative importance of each extracted

Authorized licensed use limited to: Tallinn University of Technology. Downloaded on September 19,2025 at 06:05:13 UTC from IEEE Xplore. Restrictions apply.

feature in the classification process. The results highlight the potential of this approach as a cost-effective and reliable solution for online HVCB condition monitoring. Future research will aim to expand the methodology to encompass a wider range of defect scenarios across various components of HVCB and to investigate its practical implementation in real-world settings such as substations.

REFERENCES

[1] K. Niayesh and M. Runde, *Power Switching Components*. Cham, Switzerland: Springer, 2017.

[2] P. Dehghanian, Y. Guan, and M. Kezunovic, "Real-time life-cycle assessment of high-voltage circuit breakers for maintenance using online condition monitoring data," *IEEE Trans. Ind. Appl.*, vol. 55, no. 2, pp. 1135–1146, Mar. 2019.

[3] M. Abdollah and A. A. Razi-Kazemi, "Intelligent failure diagnosis for gas circuit breakers based on dynamic resistance measurements," *IEEE Trans. Instrum. Meas.*, vol. 68, no. 9, pp. 3066–3077, Sep. 2019.

[4] A. A. Razi-Kazemi, M. Vakilian, K. Niayesh, and M. Lehtonen, "Priority assessment of online monitoring investment for power system circuit breakers—Part II: Determination of optimum number," *IEEE Trans. Power Del.*, vol. 28, no. 3, pp. 1440–1446, Mar. 2013.

[5] M. Taghizadeh Kejani, A. A. Razi-Kazemi, S. Hamid Khalkhali, and P. Heidary, "An approach to monitor medium voltage switchgear plum contact connections based on temperature rise index," *IEEE Trans. Instrum. Meas.*, vol. 73, pp. 1–10, 2024.

[6] G. Balzer and C. Schorn, *Asset Management for Infrastructure Systems*. Cham, Switzerland: Springer, 2022.

[7] Q. Yang, Z. Wang, J. Ruan, and Z. Zhuang, "Small-sample fault diagnosis method for high-voltage circuit breakers via data augmentation and deep learning," *IEEE Trans. Instrum. Meas.*, vol. 73, pp. 1–11, 2024.

[8] J. A. Grant, H. Toftaker, S. Perkin, I. B. Sperstad, and V. V. Vadlamudi, "High-voltage circuit breaker condition-dependent failure rate with covariates," in *Proc. Annu. Rel. Maintainability Symp. (RAMS)*, 2024, pp. 1–6.

[9] T. Krieg and J. Finn, *Substations* (CIGRE Green Books). Cham, Switzerland: Springer, 2018.

[10] S. Asefi et al., "Measurement and operation based condition monitoring methodology for high voltage circuit breakers," in *Proc. IEEE PES Innov. Smart Grid Technol. Conf. Eur. (ISGT-Eur.)*, Oct. 2022, pp. 1–5.

[11] A. Asghar Razi-Kazemi and K. Niayesh, "Condition monitoring of high voltage circuit breakers: Past to future," *IEEE Trans. Power Del.*, vol. 36, no. 2, pp. 740–750, Apr. 2021.

[12] A. A. Razi-Kazemi, M. Vakilian, K. Niayesh, and M. Lehtonen, "Circuit-breaker automated failure tracking based on coil current signature," *IEEE Trans. Power Del.*, vol. 29, no. 1, pp. 283–290, Feb. 2014.

[13] J. A. Grant, I. B. Sperstad, J. Foros, and V. V. Vadlamudi, "Health index calculation using failure modes, effects, and criticality analysis for high-voltage circuit breakers," in *Proc. 33rd Eur. Saf. Rel. Conf.*, 2023, pp. 1746–1753.

[14] A. Setiawan, W. Adiati, and R. A. Prasojo, "An approach of the analytic hierarchy process to acquire the weighting factor of high voltage circuit breaker health index," in *Proc. Int. Conf. Technol. Policy Energy Electric Power (ICT-PEP)*, Sep. 2020, pp. 317–322.

[15] S. Geng and X. Wang, "Research on data-driven method for circuit breaker condition assessment based on back propagation neural network," *Comput. Electr. Eng.*, vol. 86, Sep. 2020, Art. no. 106732.

[16] J. Zhong, W. Li, R. Billinton, and J. Yu, "Incorporating a condition monitoring based aging failure model of a circuit breaker in substation reliability assessment," *IEEE Trans. Power Syst.*, vol. 30, no. 6, pp. 3407–3415, Nov. 2015.

[17] S. Asefi, J. Kilter, E. Shayesteh, P. Hilber, and T. Lindquist, "High voltage circuit breaker health index evaluation considering measurement accuracy," in *Proc. IEEE PES Innov. Smart Grid Technol. Eur. (ISGT EUROPE)*, Oct. 2024, pp. 1–5.

[18] L. Zhao, I. Brandao Machado Matsuo, Y. Zhou, and W.-J. Lee, "Design of an industrial IoT-based monitoring system for power substations," *IEEE Trans. Ind. Appl.*, vol. 55, no. 6, pp. 5666–5674, Nov. 2019.

[19] R. W. Schafer, "What is a Savitzky–Golay filter? [lecture notes]," *IEEE Signal Process. Mag.*, vol. 28, no. 4, pp. 111–117, Jul. 2011.

[20] S. Lundberg and S. Lee, "A unified approach to interpreting model predictions," in *Proc. Adv. Neural Inf. Process. Syst.*, 2017, pp. 1–10.

[21] J. Seo, H. Ma, and T. K. Saha, "On Savitzky–Golay filtering for online condition monitoring of transformer on-load tap changer," *IEEE Trans. Power Del.*, vol. 33, no. 4, pp. 1689–1698, Aug. 2018.

[22] A. Savitzky and M. J. E. Golay, "Smoothing and differentiation of data by simplified least squares procedures," *Anal. Chem.*, vol. 36, no. 8, pp. 1627–1639, Jul. 1964.

[23] K. Hasan, S. T. Meraj, M. M. Othman, M. S. H. Lipu, M. A. Hannan, and K. M. Muttaqi, "Savitzky–Golay filter-based PLL: Modeling and performance validation," *IEEE Trans. Instrum. Meas.*, vol. 71, pp. 1–6, 2022.

[24] H. Sakoe and S. Chiba, "Dynamic programming algorithm optimization for spoken word recognition," *IEEE Trans. Acoust., Speech, Signal Process.*, vol. ASSP-26, no. 1, pp. 43–49, Feb. 1978.

[25] S. Asefi, M. Mitrovic, D. Ćetenović, V. Levi, E. Gryazina, and V. Terzija, "Anomaly detection and classification in power system state estimation: Combining model-based and data-driven methods," *Sustain. Energy, Grids Netw.*, vol. 35, Sep. 2023, Art. no. 101116.

Authorized licensed use limited to: Tallinn University of Technology. Downloaded on September 19,2025 at 06:05:13 UTC from IEEE Xplore. Restrictions apply.

Appendix 6

S. Asefi and J. Kilter, "Dynamic Time Warping Technique for Condition Monitoring of High-Voltage Circuit Breakers," in 2025 15th International Conference on Power, Energy, and Electrical Engineering (CPEEE), 2025, pp. 38-42.

Dynamic Time Warping Technique for Condition Monitoring of High Voltage Circuit Breakers

Sajjad Asefi
Department of Electrical Power Engineering and Mechatronics,
Tallinn University of Technology
Tallinn, Estonia
sajjad.asefi@taltech.ee
*Corresponding author

Jako Kilter
Department of Electrical Power Engineering and Mechatronics,
Tallinn University of Technology
Tallinn, Estonia
jako.kilter@taltech.ee

***Abstract*—The reliability of high voltage circuit breakers (HVCBs) is crucial for power grid operation. Therefore, it is vital to monitor the condition of HVCBs accurately. One of the online condition monitoring measurements for HVCBs is the trip/close coil current measurement which is straightforward to implement. This paper presents a novel application of dynamic time warping (DTW) to compare healthy and defective trip/close coil current signals, facilitating the detection of defects in HVCB operation. DTW is used to assess the temporal variations between different signal patterns, providing a robust comparison even under varying operational conditions. An experimental HVCB setup is used to validate the proposed method, showcasing its capability to detect different types of faults in the coil mechanism.**

***Index Terms*—Circuit breaker, Condition monitoring, Dynamic Time Warping, Measurement accuracy**

I. Introduction

HIGH voltage circuit breakers (HVCBs) are critical components for maintaining the reliability and stability of power systems [1]. HVCBs play a crucial role in protecting power systems by carrying current under normal conditions and interrupting it when a fault occurs [2]. Any failure in HVCBs can lead to stress on other equipment and can significantly affect the reliability and resilience of power systems. Because they are essential for both protection and switching. Therefore, effective maintenance and defect diagnosis systems for HVCBs are required for detecting issues at early stages [3].

There are several maintenance strategies that can be applied to HVCBs, including *time-based maintenance*: involves performing maintenance activities at predefined time intervals, *condition-based maintenance*: uses diagnostic signals such as coil current to determine the condition of the HVCB and perform maintenance when needed, and *reliability-centered maintenance*: in addition to condition monitoring it considers the criticality of the HVCBs within the power system and allocates maintenance resources to the most critical components [4].

To increase the accuracy of the maintenance, whether condition-based or reliability-centered, precise condition monitoring techniques are required. Condition monitoring of HVCBs employs various measurements to assess their health and predict potential failures. Coil current (CC) analysis measures the current in the trip/close coils, and variations in the CC waveform can indicate issues with the coil, latch, or auxiliary switches. Travel curve analysis tracks the motion of the contacts over time, which is used to evaluate the operating speed, timing, and damper condition of the HVCB. Vibration monitoring captures the vibrations generated during the operation of the HVCB, revealing anomalies in the mechanical components. Dynamic/static resistance measurement can be used to assess the condition of the main and arcing contacts. Furthermore, Partial discharge monitoring is used to detect insulation defects, particularly in gas-insulated switchgear. These methods, used alone or in combination, help to identify the condition of the HVCB [5]. However, among the mentioned techniques CC analysis can be simply implemented in an online manner, i.e., it's not required to disconnect the HVCB from the grid to implement the measurement. Moreover, it reflects approximately 25% of major failures.

Several challenges might appear while implementing the condition monitoring of HVCBs, particularly when dealing with CC signals. One significant challenge is the presence of noise in the measured signals. It can be due to the low quality of the measurement sensors or the magnetic interference of the substation environment. Noisy measurement makes it difficult to extract useful diagnostic information and might cause misinterpretation of the results. To enhance signal quality filtering techniques, such as the moving average method can be applied to the signal which has been considered in this paper.

Another challenge is that traditional methods for analyzing time series data often fall short when it comes to capturing temporal variations in the measurement signals. For instance, similarity measures, such as Euclidean distance, do not account for temporal distortions, which are common in real-world measurement signals. In this paper, dynamic time warping (DTW) has been applied to address this challenge. In other words, the objective of this study is to demonstrate how DTW can increase the accuracy of detecting and classifying defects using CC measurements.

This study was co-funded by the European Union and Ministry of Education and Research via project TEM-TA134.

The paper is organized as follows. Section II discusses the features available in CC measurement that can be useful in classifying defects. Moreover, the experimental setup that has been utilized to emulate the CC signal is demonstrated. Section III provides information about various types of defects and the measured current related to each defect is demonstrated. Additionally, it presents the proposed methodology for the detection and classification of defects. Section IV demonstrates and compares the results of defect classification. Finally, the paper is concluded in Section V.

II. Coil Current Signal Features and Experimental Setup

This section presents a typical CC measurement signal and points out the features that can be extracted for defect classification purposes. Additionally, a comparison of the raw and filtered measurement signal is demonstrated to point out the effect of filtering methods on the CC features. Finally, an experimental setup is presented which is utilized to produce realistic noisy CC measurements.

A. Coil Current Signal

Usually the HVCBs are used in environments, such as substations, where the existence of noise and electromagnetic interference is inevitable. Therefore, the CC measurements are noisy, and it's required to remove potential noise or inconsistencies in the raw CC data. Techniques like smoothing algorithms can be employed to enhance signal quality. Fig. 1 demonstrates a comparison between smoothed and raw data of CC measurement, together with the extracted features [6]. The data is based on the high accuracy laboratory measurements of a 110 kV HVCB, and it is smoothed using the moving average method with a scale factor of 0.03.

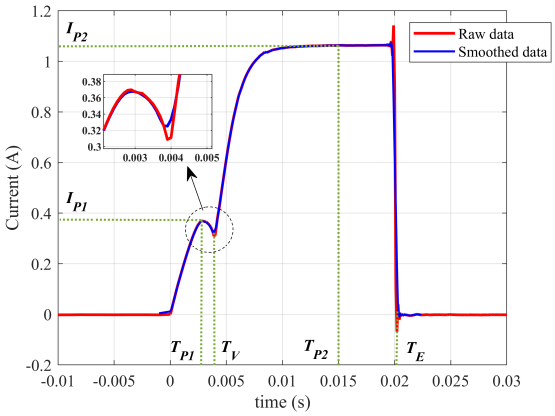


Fig. 1. Smoothing and feature extraction from CC measurement

As emphasized in Fig. 1, it's important to acknowledge that curve smoothing or other preprocessing techniques might introduce slight deviations to the extracted features' values. To mitigate this potential impact, the chosen preprocessing method should be carefully selected to minimize distortion of the underlying signal. Additionally, validating the chosen method's performance by comparing preprocessed and raw data can be beneficial.

From the preprocessed CC signal, relevant features indicative of HVCB status are extracted as shown in Fig. 1. These features include first peak current (I_{P1}), excitation time (T_{P1}), second peak current (I_{P2}), auxiliary contact operation time (T_{P2}), latching time (T_V), and total energizing time of the coil (T_E).

B. Experimental Setup

The experimental setup developed in this study is designed to emulate the behavior of an HVCB's coil mechanism. A schematic representation of the setup is shown in Fig. 2. The setup incorporates various components, including an ACS712 current sensor (5 A), which is employed to measure the CC signal.

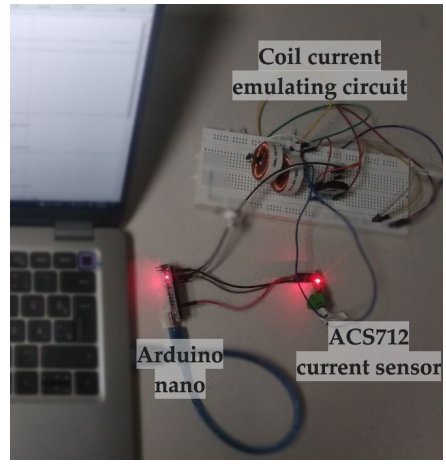


Fig. 2. Schematic representation of the experimental setup for emulating HVCB coil current behavior.

The ACS712 current sensor is a widely used Hall-effect-based sensor, known for its simplicity and affordability. While it is effective in detecting changes in the CC signal, its measurements may exhibit noise due to limited precision. This characteristic should be considered when analyzing the captured data and interpreting the results. Efforts to mitigate noise through filtering or signal processing techniques are recommended to enhance measurement reliability.

III. Methodology

A. Signal Acquisition

A typical healthy CC waveform is demonstrated in Fig. 1. However, different failures in HVCBs cause distinct changes in the CC waveforms. Supply voltage variations directly affect the electromagnetic force, causing the CC curve to shift; an overvoltage shifts the curve upwards and to the left while

undervoltage shifts it downwards and to the right. Coil issues such as increased resistance due to aging or malfunctions impact the peak currents, excitation time, and latching time, and irregularities like short circuits alter the coil's resistance and inductance, leading to significant changes in the CC features. Latch operation defects, such as sluggishness from lack of lubrication or mechanical issues, can affect the CB operation time and CC waveform, and may result in higher operation times; if the latch fails completely, the CC pattern resembles a time-independent inductance. Auxiliary contact malfunctions can influence the auxiliary contact operation time and the total energizing time of the CC; also, contact bouncing can be observed in the waveform. These changes in the CC waveform are valuable for condition monitoring by comparing measured features with reference values [7].

To illustrate the impact of various defects on the CC waveform, a conceptual figure is presented in Figure 3. This figure demonstrates the potential alterations in the waveform caused by common defects, such as auxiliary contact malfunctions (two types of auxiliary contact defects are analyzed which are labeled as Aux1 and Aux2), latch operation defects (which are labeled as soft latch and stiff latch), and supply voltage variations (in which the supply voltage has been changed in four categories, -20%, -10%, +10%, +20%). These changes in the waveform provide diagnostic signatures that can be utilized for condition monitoring and defect detection.

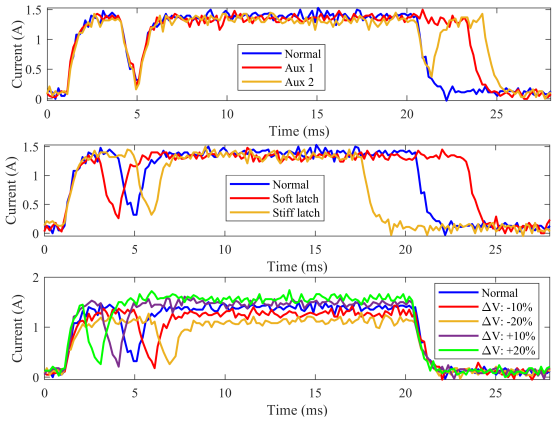


Fig. 3. Illustration of the effects of various defects on the CC waveform.

B. Dynamic Time Warping (DTW)

Euclidean distance is a widely used technique that provides a straightforward measurement of similar time series data. It assumes that both time series are of equal length and perfectly aligned in time. The Euclidean distance between two time series is calculated as:

$$d_E(X,Y) = \sqrt{\sum_{i=1}^{n}(x_i - y_i)^2} \quad (1)$$

Comparing the Euclidean distance of the normal coil current signal with the defected signals, can lead to a preliminary detection of defects. Fig. 4 demonstrates the Euclidean distance between two normal signals (called Normal-A and Normal-B) after being smoothed using the moving average method. This is the case when two measurements are perfectly aligned.

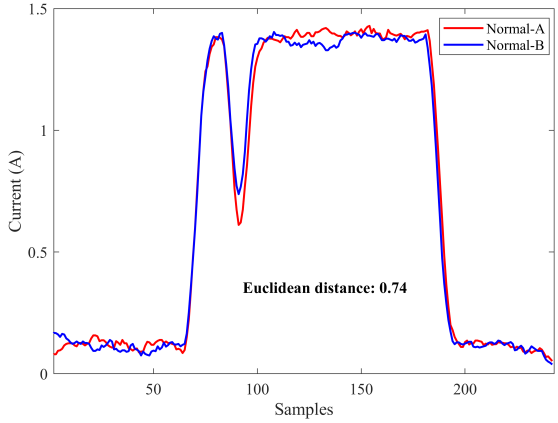


Fig. 4. Euclidean distance between two normal signals

On the other hand, Fig. 5 demonstrates the Euclidean distance between a normal and a defected signal (the defect is latch stiffness) after being smoothed using the moving average method. Again, this is the case when two measurements are perfectly aligned. Consequently using the Euclidean distance technique can easily provide the possibility to specify a threshold that distinguishes the normal and defected signals from each other.

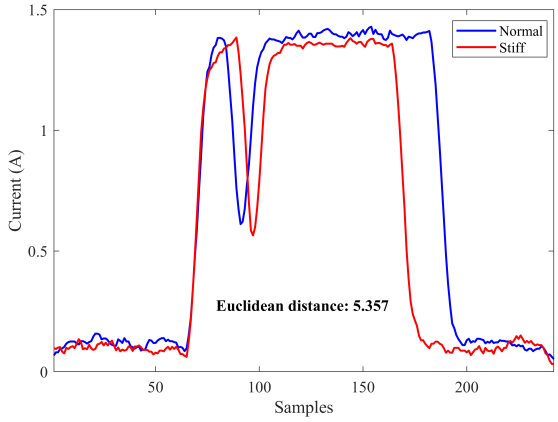


Fig. 5. Euclidean distance between normal and defected signals

However, in practical cases, the measured signals might have temporal distortions. Dynamic time warping (DTW)

is an alignment algorithm designed to compare time series, even when they are misaligned or have variable lengths [8]. DTW achieves this by dynamically stretching or compressing the sequences along the time axis to minimize the cumulative distance. Mathematically, given two sequences $X = [x_1, x_2, \ldots, x_n]$ and $Y = [y_1, y_2, \ldots, y_m]$, the DTW distance is computed as:

$$D(i,j) = d(x_i, y_j) + min\{D(i-1,j), ... \\ D(i,j-1), D(i-1,j-1)\} \quad (2)$$

where $d(x_i, y_j) = |x_i - y_j|$ is the local distance between elements x_i and y_j. The boundary conditions are:

$$D(0,0) = 0, \quad D(i,0) = \infty, \quad D(0,j) = \infty. \quad (3)$$

The warping path is determined by tracing back from $D(n,m)$, which represents the optimal alignment cost. Considering the ability of DTW to handle temporal misalignments and time series of different lengths, it is a suitable choice when analyzing coil current measurements.

IV. Results and Discussion

In this paper, DTW has been employed as a secondary index. Combining Euclidean distance with DTW, leads to a more robust and reliable condition assessment system. In other words, DTW can help ensure that a significant increase in Euclidean distance is not solely due to a time shift but rather indicates an actual change in the signal pattern.

The following figures present the application of DTW for two normal coil current measurement signals (called Normal-A and Normal-B). Fig 6 shows the scenario when two normal signals are prone to a time shift.

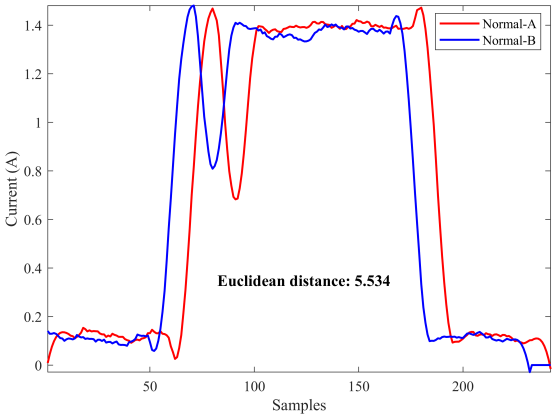


Fig. 6. Comparison of two normal signals with time discrepancy

As stated in the Fig. 6 the Euclidean distance between these two signals is 5.534. However, if the signals were completely aligned this value should have been lower than 1.8 (this value is obtained based on experimenting with 20 normal signals and comparing their Euclidean distance with respect to each other). Therefore, solely using Euclidean distance can lead to misinterpretation and detect a normal signal as defected.

Fig. 7 demonstrates the same two signals shown in Fig. 6 after applying the DTW method. As expected, the Euclidean distance after DTW has decreased and reached 0.364.

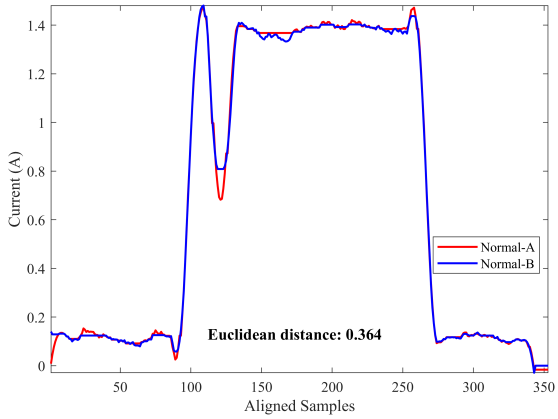


Fig. 7. Application of DTW for two normal signals' alignment

It is to be noted that the Euclidean distance threshold will also decrease after applying DTW (0.6 is an appropriate choice based on our experimental results).

Fig. 8 presents the scenario when a normal signal is compared with a defected signal which is prone to time misalignment as well. The defect signal that is presented in this figure is related to the case when the auxiliary contact malfunctions (labeled as Aux).

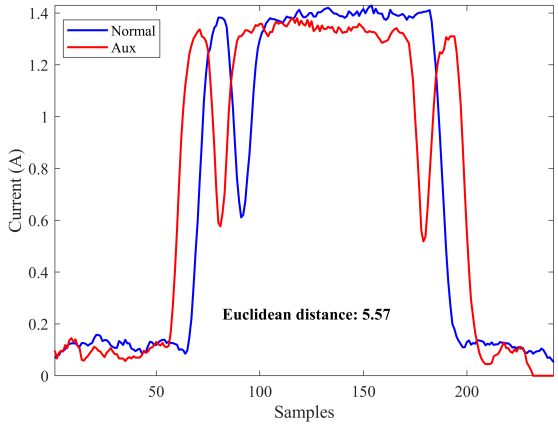


Fig. 8. Comparison of normal and defected signals with time discrepancy

The Euclidean distance is 5.57 which is above the specified threshold. To make sure that this curve represents a defect, the second stage will be to calulate the Euclidean distance

after applying DTW which is shown in Fig. 9. Although after applying DTW the Euclidean distance of two curves is decreased to 1.39, it's still higher than the specified threshold for the DTW method, and it indicates that the signal is related to a defect.

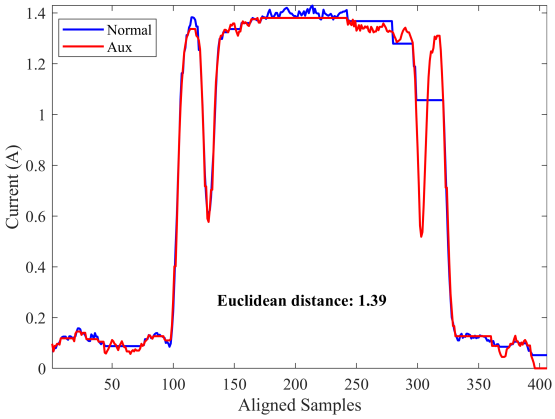


Fig. 9. Application of DTW for signal alignment

The effectiveness of DTW in detecting defects using CC signals was evaluated through a series of visual analyses. The provided figures demonstrate a clear distinction between healthy and defective signals, showcasing DTW's capability to handle temporal misalignment that often occurs for the measurement signals. Unlike traditional comparison methods, DTW dynamically aligns signals despite variations in time, effectively identifying key discrepancies caused by defects. The results validate the robustness of DTW which can improve HVCB condition monitoring.

V. Conclusion

This paper presented a novel application of DTW for condition monitoring of HVCBs, focusing on the analysis of coil current signals. Accurate condition monitoring is critical for ensuring grid reliability, yet noisy and temporally misaligned signals pose significant challenges for traditional diagnostic methods. The proposed DTW-based approach offers a robust solution by dynamically aligning time series, enabling effective comparison between healthy and defective signals. Experimental validation demonstrated that DTW can reliably detect and distinguish healthy and defected signals, even under varying operational conditions and in the presence of noise. Future work will focus on extending the proposed methodology to real-time monitoring applications, and exploring the effect of machine learning based methods and noise filtering techniques on its performance in detecting more complex fault scenarios.

References

[1] A. A. Razi-Kazemi and K. Niayesh, "Condition monitoring of high voltage circuit breakers: past to future," *IEEE Transactions on Power Delivery*, vol. 36, no. 2, pp. 740–750, 2020.

[2] S. Asefi, J. Kilter, E. Shayesteh, P. Hilber, and T. Lindquist, "High voltage circuit breaker health index evaluation considering measurement accuracy," in *2024 IEEE PES Innovative Smart Grid Technologies Conference Europe (ISGT-Europe)*. IEEE, 2024, pp. 1–5.

[3] M. Seeger, F. Macedo, U. Riechert, M. Bujotzek, A. Hassanpoor, and J. Häfner, "Trends in high voltage switchgear research and technology," *IEEJ Transactions on Electrical and Electronic Engineering*, 2024.

[4] S. Asefi *et al.*, "Review of high voltage instrument transformer condition monitoring," *IEEE Transactions on Dielectrics and Electrical Insulation*, 2024.

[5] S. Asefi *et al.*, "Measurement and operation based condition monitoring methodology for high voltage circuit breakers," in *2022 IEEE PES Innovative Smart Grid Technologies Conference Europe (ISGT-Europe)*. IEEE, 2022, pp. 1–5.

[6] J. Zhong, W. Li, R. Billinton, and J. Yu, "Incorporating a condition monitoring based aging failure model of a circuit breaker in substation reliability assessment," *IEEE Transactions on Power Systems*, vol. 30, no. 6, pp. 3407–3415, 2015.

[7] A. A. Razi-Kazemi, M. Vakilian, K. Niayesh, and M. Lehtonen, "Circuit-breaker automated failure tracking based on coil current signature," *IEEE Transactions on Power Delivery*, vol. 29, no. 1, pp. 283–290, 2013.

[8] H. Sakoe and S. Chiba, "Dynamic programming algorithm optimization for spoken word recognition," *IEEE transactions on acoustics, speech, and signal processing*, vol. 26, no. 1, pp. 43–49, 1978.

Curriculum Vitae

1. Personal data

Name	Sajjad Asefi
Date and place of birth	19 September 1992, Talesh, Iran
E-mail	sajjad.asefi@taltech.ee

2. Education

2021–...	Tallinn University of Technology, School of Engineering, Electrical Power Engineering and Mechatronics, PhD studies
2015–2018	University of Mohaghegh Ardabili, Ardabil, Iran, Electrical Engineering, MSc (Excellent)
2011–2015	Guilan University, Rasht, Iran, Electrical Engineering, BSc

3. Professional employment

2024–...	Tallinn University of Technology (TalTech), Early-stage researcher
2025–2025	INESCTEC, Centre for Power and Energy Systems (Portugal), Visiting researcher
2024–2024	KTH Royal Institute of Technology (Sweden), Visiting researcher

4. Defended theses

- 2018, Optimal sizing and energy dispatch of distributed generation sources considering demand response, MSc, University of Mohaghegh Ardabili
- 2015, Analysis of distribution system reliability indices accounting time to switch using Monte Carlo simulation, BSc, Guilan University

5. Scientific work
Publications

1. Asefi, S., Asefi, S., Afshari, H., Kilter, J., Shayesteh, E., Hilber, P., & Lindquist, T. (2025). Machine Learning based High-Voltage Circuit Breaker Defect Classification Utilising Savitzky-Golay Filter. *IEEE Transactions on Instrumentation and Measurement*.
2. Asefi, S., Asad, B., Leinakse, M., Manninen, H., Kilter, J., Vaimann, T., Kallaste, A., Tealane, M., & Landsberg, M. (2024). Review of High-Voltage Instrument Transformer Condition Monitoring. *IEEE Transactions on Dielectrics and Electrical Insulation*.
3. Asefi, S., & Kilter, J. (2025). Dynamic Time Warping Technique for Condition Monitoring of High-Voltage Circuit Breakers. In *2025 15th International Conference on Power, Energy, and Electrical Engineering (CPEEE)*. IEEE.
4. MohammadNezhad, H., Asefi, S., & Kilter, J. (2024). Application of Multi-Agent Reinforcement Learning for Renewable Energy Sources Management. In *2024 IEEE PES Innovative Smart Grid Technologies Conference Europe (ISGT-Europe)*. IEEE.
5. Asefi, S., Kilter, J., Shayesteh, E., Hilber, P., & Lindquist, T. (2024). High-Voltage Circuit Breaker Health Index Evaluation Considering Measurement Accuracy. In *2024 IEEE PES Innovative Smart Grid Technologies Conference Europe (ISGT-Europe)*. IEEE.

6. Asefi, S., Kilter, J., Akroud, N., Hurtado, A., Gilbert, I., & Orue, I. (2024). Application of Transfer Learning for Instrument Transformer Condition Monitoring. *International Conference on Diagnostics in Electrical Engineering (Diagnostika)*.

7. Asefi, S., Kittam, I., Mannenin, H., Kilter, J., Tealane, M., & Landsberg, M. (2023). Variability of High-Voltage Circuit Breaker Performance Parameters for Condition Monitoring. In *2023 International Conference on Condition Monitoring, Diagnostics, and maintenance (CMDM)*. CIGRE.

8. Asefi, S., Leinakse, M., Kilter, J., & Landsberg, M. (2023). Capacitor Coupled Voltage Transformer Defect Identification in the Presence of Tap Changer. In *2023 IEEE PES Innovative Smart Grid Technologies Conference Europe (ISGT-Europe)*. IEEE.

9. Asefi, S., Kilter, J., & Landsberg, M. (2023). Non-intrusive defects identification for the high-voltage instrument transformers. In *2023 IEEE 17th International Conference on Compatibility, Power Electronics and Power Engineering (CPE-POWERENG)*. IEEE.

10. Asefi, S., Kilter, J., & Landsberg, M. (2023). Incorporating Service Type in Ageing Failure Model of High-Voltage Circuit Breaker. In *2023 27th International Conference Electronics*. IEEE.

11. Asefi, S., Andreesen, G., Kilter, J., & Landsberg, M. (2023). Capacitor Coupled Voltage Transformer Inaccuracy Effect on Circuit Breaker Operation. In *2023 23rd International Scientific Conference on Electric Power Engineering (EPE)*. IEEE.

12. Asefi, S., Andreesen, G., Leinakse, M., Kilter, J., Kalmet, T., Manninen, H., & Landsberg, M. (2022). Measurement and Operation Based Condition Monitoring Methodology for High-Voltage Circuit Breakers. In *2022 IEEE PES Innovative Smart Grid Technologies Conference Europe (ISGT-Europe)*. IEEE.

Elulookirjeldus

1. Isikuandmed

Nimi	Sajjad Asefi
Sünniaeg ja -koht	19.09.1992, Talesh, Iran
E-mail	sajjad.asefi@taltech.ee

2. Haridus

2021–…	Tallinna Tehnikaülikool, Inseneriteaduskond, Elektroenergeetika ja mehhatroonika, doktoriõpe
2015–2018	Mohaghegh Ardabili Ülikool, Elektroenergeetika, MSc
2011–2015	Guilani Ülikool, Elektroenergeetika, BSc

3. Teenistuskäik

2024–…	Tallinna Tehnikaülikool, Nooremteadur
2025–2025	INESCTEC (Portugal), Külalisteadur
2024–2024	KTH Kuninglik Tehnoloogiainstituut (Rootsi), Külalisteadur

4. Kaitstud lõputööd

- 2018, Optimal sizing and energy dispatch of distributed generation sources considering demand response, MSc, Mohaghegh Ardabili Ülikool
- 2015, Analysis of distribution system reliability indices accounting time to switch using Monte Carlo simulation, BSc, Guilani Ülikool

5. Teadustegevus

Teadusartiklite, konverentsiteeside ja konverentsiettekannete loetelu on toodud ingliskeelse elulookirjelduse juures.

ISSN 2585-6901
ISBN 978-9916-80-545-9